MSc thesis in Geomatics

(Semi-)automatic modeling of indoor building 3D models for daylight simulation with Lidar-enabled mobile devices

Giorgos Iliopoulos

January 2026

A thesis submitted to the Delft University of Technology in partial fulfillment of the requirements for the degree of Master of Science in Geomatics

The work in this thesis was carried out in the:

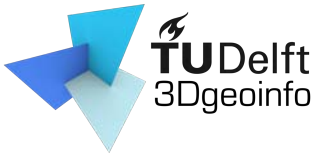

3D geoinformation group
Delft University of Technology

Supervisors:	Ken Arroyo Ohori
	Eleonora Brembilla
	Nima Forouzandeh Shahraki
Co-reader:	Azarakhsh Rafiee

Abstract

This project evaluates the suitability of 3D interior space models acquired using Apple's RoomPlan API for daylight simulations. The main contribution is a Python-based tool that converts RoomPlan output into Honeybee JSON file format (HBJSON) by automatically reconstructing the ceiling and adding window frames, which are missing in RoomPlan's output. Although RoomPlan is also able to capture furniture, these elements were not used in the geometric evaluation or in the daylight simulations. The resulting models can be directly used in Grasshopper for daylight simulations, reducing the modeling time required by practitioners. To assess the suitability of RoomPlan, three office interiors were scanned using a Terrestrial Laser Scanning (TLS) and modeled both manually and with an iPhone 12 Pro. The manual models were used as ground truth. For each room, a geometric evaluation and a daylight simulation evaluation were performed using three model versions: manual, RoomPlan with extruded window frames, and RoomPlan without extruded window frames. For both the geometrical and the daylight performance evaluation, it is apparent that the windows' frames extrusion is significant to achieve more accurate results. Geometric accuracy was evaluated using Chamfer and Hausdorff distances, showing good overall accuracy. However, errors were observed in wall heights when the ceiling was not clearly visible and in the separation of windows located close to each other. The models were used for point-in-time grid-based illuminance and view-based luminance simulations in Grasshopper using Honeybee. For the illuminance simulations, the Mean Absolute Error (MAE) is approximately 269 lux and the Mean Absolute Percentage Error (MAPE) is 19.5%. For Daylight Glare Probability (DGP), the MAPE is 7.6% for the RoomPlan models with extruded window frames, with only one misclassification of the DGP category. The results indicate that RoomPlan can be used for visual comfort studies but not for daylight availability studies. Despite these results, suggestions for further work are given, considering both the geometrical and the daylight simulation performance evaluation of the RoomPlan models.

Contents

List of Figures

List of Tables

Acronyms

1. Introduction

1.1. Background and motivation

In the European Union 40% of the energy is consumed for the operational purposes of buildings such as heating, cooling and lighting [Dir, 2024]. The same Directive stresses the significance of energy usage reduction and sets goals towards this direction mainly by means of retrofit. One key aspect that has to be taken into account during the planning of the renovation is the daylight and its effect on occupants' health and well-being. More precisely, daylight affects not only the energy consumption of the building but also the the users of the building psychologically and physiologically [López-Lovillo et al., 2023; Doulos and Tsangrassoulis, 2022]. In addition, many standards for buildings (e.g., EN17037, WELL, BREEAM) highlight the importance of daylight and visual comfort for building occupants since they incorporate the concept of light in their core [Royal Netherlands Standardization Institute (NEN); International WELL Building Institute, n.d.b] Both in new building projects and renovation projects simulations are a great tool for practitioners to forecast the lighting conditions and optimize the design in favor of occupants' well-being.

To run daylight simulations one must have the properly oriented 3D model of the space in question. Although for new projects the 3D models exists, since they are digitally designed, for renovation projects this condition does not apply since older buildings lack digital representations or only rudimentary or outdated models exist [Hübner et al., 2021]. A promising solution to this lack of information are LiDAR scanners. However, the reconstruction of 3D models of indoor environments from point clouds is a complicated task since interiors are complex and may contain multiple objects in addition to the permanent structures (i.e., walls, floors, and ceiling) [Lehtola et al., 2021]. For this reason automatic reconstruction of indoor 3D models for building simulations is still an active research field. Despite the plethora of professional LiDAR scanners in the market, they still have drawbacks which limit their usage by practitioners. First of all, their high cost restricts the accessibility to professionals [Lehtola et al., 2021]. Secondly, their use requires technical knowledge and training. A promising solution to these challenges as Askar and Sternberg [2023] state, is "the democratization of 3D scanning" with the release of iPhone's Pro version which is equipped with LiDAR sensors. In addition to that, Apple has release RoomPlan API which is capable of reconstructing the 3D model of indoor spaces including the architectural components and some types of interior objects [Apple Inc., 2022a] Based on the aforementioned need for a solution to rapidly and easily generate 3D models of indoor spaces for simulations purposes, the current study will assess RoomPlan API as a potential source of information to incorporate in the automatic 3D modeling process.

1.2. Research questions

The goal of this thesis is to test the feasibility of utilizing the 3D models of indoor spaces generated from RoomPlan API. To ensure that all significant aspects of the topic are considered, this section formulates the research questions which will be addressed during the thesis. Initially, the following main research question phrases the goal of the current work. Following that, the sub-questions create the framework based on which the methodology was designed. The formulation of the sub-questions and the methodology was done in a two-way fashion.

Main research question

> How feasible and accurate is the use of iPhone for generating 3D indoor models suitable for daylight simulation?

Sub-questions

1. What are the possibilities of using the RoomPlan API and accessing data from iPhone's sensors for daylight simulations?
2. How can the RoomPlan API's model be transformed into a format compatible with daylight simulation tools?
3. How do RoomPlan generated models perform compared to manually reconstructed models with respect to geometrical accuracy and daylight simulations results?

2. Theoretical background & related work

This chapter provides the theoretical foundation for the research, reviewing the core concepts and technologies underpinning indoor 3D modeling and daylight simulation. It begins by categorizing different techniques used for reconstructing indoor environments, distinguishing between manual, semi-automatic, and automatic approaches. These distinctions are essential for understanding the trade-offs between modeling accuracy, time, and accessibility.

The chapter then introduces the fundamentals of daylight simulation, including its physical basis, typical use cases in architecture, and the tools commonly used in practice. Finally, the capabilities of Apple's RoomPlan API are examined in detail, including the structure of its 3D outputs and the machine learning models it relies on for real-time geometry generation. This review frames the relevance and novelty of investigating RoomPlan as a data source for simulation-ready 3D indoor models.

2.1. 3D Modeling of Indoor Spaces

3D modeling of the built environment is a wide and significant topic in the field of Geomatics due to the importance of 3D models as input for a wide spectrum of applications. Some examples of applications that need 3D models are: indoor and/or outdoor navigation, facility management, emergency management, heritage preservation, wind modeling, and daylight analysis, which is the focus of the current research. It is understandable that these applications require different 3D models as input in terms of semantic information and geometrical detail. As a result, different data sources are utilized and different techniques are applied depending on the application's needs. The most fundamental distinction that can be made is whether the 3D model that need to be reconstructed represents an indoor or outdoor spaces, for instance a room, a house, a facade, the shell of a building or a city. Since this research focuses on indoor environments, this chapter will explore the different and reconstruction techniques applied in the case of indoor space 3D modeling.

When someone needs to reconstruct a 3D model of an indoor environment there are different potential approaches to follow. The approaches can vary on the source used to collect the data as well as the degree of automation incorporated in the reconstruction technique. For instance, the one who needs needs a 3D model might make measurements of the space using a measuring tape or total station and then digitize them in a CAD software. This would be feasible in the case of a single room but in most cases more spaces are needed and therefore this approach would be excessively time-consuming. Another potential source of information to base 3D reconstruction on, are CAD files and blueprints of the buildings, but they are usually outdated or non-existing [Tang et al., 2010]. The advancement of technology though, has equipped practitioners with new novel tools and techniques which accelerate data collection and processing.

Specifically, for daylight analysis in addition to the geometry of constituting elements of the building (i.e., walls, roof and floors), the geometry of those surfaces of the building through which natural light can enter the building is also required [Díaz-Vilariño et al., 2014].

According to Kang et al. [2020]; Tang et al. [2010], 3D modeling is a multi-aspect process and consists of: (i) geometric; (ii) semantic; and (iii) relationship modeling. The discretization into those 3 individual types of modeling assists in understanding the challenging and complicated nature of 3D modeling.

Geometric modeling As its name suggest, refers to the process of recovering the 3D geometry of the indoor environment, or in other words the reconstruction of walls, doors, floors, ceiling, etc[Kang et al., 2020].

Semantic modeling Also referred as object detection, semantic modeling deals with the understanding what is present in the scene and labeling geometries with semantic information[Kang et al., 2020; Tang et al., 2010].

Relationship modeling According to Abreu et al. [2023], it refers to the modeling of spatial relations between objects. The relationships can be distinguished into:

1. aggregation (e.g., wall contains a door).
2. topological (e.g., wall 1 is connected to wall 2).
3. directional (e.g., the second floor is above the first floor) [Abreu et al., 2023].

2.1.1. 3D modeling

Manual modeling

Manual modeling can be approached in the most primitive way of measuring the dimensions and digitizing the manually the model using for instance a CAD software. In this approach the user has full control over the generation of the model, but its prone to human error along with the many hours needed to complete the process. An initial solution to that is the usage of point clouds acquired by LiDAR scanners. The point clouds is imported into an appropriate software (e.g., Rhino3D) and the user generates the geometries by using the points.

Automatic modeling

Geometric modeling focuses on reconstructing the shape and spatial structure of indoor environments from point cloud data, without explicitly assigning semantic meaning or modeling spatial relationships. The primary objective is to transform unstructured 3D point samples into explicit geometric representations, such as surfaces, meshes, or parametric primitives, that approximate the physical indoor space [Kang et al., 2020; Tang et al., 2010].

Some geometric modeling techniques relies on primitive-based approaches, motivated by the strong structural regularity of indoor environments. Architectural elements such as walls, floors, and ceilings are predominantly planar and can therefore be approximated using simple geometric primitives. Kang et al. [2020], describe multiple methods that detect planar surfaces by analyzing local point neighborhoods, estimating surface normals, and grouping points with similar geometric properties. Lim and Doh [2021],), for example, describe moving

from earlier RANSAC-based plane extraction toward region-growing-based plane extraction to better capture smaller planar patches (e.g., stairs, openings) in cluttered indoor data. Their related-work also illustrates how the same goal (structural surface extraction) can be pursued via Hough transform, PCA-based planar segmentation, or RANSAC plane fitting [Lim and Doh, 2021]. Some geometric modeling techniques rely on surface-based reconstruction methods, where the goal is to directly generate a triangle mesh from point samples (Tang et al., 2010; Kang et al., 2020). These approaches are often used when a detailed surface representation is desired, and they generally treat the point cloud as samples of an unknown surface to be reconstructed (Tang et al., 2010). Representative techniques include Poisson surface reconstruction and Screened Poisson reconstruction. Other commonly cited mesh-from-points approaches include Ball Pivoting and Delaunay/α-shape–based reconstruction. Kang et al. [2020] summarize surface-oriented reconstruction as one of the core geometric modeling directions for indoor environments, particularly when the output is intended for visualization or further geometric processing [Kang et al., 2020]. Some geometric modeling techniques rely on volumetric reconstruction, where geometry is represented first as a 3D field (e.g., distance or occupancy values in a voxel grid) and the final surface is extracted afterward [Kang et al., 2020; Tang et al., 2010]. A widely used family of volumetric methods is based on TSDF fusion, introduced for integrating multiple range/depth observations into a consistent volumetric model. A well-known indoor reconstruction system in this direction is KinectFusion, which combines tracking with TSDF-based surface fusion for dense indoor reconstruction. After volumetric fusion, the surface is commonly extracted using Marching Cubes. Volumetric occupancy approaches are also represented in the literature through space carving / volumetric carving formulations. More recent indoor work also follows the same "implicit field then mesh extraction" idea using learned or optimized SDF-style implicit representations, with meshes extracted using Marching Cubes [Lin et al., 2024].

Another important aspect of modeling is semantic segmentation which can be applied directly on the point clouds or on intermediate geometric elements [Kang et al., 2020]. Semantic segmentation can be performed at different resolutions, such as point-wise labeling, voxel/supervoxel labeling, or labeling of pre-segmented geometric regions, depending on the pipeline [Kang et al., 2020]. Kang et al. [2020] describe classical semantic pipelines that use handcrafted geometric and appearance features with standard classifiers (e.g., SVMs or random forests) and often apply spatial-regularization models (e.g., CRFs/MRFs) to encourage consistent labels in neighboring regions [Kang et al., 2020]. More recent work is dominated by deep learning, including point-based networks such as PointNet, and PointCNN, as well as convolutional approaches that operate on voxelized representations using sparse 3D convolutions for large indoor scenes. In Scan-to-BIM settings, semantic modeling is often framed as component recognition, where the target classes align with BIM-relevant elements, and Tang et al. (2010) describe workflows that move from segmented geometry to identifying building objects (e.g., walls, doors, windows) as part of as-built BIM reconstruction [**?**].

2.2. Daylight simulations

Daylight plays a critical role in shaping the indoor environment of buildings, influencing both energy performance and occupant well-being. Beyond its contribution to reducing energy demand through solar gains and lowered reliance on electric lighting, daylight significantly impacts the physiological and psychological health of occupants by supporting circadian rhythms and visual comfort [López-Lovillo et al., 2023; Doulos and Tsangrassoulis, 2022].

Daylight performance is regulated through national and international standards (e.g., EN 17037), and is often a key component of sustainability certification systems (e.g., WELL, BREEAM). To meet these performance targets in both new construction and retrofitting projects, daylight simulation tools are widely used in architectural, engineering and construction practice, since they can assist design teams predict lighting conditions and interpret results by the mean of metrics [Jan L.M. Hensen and Roberto Lamberts, 2019; Montiel-Santiago et al., 2020].

This section reviews the motivation for daylight simulation, introduces its underlying principles and metrics. Following that, it presents the most commonly used tools in performance-based daylight analysis.

2.2.1. Purpose and applications

Daylight simulation serves as a valuable tool in building design and rehabilitation, driven by its dual impact on occupant well-being and building energy performance [Montiel-Santiago et al., 2020]. In recent years, its role has become more prominent due to the increasing regulatory pressure and the integration of daylight metrics in building certification systems. Simulations can provide significant insight of buildings' behavior and be utilized for multi-objective design optimization [Montiel-Santiago et al., 2020].

Occupants Health and Visual Comfort

Exposure to natural daylight directly affects occupants' circadian rhythms, which regulate sleep cycles, hormonal activity, and cognitive function. Inadequate daylight in indoor spaces has been linked to reduced alertness, impaired concentration, and increased stress levels[Boubekri et al., 2020; Jamrozik et al., 2019]. In contrast, studies have shown that well-daylit environments improve academic performance in schools, productivity in office settings, and patient recovery rates in healthcare facilities [Boubekri et al., 2020; Jamrozik et al., 2019; Jafarifiroozabadi et al., 2023; Baloch et al., 2021]. A European study involving 2,670 schoolchildren across 12 countries found that classroom day-lighting parameters, especially the window-to-floor area ratio and shading quality, were significantly associated with higher scores in math and logic tests, suggesting that better access to daylight supports cognitive performance in educational settings [Baloch et al., 2021] In their experimental study, Boubekri et al. [2020] found that workers in environments with optimized daylight and outdoor views slept 37 minutes longer per night and scored 42% higher on cognitive performance tests, compared to those working in traditionally shaded offices. Similarly, [Jamrozik et al., 2019] demonstrated that office workers with access to daylight and exterior views—achieved via modern mesh shading and electrochromic glazing—reported significantly higher satisfaction, reduced eyestrain, and improved working memory and inhibition performance compared to those in blackout environments. In the same vein, in healthcare settings, Jafarifiroozabadi et al. [2023] conducted a retrospective analysis of 2,319 cardiac ICU patients and found that those with beds positioned toward south-facing windows—offering both daylight and exterior views—had significantly shorter lengths of stay compared to patients in windowless or daylight-only rooms. These findings emphasize that daylight design is not only a sustainability measure, but a health and productivity intervention that can yield measurable cognitive, behavioral and health benefits.

In addition to its physiological and psychological effects, daylight also plays a key role in determining visual comfort. According to the European Standard EN 12665, visual comfort is a "subjective sense of well-being resulting from the visual environment", as reported by Carlucci et al. [2015, p. 6]. The reason that makes it highly subjective and thus differing significantly between individuals is that it depends: (i) on the physiology of the human eye, (ii) on the physical quantities describing the amount of light and its distribution in space, and (iii) on the spectral emission of the light source. The assessment of visual comfort is based on the following factors: (i) the amount of light, (ii) the uniformity of light, (iii) the quality of light in rendering colors, and (iv) the prediction of the risk of glare for occupants [Carlucci et al., 2015]. Each of these factors can have positive and negative effects. The European standard EN 12464-1:2021 "Light and lighting - Lighting of work places" for lighting in work places states that "... a person's ability to perceive and perform a visual activity quickly, safely, and comfortably depends greatly on the amount of light and how it is distributed in the task area and the surrounding environment.", as reported by Tzouvaras et al. [2023, p. 188]. By linking the definition of visual comfort from EN 12665, its assessment factors and the dependence of persons' ability on lighting conditions, it can be concluded that visual comfort has a significant impact on building occupants. Although adequate and evenly distributed light can support visual clarity and task efficiency, poorly managed daylighting, such as insufficient illuminance, high brightness contrast, or excessive glare, can result in visual discomfort, eye strain, and cognitive fatigue [Hamedani et al., 2020]. In experimental studies, discomfort glare was shown to degrade both physiological responses and visual task performance, highlighting the need for daylight design to go beyond the quantity of light and address perceptual quality [Hamedani et al., 2020].

Standards and Building certificates

Given the importance of these factors, several international standards and certification frameworks have incorporated visual comfort into their core performance criteria.

European standard EN 17037 "Daylight in Buildings" The European Standard EN 17037 explicitly addresses visual comfort through its assessment criteria for (i) Indoor daylight provision, (ii) View out, (iii) Exposure to sunlight, and (iv) Protection from glare [Brembilla et al., 2021].

WELL Building Standard The WELL Building Standard, it is a performance-based certification system developed by the International WELL Building Institute (IWBI) and promotes human health and well-being within buildings [International WELL Building Institute, n.d.b]. The approach includes ten core concepts, with each having specific health goal (see Figure 2.1). Each of these concepts include a series of features, from which some are preconditions, mandatory for certifications, and others are optimizations, optional pathways to collect points. Recognizing the importance of light for humans' health and well-being, one of the ten concepts is devoted to light. As stated in International WELL Building Institute [n.d.a], "the WELL Light concept promotes exposure to light and aims to create lighting environments that promote visual, mental, and biological health". The light concept includes nine key features which are listed in Table 2.1. It can be noted that they provide a holistic approach to light treatment in indoor environments. The features are not limited only to daylight but also extend to artificial light. Moreover, there is a close relationship between the features, visual comfort and its

assessment factors as they are described in Section 2.2.1. Table 2.2 lists the correspondence between the visual comfort assessment factors and the relevant light features of the WELL standard.

Figure 2.1.: The ten concepts of the WELL building standard. Source: IWBI

Feature	Description
L01: Light Exposure (precondition)	Provide indoor light exposure through daylight and electric light strategies.
L02: Visual Lighting Design (precondition)	Provide visual comfort and enhance visual acuity for all users through electric lighting.
L03: Circadian Lighting Design	Support circadian and psychological health through indoor daylight exposure and outdoor views.
L04: Electric Light Glare Control	Minimize glare caused by electric light.
L05: Daylight Design Strategies	Provide daylight exposure indoors through design strategies.
L06: Daylight Simulation	Ensure indoor daylight exposure through daylight simulation strategies.
L07: Visual Balance	Create lighting environments that enhance visual comfort.
L08: Electric Light Quality	Enhance visual comfort and minimize flicker for electric light.
L09: Occupant Lighting Control	Provide individuals with access to customizable lighting environments.

Table 2.1.: Key features of WELL's standard light concept [International WELL Building Institute, n.d.a]. L01 and L02 are preconditions while the rest are optimizations.

2.2.2. Basic daylight simulations' principles and units

Daylight simulation refers to the computational modeling of how natural light enters, distributes, and interacts within interior spaces. Different algorithms/methods to perform daylight simulation exist, which are: such as, British Building Research Establishment (BRE) split-flux, ray-tracing, radiosity and photon mapping [Dolníková, 2025; Jan L.M. Hensen and Roberto Lamberts, 2019; Iversen et al., 2013]. Figure 2.2 illustrates all the necessary elements

Visual Comfort Assessment Factor	Relevant WELL v2 Light Feature(s)	Explanation
(i) Amount of light	L01 – Light Exposure	L01 addresses appropriate light exposure.
	L02 – Visual Lighting Design	L02 addresses appropriate illuminances on work planes.
(ii) Uniformity of light	L07 – Visual Balance	L07 targets spatial lighting uniformity and luminance ratio limits.
	L02 – Visual Lighting Design	L02 supports even distribution of light across task areas.
(iii) Quality of light in rendering colors	L08 – Electric Light Quality	L08 ensures high CRI ($\geq$90), low flicker, and consistent spectral output for better color perception and visual comfort.
(iv) Prediction of the risk of glare for occupants	L04 – Electric Light Glare Control	L04 requires shielding, beam angles, and design controls for electric glare.
	L05 – Daylight Design Strategies	L05 promotes daylight integration while managing potential daylight glare through spatial and facade strategies.

Table 2.2.: WELL v2 features related to visual comfort assessment

to perform daylight simulations. Although depending on the goal of the simulations and the calculations to be conducted, not all the elements must be present. The ones that are strictly needed is the geometry, the area of interest, and the sky model.

2.3. RoomPlan API and USD Format

According to Apple Inc. [2022c], RoomPlan is Apple's Application Programming Interface (API) which is capable of generating semantically enriched 3D floor plan of a single room or a building (see Figure 2.3. This is done by utilizing the camera and LiDAR scanner on LiDAR enabled iPhones and iPads. The collected data which are essentially RGB and Depth images are processed by a Machine Learning (ML) enabled pipeline—running as the backbone of RoomPlan—which generates the 3D model of the scanned scene. The 3D model includes the identified architectural components and objects which are present in the room. Finally it exports the data using Universal Scene Description (USD) framework Apple Inc. [2022c]. An example of a generated 3D as it is depicted on the iPhone can be seen in Figure 2.3. The way RoomPlan processes the RGB and Depth images to reconstruct the 3D model of the room is detailed in the following sections.

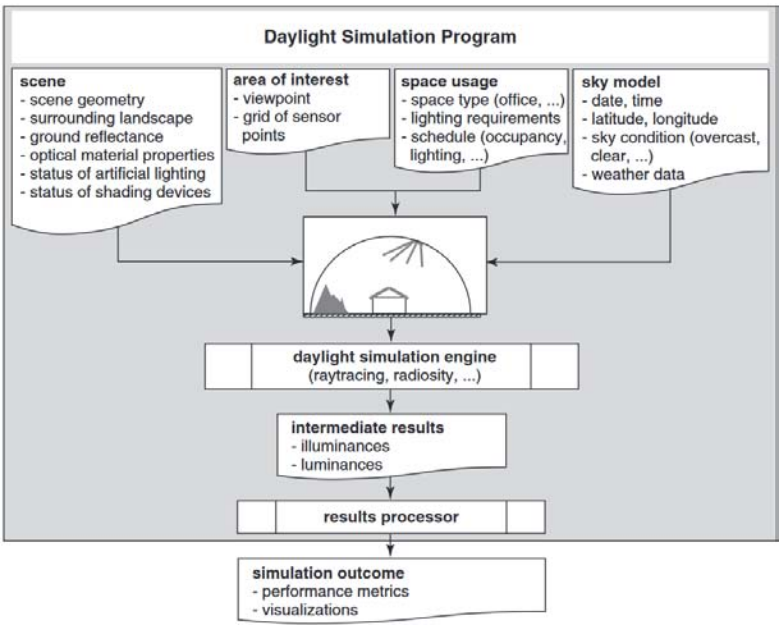

Figure 2.2.: Elements needed for daylight simulations (taken from [Jan L.M. Hensen and Roberto Lamberts, 2019]).

Figure 2.3.: Example of RoomPlan's output as it appears at the end of the scanning process on the iPhone's screen. It depicts the result of the scanning process of an open-plan living room and kitchen, not used in the current project.

2.3.1. 3D scene reconstruction pipeline

According to Apple Inc. [2022a], the reconstruction of the 3D scene by RoomPlan is discretized in two components: (i) 3D room layout estimation; and (ii) 3D object-detection pipeline. The former is responsible for detecting the architectural components of the scanned scene and later for detecting objects. As architectural components are considered the permanent structures of a room while objects are the various objects present in a room. All the different types of identifiable structures and objects are listed in Table 2.3 [Apple Inc., 2022a].

Architectural components	Objects	
walls	bathtub	bed
doors	chair	dishwasher
windows	fireplace	oven
openings	refrigerator	sink
	sofa	stairs
	storage	stove
	table	television
	toilet	washer / dryer

Table 2.3.: Different structures and objects types identifiable by RoomPlan.

3D Room Layout Estimation

As reported in Apple Inc. [2022a], the pipeline for the 3D Room Layout Estimation consists of two neural network-enabled components each responsible for a different task (see Figure 2.4). Both components use as input semantically enriched point clouds of the scene, but it is not clear how the point clouds get labeled.

To detect the walls and the openings (Figure 2.4a), the point cloud is being projected into a semantic map (image) of size $H \times W \times K$ where H, W, and K are image length, width, and number of semantic classes respectively. In addition, the points are mapped into $H \times W \times Z$ voxel space, where Z is the number of slices along the gravity direction. Specifically, H, W, and Z are set to 512, 512, and 12 respectively, allowing to support room with a maximum size of 15 meters by 15 meters and maximum height of up to 3.6 meters. Then, an end-to-end line-detection network takes as input the concatenation of the semantic map and the Z-slicing to perform 2D room layout estimation. Finally, the estimated corners and edges are optimized and lifted into 3D based on the estimated wall height by using post-processing algorithms [Apple Inc., 2022a].

The detection of doors and windows is formulated as a 2D detection problem(Figure 2.4b) by projecting the wall information into wall planes. For each wall from the walls and openings detection component a projection map is generated. Each projection map consists of a) a semantic map, b) an RGB map, and c) a point-distance map. The semantic map is created by the orthographic projection of the points onto the wall's surface which results in a map of size $H \times W \times K$ where $K = 10$ for performance purposes. The RGB map is a $H \times W \times 3$ vector which is created after applying the same projection method to the point cloud. The point-distance map $H \times W \times 1$ vector which encodes the normalized distance between between points and nearby walls. The projection maps are passed to the "2D Orthographic Detection"

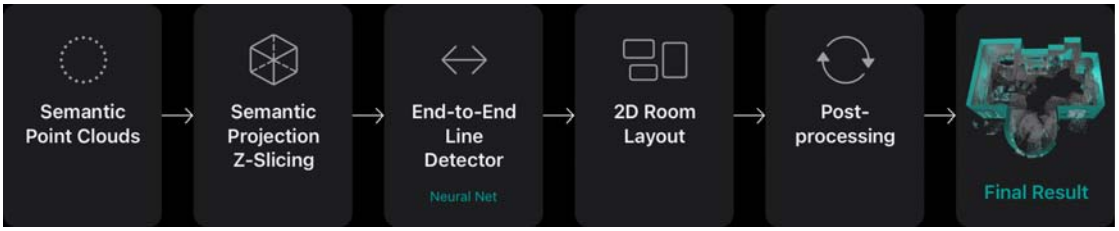

(a) Component to detect walls and openings.

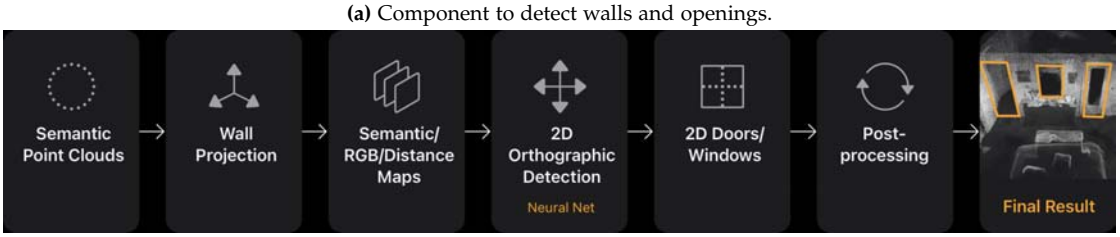

(b) Component to detect doors and windows.

Figure 2.4.: RoomPlan's 3D room layout estimation pipeline components. Source: Apple Inc., *3D Parametric Room Representation with RoomPlan*, https://machinelearning.apple.com/research/roomplan

neural network which predicts the location of the doors and windows in 2D planes. Finally the predicted doors and windows are lifted into 3D by utilizing the wall and camera pose information [Apple Inc., 2022a].

3D Object Detection

The pipeline for 3D Object Detection (3DOD) consists of a local detector, a global detector, and a fusion algorithm, each responsible for different tasks (see Figure 2.5). It detects objects that belong to on of the categories listed in Table 2.3. In addition, to an assigned category, each object gets a set of attributes which describes the object. For instance, a chair has:(i) a ChairType; (ii) a ChairArmType; (iii) a ChairLegType; and (iv) ChairBackType.

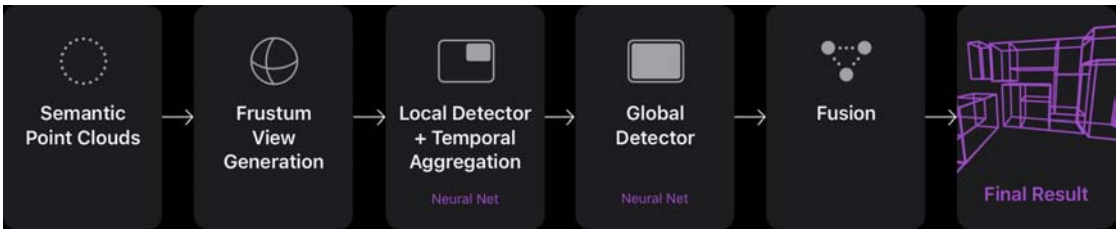

Figure 2.5.: RoomPlan's 3D objects detection component. Source: Apple Inc., *3D Parametric Room Representation with RoomPlan*, https://machinelearning.apple.com/research/roomplan

The local detection pipeline begins by accumulating semantic point clouds into a wide frustum view which is fed into the local 3DOD network. This network predicts oriented bounding boxes of room-defining elements during online scanning. The detected boxes are aggregated, tracked over time, and presented to the user during the scan. The input frustum is set to $7.2 \times 4.8 \times 3.6$ meters with a voxel resolution of 15 cm, resulting in a $48 \times 32 \times 24$ voxel grid.

Each voxel carries a 35-dimensional feature vector combining xyz coordinates, normalized height, and semantic features. A 3D Convolutional U-Net backbone processes the input and outputs predictions for objectness, center, type, size, and orientation, using a total of $2 + 3 + 2H + 4S + N$ channels, where $N = 16$, $H = 12$, and $S = 16$.

After the scanning session, a global detector refines detection by using the full reconstructed scene instead of a limited frustum. The global model focuses on larger objects such as storage units, beds, sofas, and tables, using fewer object categories ($N = S = 4$). This allows the network to leverage broader scene context that might be unavailable during online scanning.

Finally, both local and global detections are merged in a fusion pipeline. This pipeline adjusts bounding boxes based on the surrounding wall geometry obtained from Room Layout Estimation and ensures logical placement, such as preventing boxes from intersecting walls. The fusion step also handles object relationships, for example, by aligning multiple sofa segments to form an L-shaped configuration [Apple Inc., 2022a].

2.3.2. RoomPlan's Output

As mentioned in the introduction of the current chapter, RoomPlan uses USD framework to store the reconstructed 3D models. In addition, it offers three (3) export options to store the data, namely: (i) Parametric; (ii) Mesh; and (iii) Model (see Figure 2.6)[Apple Inc., 2022b]. It can be observed that there are significant differences between the geometries of the architectural components and the objects across the three options.

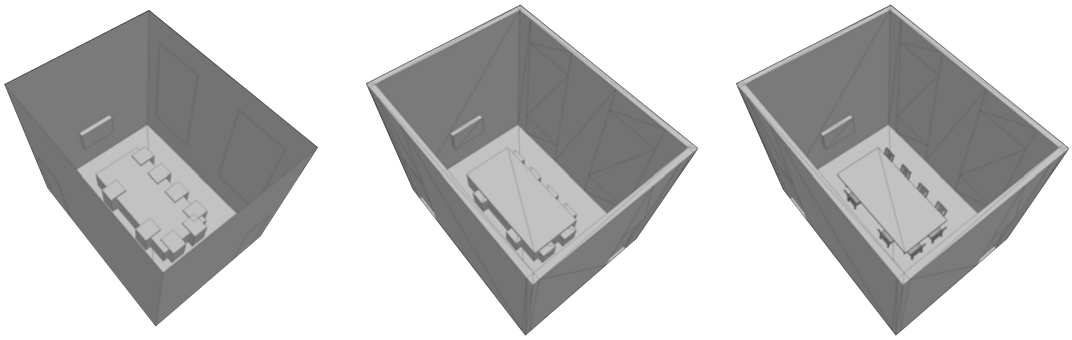

(a) Parametric option. It represents architectural components as planar surfaces and furniture as bounding boxes.

(b) Mesh option. It represents architectural components as volumes and furniture as bounding boxes. All the geometries are triangulated meshes.

(c) Model option. It represents architectural components as volumes and bounding boxes are replaces by furniture meshes.

Figure 2.6.: Visualization of the three different geometrical representations of Room BGW640 as exported from RoomPlan API.

Regarding the difference of the architectural components, the parametric option represents them as planar surfaces. In contrast, the Mesh and the Model option represent them as triangulated meshes which have width. Moreover, in the Mesh and the Model option, the windows, doors, and other openings cut out of wall geometry.

With respect to the differences of the objects' representation, the Parametric (Figure 2.6a) and the Mesh (Figure 2.6b) option represent the objects as bounding boxes. On the other hand, in

the Model option (Figure 2.6c) the bounding boxes have been replaces by 3D mesh models. This is option provided by RoomPlan, that based on the object's attributes, such as the example with the chair in Section 2.3.1, the bounding boxes gets replaced by a 3D mesh from a model library which can be customized. The characteristics of the export options are summarized in Table 2.4

		Export option		
	Representation	Parametric	Mesh	Model
Architectural components	Planar	✓		
	Volume		✓	✓
Objects	Bounding boxes	✓	✓	
	Models			✓

Table 2.4.: Representation of architectural components and objects in the different export options. Architectural components can be represented as either planar surfaces or volumes and objects as bounding boxes or 3D mesh models.

2.3.3. USD

USD is an open source framework developed by Pixar Animation Studios for the robust interchange and collaborative editing of 3D scene data. It facilitates a standardized way to integrate 3D geometry, shading, lighting, and physics into a scene Pixar Animation Studios [2021]. Apple's RoomPlan API leverages USD to export room scans in the .usdz format which contains 3D geometry, textures, and metadata [Pixar Animation Studios, 2021; Apple Inc., 2022a].

USD data structure

USD files have a hierarchical structure and allows for expressing complex and flexible relationships between asset data via composition Apple Inc. [2023]. The USDZ file exported from RoomPlan is a compressed file which contains a 'master' USDA file which describes the scene and refers to other USDA files which describe each individual asset (e.g., a wall, a chair). A non-exhausting example of the directory tree after the extraction the of a .usdz file can be seen in Figure 2.7.

By composing all the assets together, someone can reconstruct the whole scene. The API has the capability to export the scene in three different geometrical representations of the captured scene as depicted in Figure 2.6. The difference stems from the way the geometries are defined, but the semantic information is the same across the different models.

The file has a hierarchical structure and contains all the three different geometrical representations of the captured scene organized in different groups, namely the *Parametric_grp*, the *Mesh_grp* and the *Model_grp* (Figure 2.8). In all three groups, the objects are stored in the same three sub-groups:

1. *Arch_grp* which stores the architectural components (i.e., walls, doors, windows).
2. *Floor_grp* which stores the floor.
3. *Object_grp* which store the objects of the scene (e.g., chairs, table, television).

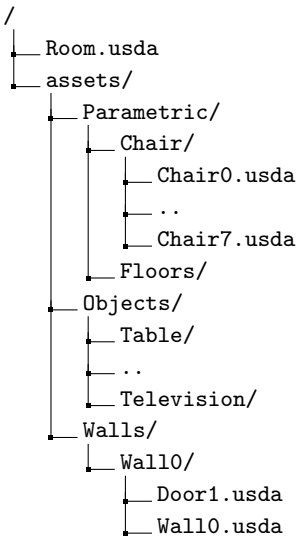

Figure 2.7.: USD Directory Structure

(a) Hierarchical structure of *Parametric_grp*.

(b) Hierarchical structure of *Mesh_grp*.

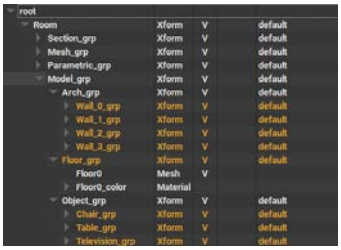

(c) Hierarchical structure of *Model_grp*.

Figure 2.8.: Hierarchical structure of USDZ file exported from RoomPlan corresponding to room BGW640 as visualized in usdview. It contains all the three different representations of the captured room, namely the Parametric model (Parametric_grp), the Mesh model (Mesh_grp) and the Mesh model with furniture (Model_grp). All the groups organize the objects in the same way.

Despite the different geometrical representations the same semantic information (e.g., which object is a chair or which door belong to which wall) is implicitly described and maintained across the geometric groups by the grouping of the objects (Figure 2.9). For instance, it is known that *'Door1'* belongs to *'Wall0'* because they both belong in *'Wall_0_grp'* group. Regarding the geometrical representation it can be seen in Figure 2.9 that *'Door1'* and *'Wall0'* are defined as Cubes in the *Parametric_grp* (Figure 2.9a) and as Meshes in *Mesh_grp* (Figure 2.9b) and *Model_grp* (Figure 2.9c). In any of the three cases, the objects are defined parametrically. Thiss mean that either a primitive (in this case a Cube) or a Mesh is transformed using a transformation matrix in order to be placed with correct size and orientation in the scene. By reconstructing all the objects in the same fashion, someone can reconstruct the whole scene.

It can be noted that the API's output do not include the ceilings of the scanned rooms. To tackle this issue, since a closed volume is needed for indoor daylight simulations, the ceiling is generated automatically based on the walls of the structure. The reconstruction of the geometries to bu used in the simulations is described in Section 3.2.

(a) Hierarchical structure of *Parametric_grp*.

(b) Hierarchical structure of *Mesh_grp*.

(c) Hierarchical structure of *Model_grp*.

Figure 2.9.: Implicit description of relations between different components of the scene.

3. Methodology

This research follows a comparative experimental case study approach. This is based on comparing the geometric accuracy and corresponding dayligth simulation results of 3D models from RoomPlan API to 3D models manually reconstructed using data from TLS. Figure 3.1 illustrates an overview of the methodology which is described in the following sections.

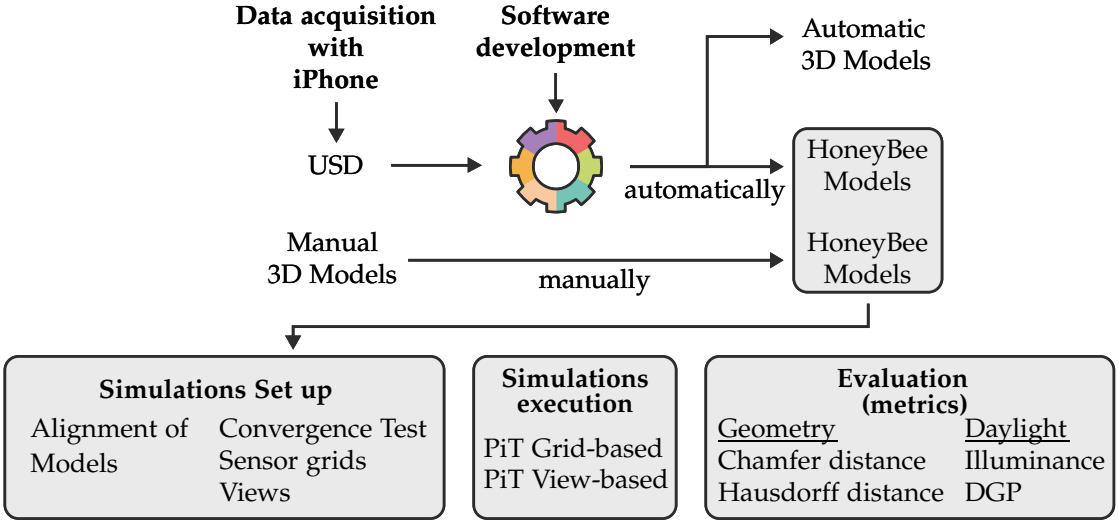

Figure 3.1.: Methodology overview. The colorful gear represents the steps for transformation of USDZ to HBJSON.

3.1. Datasets

3.1.1. Case selection

Three rooms in the TU Delft's Architecture (Bowkunde (BK)) building were selected as case studies. These rooms were selected based on their different size, shape and complexity in terms of structure and presence of objects. The characteristics of the room are listed in Table 3.1.

As documented in Table 3.1 and Figure 2.6, room BGW 640 is the simplest of the selected cases. Regarding the architectural components, it has 4 walls (shoebox shape), 2 windows on one of the walls and 2 doors on 2 different walls. Object-wise, during the scanning process there was 1 long table and 10 chairs. In addition to these, there were 2 televisions (1 attached to the wall, 1 on rack), a flipboard stand and a plant pot. Room W01050 (see Figure 3.4 is

slightly more complicated due to its L-shape (6 walls). It has 1 window and 2 doors on 2 different walls. Similarly to BGW640 there is a long table, 5 chairs and a television on a rack. The last room, GeoinfoLab is the most complicated (see Figure 3.3). It has a rectangular foot print but the ceiling has 2 different horizontal levels. Therefore, the walls are not rectangular (see Figure 3.3a. Furthermore, it has multiple working desks and chairs, 2 storage cabinets, a sofa, a fridge, a dining table, and 2 plant pots. On the ceilings of all of the rooms there are ceiling-mounted light fixtures, while the pipes for heating and the ventilation system are visible.

The different levels of complexity allow for solid assessment of the capabilities of the RoomPlan API in capturing different rooms. In addition, it provides different cases to handle during the development of the software. The selected rooms represent lots of working spaces where daylight evaluation may be relevant.

Room	Plan shape	Doors	Windows
W01050	L-shaped	2	1
BGW640	Rectangular	2	2
GeoinfoLab	Rectangular with uneven ceiling	2	9

Table 3.1.: Characteristics of the case study rooms.

(a) **(b)**

(c) **(d)**

Figure 3.2.: Photos of the meeting room BGW640.

(a) (b)

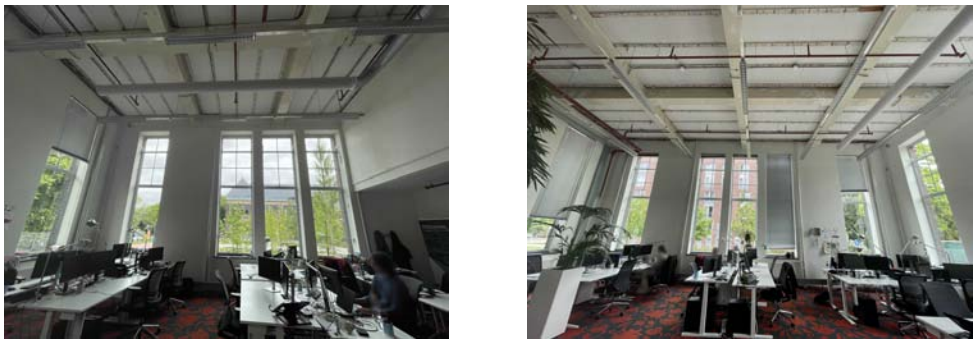

(c) (d)

Figure 3.3.: Photos of the office room GeoinfoLab

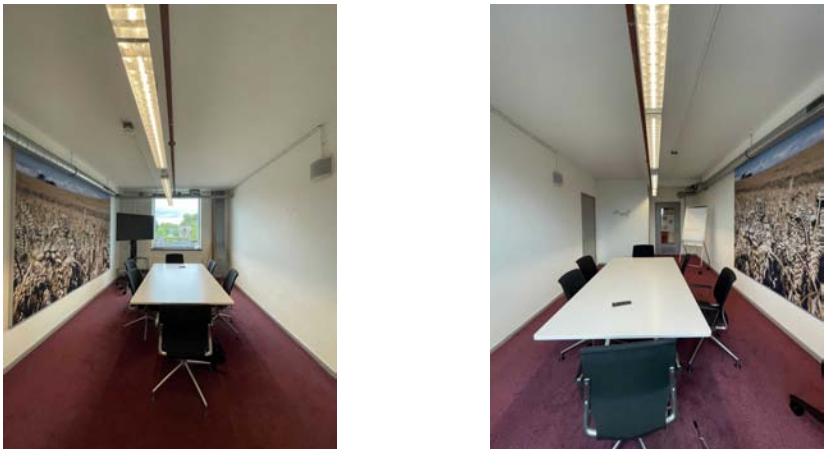

(a) (b)

Figure 3.4.: Photos of the meeting room W01050.

3.1.2. Data acquisition

Manual models

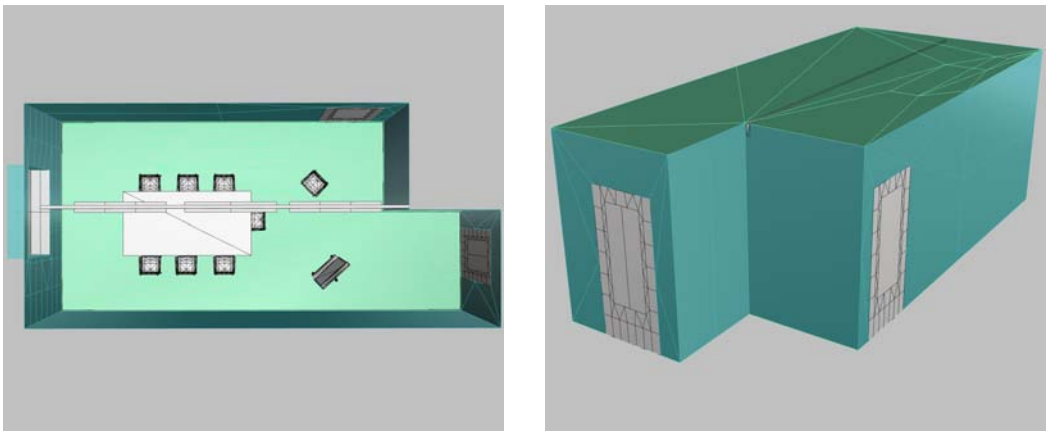

(a) Top-down view. **(b)** Perspective view of the exterior.

Figure 3.5.: Manual model of Room W01050.

Manual 3D models were created in Rhinoceros 3D software based on point clouds acquired by TLS Leica P40 and manual modeling techniques, ensuring high-fidelity representations to serve as ground truth. To minimize the occlusions multiple scans were performed for each room which were registered before reconstructing the geometries on top of the complete point cloud. Note that the generation of the manual models was not part of the current project. The models are visualized in Fig. 3.5, Fig.3.6, and Fig. 3.7.

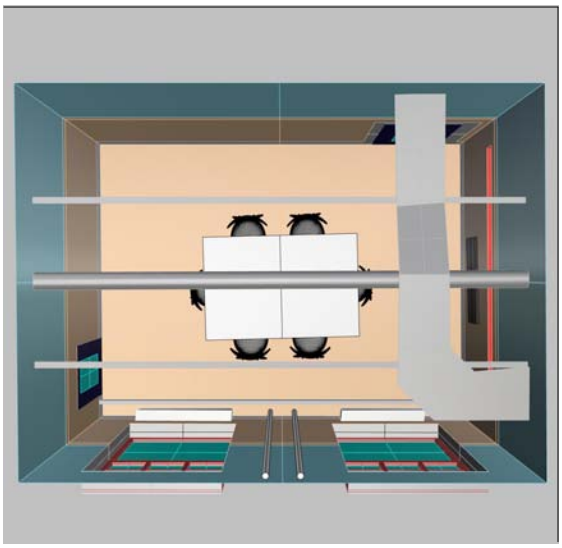

(a) Top-down view.

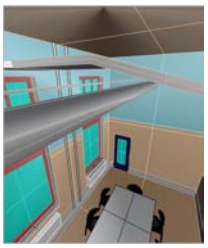

(b) Interior detail view of the the ventilation system.

(c) View of the interior.

(d) View of the interior.

Figure 3.6.: Manual 3D model of Room BGW640.

(a) Top-down view.

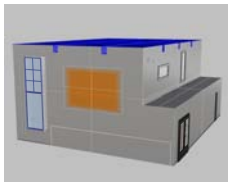

(b) Perspective view of the exterior.

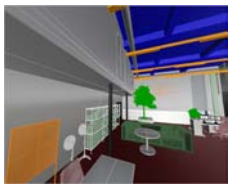

(c) Detail view of the interior.

(d) Detail view of the interior.

Figure 3.7.: Manual 3D model of GeoinfoLab.

Automatic models

Each one of the selected rooms was captured using the RoomPlan API on an iPhone 12 Pro equipped with a LiDAR sensor. The API was utilized, using the sample code provided by Apple [Apple Inc., 2025a]. To replace the furniture bounding boxes with 3D models of furniture, the sample code and the sample catalog of 3D assets were used [Apple Inc., 2025b]. Figure 3.9 illustrates the data captured as they are imported and visualized in Blender software in USD format. The figure shows the differences that three export options RoomPlan has. A visualization of those options from different points of view is presented in Appendix B.

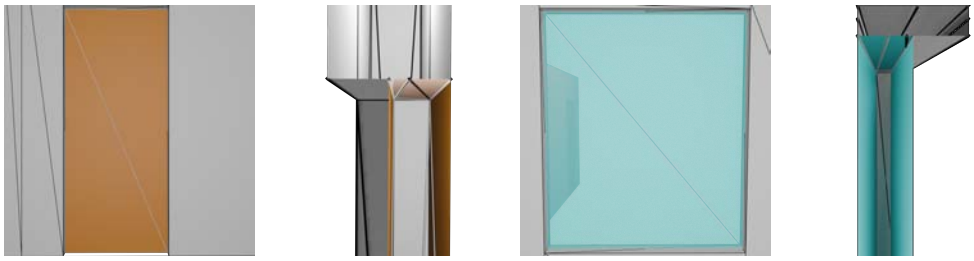

(a) Front view of the door. **(b)** Side section detail of the top part of the door and how it connects to the wall. **(c)** Front view of the window. **(d)** Side section detail of the top part of the window and how it connects to the wall.

Figure 3.8.: Detailed views of the wall (gray), the door (orange) and the window (blue) of Room W01050. The black wireframe belongs to the wall and the white one to the individual objects.

It is prominent that the models do not have a ceiling. This is due to how RoomPlan works and is known from RoomPlan's documentation. The automatic reconstruction of the ceiling is of main focus in the development of the software to ensure watertightness. In addition, all the architectural components (i.e., walls, floors, doors and windows) and the furniture (e.g., table, chairs, television) have the same material. The Parametric is the simplest representation of all, in which the architectural components are planar surfaces. It should be noted that the walls do not have holes for the doors and the windows. Moreover, the furniture are represented as bounding boxes, same as in the Mesh option. In contrast to the Parametric option, the Mesh and the Model options represent the architectural components as volumes (i.e., the walls, the floor, the doors and the windows have thickness which is arbitrary). Another significant difference between the Parametric and the other two options is that the parametric does not store architectural components with not canonical shapes. For instance, in the case of GeoinfoLab room which has two ceiling in different heights connected with a vertical wall, it can be noticed that the Parametric version of the model does not carry this information, while the Mesh and the Model options do (see Figures 3.9g - 3.9i). This difference is also considered during the development of the software. Moreover, the walls do have holes for the windows and the doors (see Figure 3.8).

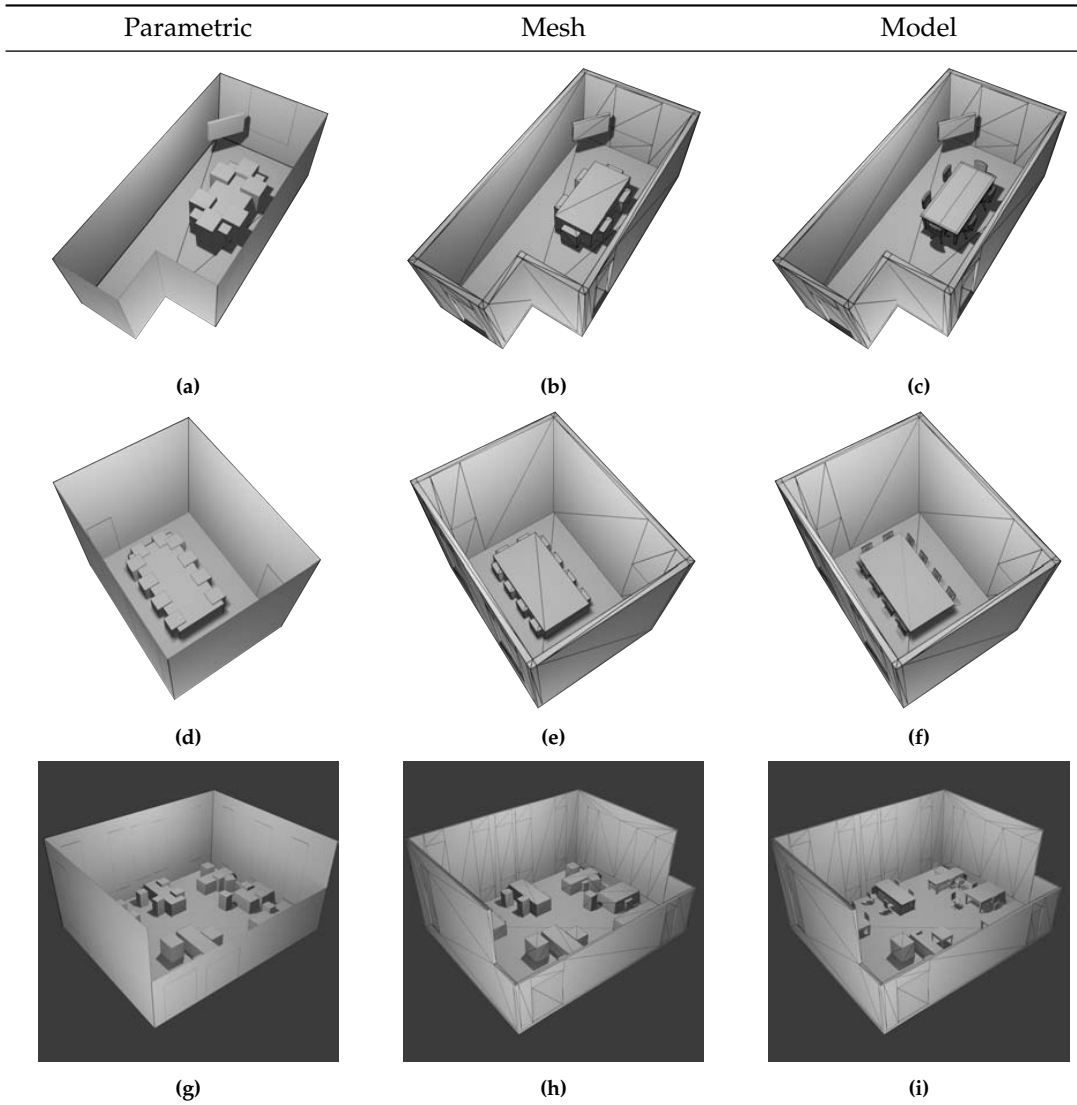

Figure 3.9.: RoomPlan's output in USD format of the 3 models. The models in the three rows correspond to Room W01050, BGW 640 and GeoinfoLab. In the three columns the different output settings of RoomPlan are visualized, namely: Parametric, Mesh and Model. The models are visualized in Blender Open Source 3D Creation Software.

3.2. Simulation ready geometry - From USD to HoneyBee

The scope of the current project is to develop a tool that can be used by practitioners who need to perform daylight simulations seamlessly, and minimize the time of manual modeling and data processing. This is done by first reading the USDZ files and then converting them into Honeybee JSON format (.hbjson), which will be later used for daylight simulations. This section describes the proposed approach for converting between the two formats as well as how this is implemented. The developed software is developed in Python. At the core of the software, the OpenUSD, Trimesh and HoneyBee APIs were utilized.

3.2.1. Solution Strategy

As discussed in Section 3.1.2, the different export options from the RoomPlan API store different information (see Figure 3.9). To capture the highest level of detail, it is chosen to use the Model export option (see Figures 3.9g - 3.9i) - not only for the architectural components but also for the furniture.

The main pursuit of the software was to be able to create a watertight multi-surface mesh to represent the room. To achieve that, 3D models are represented as solids, as defined by ISO19107. This allows for easier conversion of the geometries to HoneyBee models utilizing HoneyBee's Python API and future development to integrate the software with the Ladybug ecosystem. Therefore, the shell of the room should be represented as a set of surfaces without holes or cavities, as illustrated in Figures 3.10 and 3.11. In the case of windows, the software offers the option to create either windows that are coplanar with the walls, as well as windows that are extruded as illustrated in Figure 3.12. To achieve that, one approach would be to keep the interior faces of the walls, doors and windows, and create the ceiling. However, this is not possible due to the nature of the models.

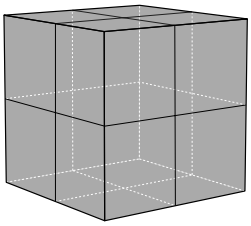

Figure 3.10.: Example of a cube-shaped room without windows or doors. Each side of the cube is a different entity, which is how HoneyBee expects the geometries. This allows for assigning different materials to each surface.

The following sections focus on the description of the input data and the challenges that need to be addressed in order to create models that have the required characteristics as described.

Characteristics of the input data, challenges and solution approach

First of all, each object in the model (e.g., wall, chair) is represented as a separate mesh. Next, within each mesh, its vertices are duplicated according to the number of faces that reference them. For example, to represent a solid rectangular object (such as a window), the model

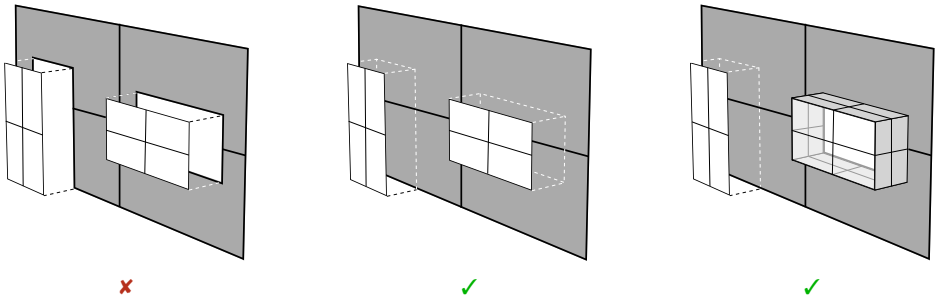

Figure 3.11.: Examples of different ways to represent a wall with one door and one window. Based on HoneyBee's requirements the variations in the middle and on the right will be used in the current project.

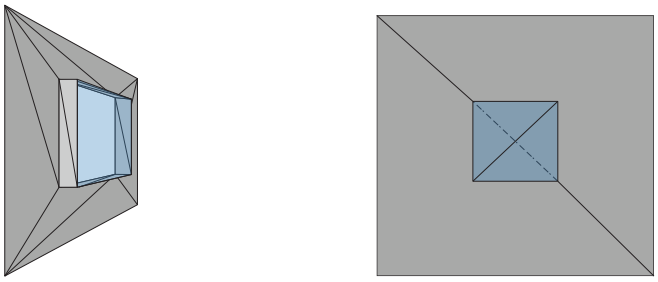

Figure 3.12.: Illustration of a wall with an extruded window. The mesh is a multisurface.

contains 24 vertices instead of 8, meaning that each of the six faces is defined by its own set of four unique vertices. To verify this conclusion, the same files were opened in Blender.

As illustrated in Figures 3.13 and 3.14, the floor geometry extends to the outer boundary of the walls. However, the floor and walls are not topologically connected, in the sense that there are no vertices on the floor mesh that correspond to the vertices of the interior part of the wall meshes.

Given the characteristics of the models that were extracted from the RoomPlan API, the following **challenges** need to be addressed:

1. Isolation of the interior faces of the walls.
2. Creation of faces without holes or cavities.
3. Creation of the floor and the ceiling.

Isolation of the interior faces of the walls. This would be trivial if all the floor surface of the rooms were all convex (see Figure 3.15). This is because for instance, it would be possible to choose all the faces that face the center of the room, which could be computed by using the extent of the 3D model. Since it is common for rooms have concave floor plans as reflected in one of the rooms, i.e., Room W01050, a different approach was designed, which is described in Section 3.2.2.

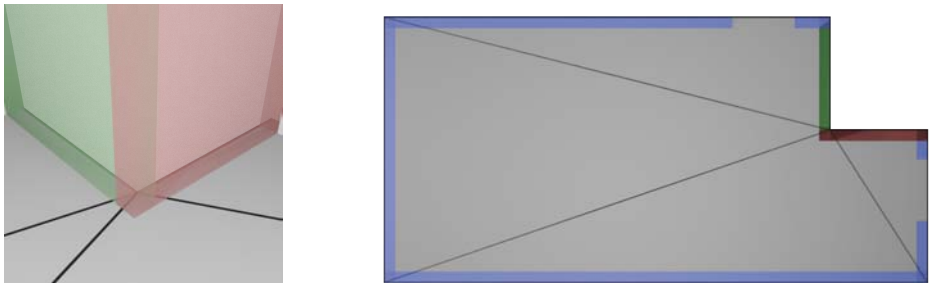

(a) Detail of how the walls connects with the floor.

(b) Top-down floor plan view of the room.

Figure 3.13.: Connection of the walls to the floor. The specific example is from Room W01050. The floor is in gray overlapped with its wireframe. The walls are colored in blue while the the red and green walls are the same as in Figure 3.14.

(a) Top-down view.

(b) Perspective view.

Figure 3.14.: Overlapping walls of Room W01050.

Creation of faces without holes or cavities. Since the walls in the model output option from RoomPlan API have holes and cavities for the windows and the door, it is necessary to remove them and obtain meshes as the ones illustrated in Figure 3.16. To resolve this problem, the meshes of the door and the windows are used.

Creation of the floor and the ceiling. As illustrated in Figure 3.13, the floor includes the exterior sides of the walls. This observation leads to the third challenge to create a surface for the floor. The approach for this issue was to use the bottom vertices of the walls to define the boundary of the floor. The same approach was followed to create the ceiling, but in this case

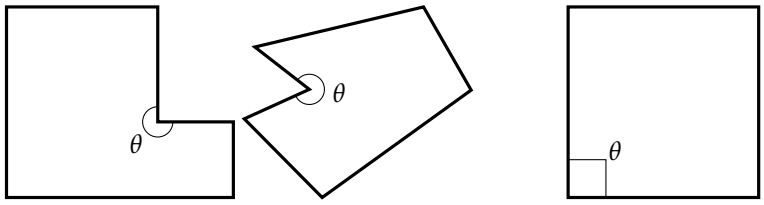

(a) Concave shapes.

(b) Convex shape

Figure 3.15.: Examples of convex and concave shapes. Concave shapes have at least one interior angle θ that is $180^\circ < \theta < 360^\circ$.

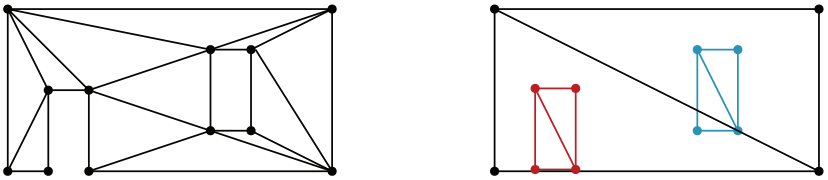

Figure 3.16.: Triangulation of planar surfaces, which represent a wall with one door and one window. Left: the surface has one hole for the door and another for the window. Right: each component (wall, door, window) is a different surface, where the wall overlaps with both the door and the window.

the top vertices of the walls were used. In the edge case of GeoinfoLab, in which the ceiling contains two different surfaces at different heights, an adjusted approach was used.

To achieve watertightness, the entire model is constructed with the walls as the geometric reference from which the floor and ceiling are derived as it is described in the following subsections.

3.2.2. Extraction of wall's boundaries

Isolating interior faces

The chosen approach simplifies the problem by projecting the 3D interior faces to 2D. This is done by utilizing a raster map, which encodes the interior and exterior areas of the model in question. An example of such a raster map and how it is created is illustrated in Figure 3.17. Having this map allows for labeling the faces as interior or exterior by utilizing the centroids of the faces.

Raster map

The steps to create the raster map are the following:

1. Voxelize the 3D model using only the vertical faces.

2. Create a the 2D raster within the extends of the bounding box and label all the cells with the same value (0).

3. Project the voxel grid on the raster map and label the corresponding cells with a different value (1).

4. Finally, label the interior cells by using flood fill with a third value (2).

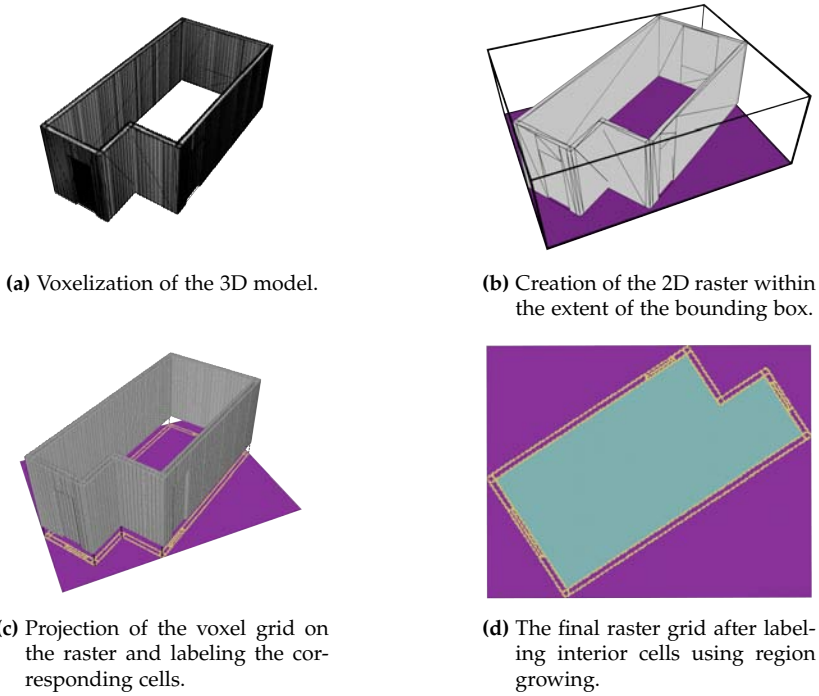

(a) Voxelization of the 3D model.

(b) Creation of the 2D raster within the extent of the bounding box.

(c) Projection of the voxel grid on the raster and labeling the corresponding cells.

(d) The final raster grid after labeling interior cells using region growing.

Figure 3.17.: Creation of the raster map. The purple cells illustrate the exterior, yellow the walls and blue the interior.

Labeling the faces

Having this raster map allows for identification of interior and exterior faces. This is achieved by utilizing the centroid and the normal of each face (see Figure 3.18).

More precisely:

1. The centroid of each face is shifted along the normal of the face by twice the raster cell size and the new 3D position is translated to the index of a 2D cell on the raster map. This can be done because the normals of the meshes are consistently oriented and point outwards.
2. The new position is projected on the raster and the value of the corresponding cell is retrieved. If the label of the cell is 'interior', then the face is considered to belong to the interior of the room and and is kept for the next steps (see Figure 3.18a). The opposite holds for the faces whose centroid when shifted lays on a raster cell labeled as 'exterior'.

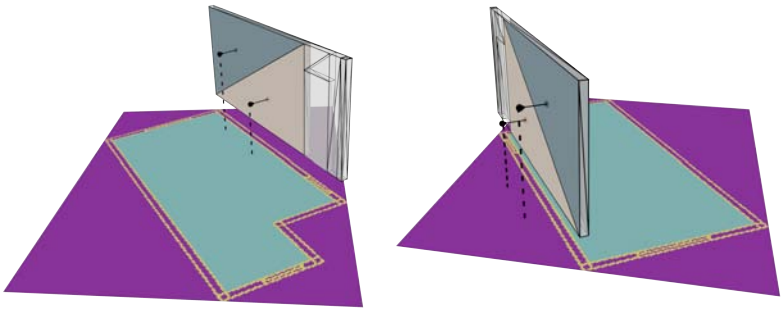

(a) Interior faces. **(b)** Exterior faces.

Figure 3.18.: Labeling interior and exterior faces by utilizing the raster map. For each wall face, the centroid is computed and shifted along the normal of the face. The new position is then projected onto the 2D raster, and the value of the corresponding pixel is checked (interior or exterior).

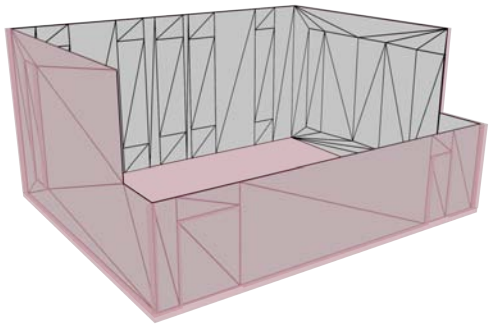

Figure 3.19.: Interior faces of GeoinfoLab model in gray with black wireframe. In transparent red are the initial meshes before the isolation of the interior.

Treating cavities and holes

After completing the previous steps, the interior faces of the architectural components are isolated, as illustrated in Figure 3.19. The next objective is to convert those components (see Figure 3.20a) into suitable surfaces to use in Honeybee (see Figure 3.20b). To explain the steps, the wall in Figure 3.21 is used as an example. The steps are the following:

1. For each wall, its mesh gets merged into a single mesh with each child entity (i.e., doors and/or windows). Due to the way Trimesh works and the functions it provides when the meshes are merged, they are simply concatenated. This means that they remain separate entities.

2. Starting from the merged mesh, its 3D outline is extracted. The outline of a mesh is defined as every edge which is only included by a single triangle (see Figure 3.22a, Figure 3.24).

3. The outline is projected into 2D, as shown in Figure 3.22, to create a raster map. Another example of the raster map of the side wall of GeoinfoLab is depicted in Figure 3.23.

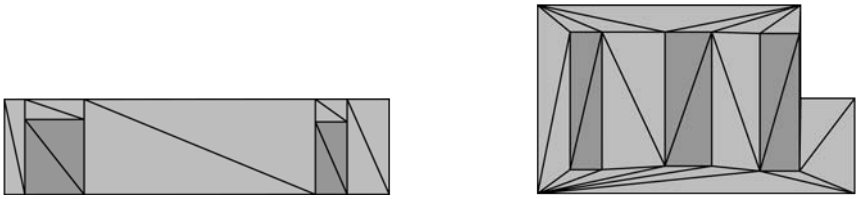

(a) Initial triangulation of the walls.

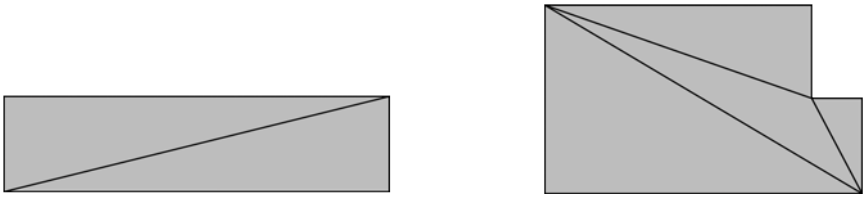

(b) Triangulation of the walls after removing the cavities for the doors and the holes for the windows.

Figure 3.20.: Interior faces of two walls with doors (left) and windows (right).

4. As illustrated in Figure 3.24, the outline is then projected and the segments which belong to the boundary are kept.

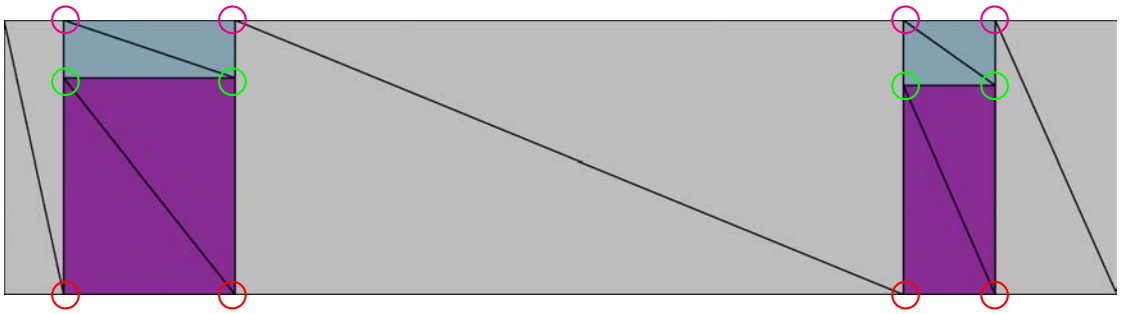

Figure 3.21.: Mesh of the entrance wall of GeoinfoLab with two doors. The different circles highlight different vertices. The doors do not share any vertices with the rest of the faces, consequently the vertices in red and green are duplicated. In addition, it must be noticed that the vertices in green are not present in the faces colored in gray. The vertices in magenta are shared between the blue and the gray faces.

(a) Initial 2D outline of the mesh.

(b) Initial raster map after burning the outline in white.

(c) The raster map after labeling the exterior cells in green.

(d) Binary mask of the exterior around the wall.

(e) Binary mask after dilating the exterior using a 3×3 kernel.

(f) Exterior boundary of the wall in yellow. This is extracted by intersecting the outline (b) and the dilated mask (e).

(g) Final raster map with exterior, interior, boundary and outline.

Figure 3.22.: Steps of the rasterization of the 2D outline of GeoinfoLab's entrance wall and labeling of the cells; in purple is the default value, in white are the outlines, in green is the exterior and in yellow is the exterior boundary.

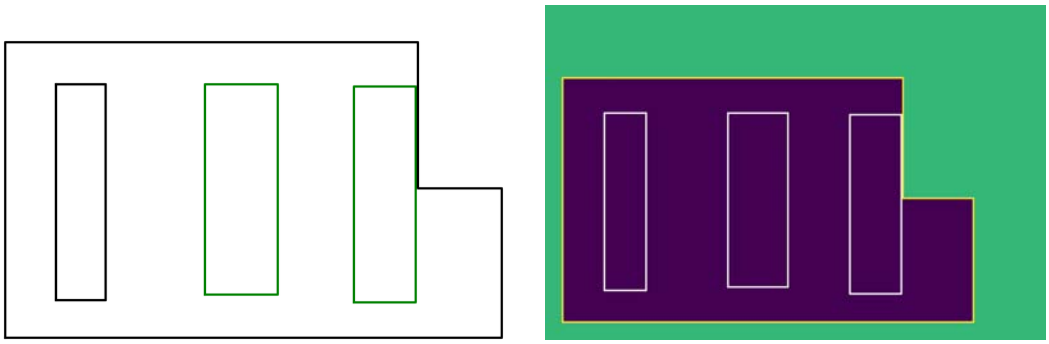

(a) Initial 2D outline of the mesh.

(b) Final raster map with exterior, interior, boundary and outline.

Figure 3.23.: Steps of the rasterization of the 2D outline of GeoinfoLab's side wall and labeling of the cells; in purple is the default value, in white are the outlines, in green is the exterior and in yellow is the exterior boundary.

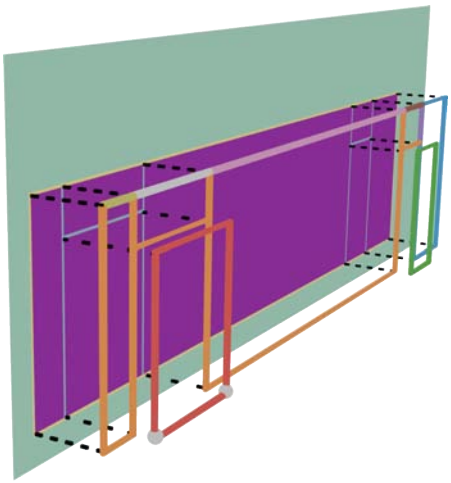

Figure 3.24.: Projection of the 3D outline onto the 2D raster map (Figure 3.22g). Each path of the outline has different color as shown in Figure 3.22a. Each path is divided in segments. For instance, one segment of the red path (door) is between the two vertices (in gray). Each segment is projected individually onto the raster. The rule to consider a segment as part of the outline is that the whole segment intersects with cells labeled as boundary. In that way, Segments that have their start and/or end vertex on the boundary, but do not lie entirely on the boundary, are discarded.

3.2.3. Creation of missing geometries

Window frames

In order to add extruded window frames in the model the steps which are visualized in Figure 3.25 are followed.

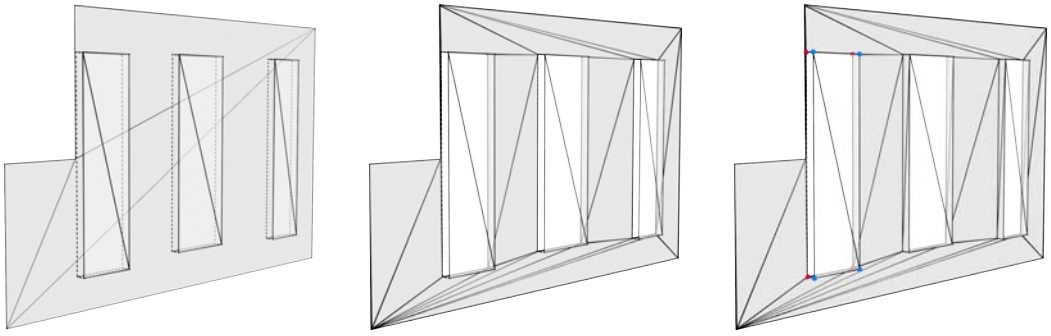

(a) The windows surface and the initial state of the wall without holes.

(b) Triangulation of the wall after creating holes using the windows.

(c) The vertices of the holes (red) and the windows (blue) are used to create the window faces.

Figure 3.25.: Creation of the window reveal.

Ceiling and floor

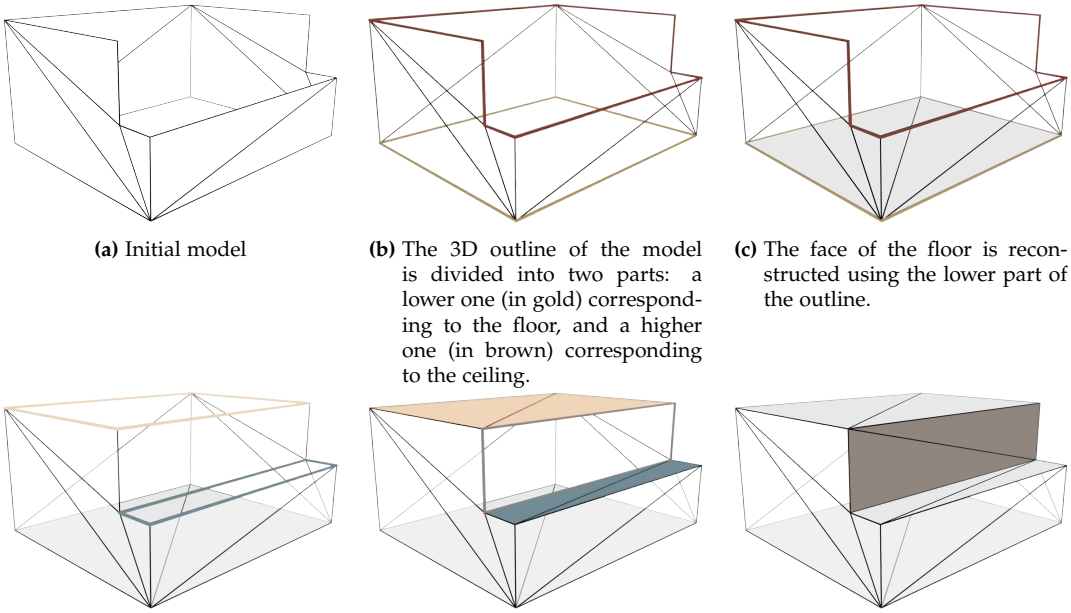

(a) Initial model

(b) The 3D outline of the model is divided into two parts: a lower one (in gold) corresponding to the floor, and a higher one (in brown) corresponding to the ceiling.

(c) The face of the floor is reconstructed using the lower part of the outline.

(d) The higher part of the outline can be divided into two subparts (in beige and teal), each of which has vertices at the same height.

(e) Reconstruction of the two surfaces. The updated outline of the model is the ring in gray.

(f) Reconstruction of the last surface of the model's ceiling.

Figure 3.26.: Reconstruction of the model's floor and ceiling using the 3D outline of the model.

3.3. Software architecture

3.4. Workflow – Experimental set-up

This section describes the individual steps to prepare the experimental set-up. These steps include:

1. Creation of the HoneyBee models for:
   a) the Automatic models.
   b) the Roomplan models.
2. Alignment of the HoneyBee models.
3. Set up of the sensor grids and the views.
4. Convergence test.

In contrast to the HoneyBee models for the manual 3D models which are created manually in Grasshopper, the HoneyBee models for the models captured using the iPhone are generated automatically from the developed software. Having the HoneyBee models for all the rooms, setting up the models includes (1) the alignment of the models so that they have the same relative orientation with respect to the North, (2) setting up the sensor grids and the

views, (3) a convergence test to choose Radiance parameters, and (4) performing the daylight simulations.

3.4.1. Data processing

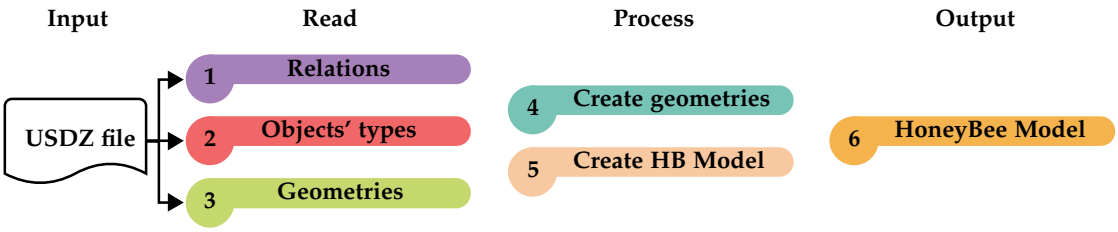

Figure 3.27.: Data processing overview

Following the acquisition of the data using the RoomPlan API, the datasets need to be converted to HBJSON (see Figure 3.27). HBJSON is Honeybee (HB)'s JSON-based model schema used for daylight and energy simulation and describes building geometry, simulation settings, and environmental conditions for the simulations [Ladybug Tools, 2024]. The conversion is performed by the developed software (for details see Section 3.2). The software, reads the output of the RoomPlan API (USDZ files) (i.e., relations, objects' types and geometries), keeps the interior faces, reconstruct the missing geometries the and creates a HBJSON.

3.4.2. Daylight simulations

(a) Honeybee logo.

(b) Grasshopper logo.

(c) Rhinoceros 3D logo.

Figure 3.28.: Tools used for the daylight simulations.

The daylight simulations were performed using the Honeybee plugin in Grasshopper for Rhino (Figure 3.28). Using the developed tool, the RoomPlan scans were converted to HB models. For the manually reconstructed models, the HB models were created manually in Grasshopper. The HB models for both the manual and RoomPlan models are illustrated in Figures 3.29 - 3.31.

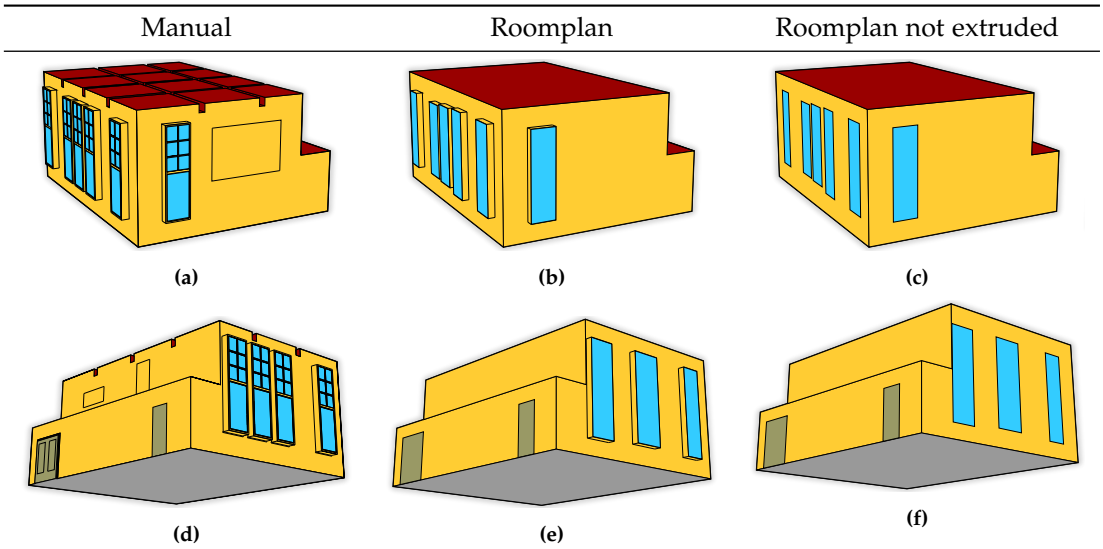

Figure 3.29.: HoneyBee Models of GeoinfoLab.

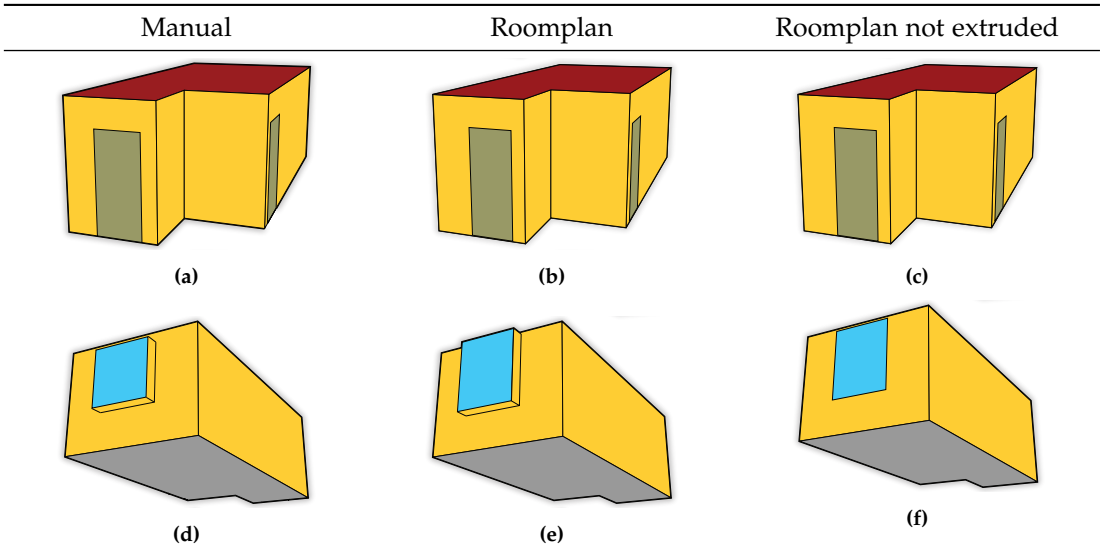

Figure 3.30.: HoneyBee Models of Room W01050.

Manual	Roomplan	Roomplan not extruded
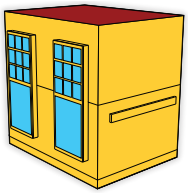 (a)	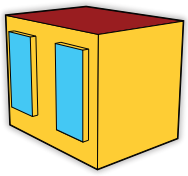 (b)	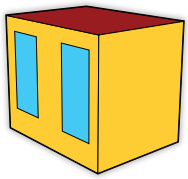 (c)
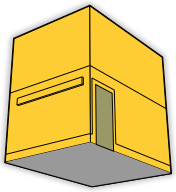 (d)	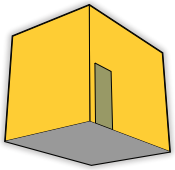 (e)	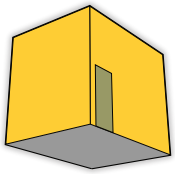 (f)

Figure 3.31.: HoneyBee Models of Room BGW640.

Alignment of models

Since the automatically and manually generated models use different reference systems, they are manually aligned in Rhinoceros 3D. The alignment process considers only their relative alignment and does not reflect their true orientation with respect to the north. The orientation of each model is visualized in Figure 3.32. The alignment is performed to ensure that the two models have the same relative orientation for the daylight simulations.

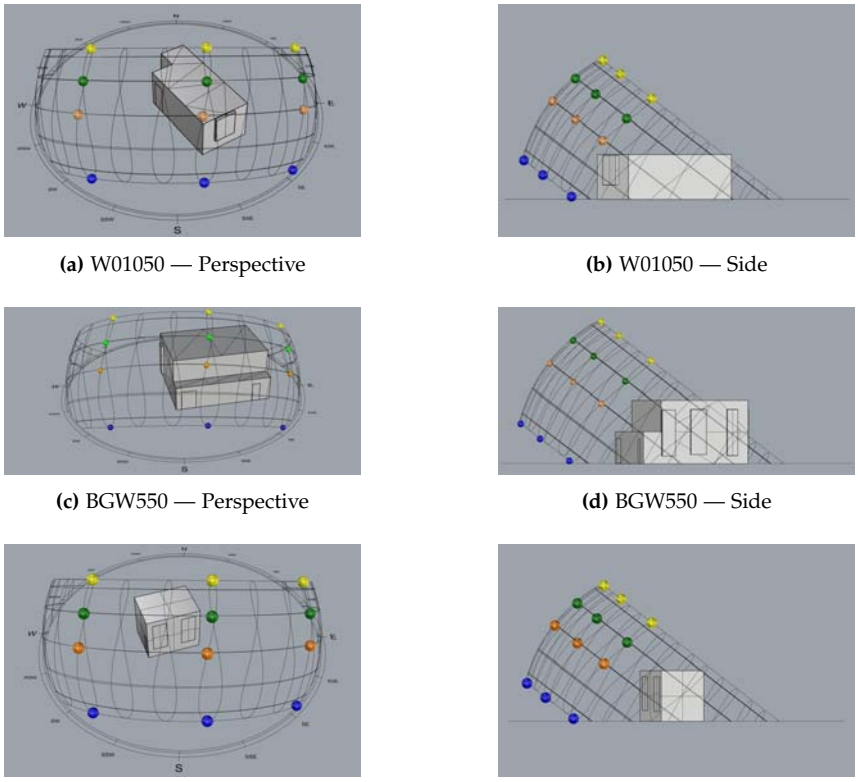

(a) W01050 — Perspective

(b) W01050 — Side

(c) BGW550 — Perspective

(d) BGW550 — Side

(e) BGW640 — Perspective

(f) BGW640 — Side

Figure 3.32.: The sun path relative to Rooms W01050, BGW550, and BGW640 is shown for four days at three time steps (9 AM, 12 PM, and 3 PM). The yellow, green, orange, and blue spheres represent the sun position during the summer solstice, spring equinox, autumn equinox, and winter solstice, respectively.

Sensor grid set up

Following the alignment of the models, a rectangular sensor grid of size 0.5 meters was generated based on the automatically generated model. The vertical position of the grid was set to 0.8 meters above the floor. Using the same grid allows for easier comparison of the results. The position of the sensors relatively to the models is illustrated in Figure 3.33.

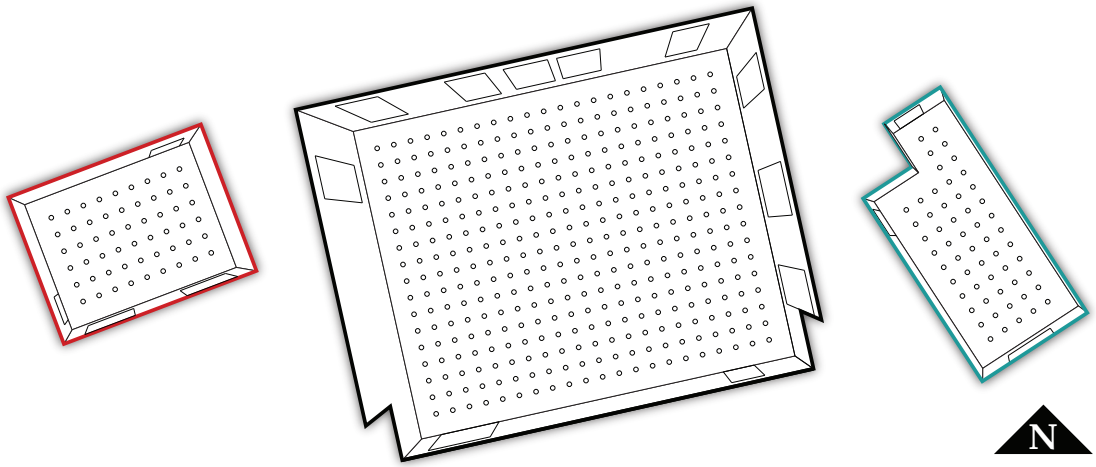

Figure 3.33.: The sensor grids used in the simulations. From the left to the right, the red room is **BGW640**, the black room is **BGW550**, and the one in blue is room **W01050**. The three grids have the same characteristics, i.e., the sensors are arranged on a rectangular grid 0.5 $\times$ 0.5 meters, 0.8 meters from the floor and 0.5 meters offset from the walls.

Convergence test

Since Radiance uses a stochastic sampling approach, the results might not always be the same between different runs of the simulation. For this reason, a convergence test must be conducted. Although Radiance has in total 18 parameters, only 5 of them directly affect the results and the accuracy, which are: (i) ambient divisions (ad); (ii) ambient super-samples (as); (iii) ambient resolution (ar); (iv) ambient accuracy (aa); and (v) ambient bounces (ab) [Kharvari, 2020; Radiance]. The goal of the convergence test is to choose the values for these parameters that stabilize the results across different runs. The test is performed by running multiple iterations of the simulation and tweaking the parameters until the difference of the results from different runs are within a range of $\pm 5\%$.

Initially, the parameters are set to `-ab 1 -aa 0.4 -ar 8 -ad 32 -as 16`. These values give the least accurate results, but in significantly less time. The optimization of the parameters is performed starting from the `ad` and `as` which are related. Once the results converge, these values are kept constant and `ar` is optimized. In the same fashion, the `aa` and finally the `ab` are optimized. The values tested for the parameters are listed in Table 3.2.

Room W01050 was selected for the convergence test because it is the darkest room among the 3 cases. The test was conducted by testing the convergence of the illuminance results. The illuminance was measured at a virtual sensor which was placed as far away as possible from the window. Using a single sensor instead of a grid accelerates the execution of the test. In some cases, it was noticed that even with the same parameters there is a high variance of the results. For this reason it was regarded as beneficial to perform five (5) times the test for each set of parameters settings. This decision was made to evaluate both the accuracy and the precision of the simulations. One fruitful parallelism to explain the difference between accuracy and precision is visualized in Figure 3.35. In illuminance simulations precision would refer to getting similar results and accuracy getting results as close to reality as possible.

	Parameters				
	ad	**as**	**ar**	**aa**	**ab**
Set 1	32	16	8	0.4	1
Set 2	64	32			
Set 3	128	64			
Set 4	256	128			
Set 5	512	256			
Set 6	1024	512			
Set 7	2048	1024			
Set 8	**4096**	**2048**	16		
Set 9			32		
Set 10			64		
Set 11			128		
Set 12			**32**	0.2	
Set 13				0.1	
Set 14				0.05	
Set 15				**0.2**	2
Set 16					3
Set 17					**4**
Set 18					5
Set 19					

Table 3.2.: The sets of Radiance parameters used in the convergence test. The values in bold font are the ones chosen (Set 18).

Table C.1 documents the illuminance results for each set of parameters along the five runs. Figures 3.36 - 3.38, illustrate the results of. In Figure 3.36 one can notice the exact reason why it was necessary to execute multiple runs with the same settings. Sets 1 - 7 give results that vary significantly. For instance, with 'Set 1' while four out of five runs result in 0 lux, one results in 88. The convergence starts to occur after 'Set 8', in terms of precision, meaning that the results with the same settings are getting closer with $CV < 12\%$. A potentially good set of parameters could be Set 13 which has $CV = 1.02\%$ and the difference of the average illuminance is less than 5%. Nevertheless, while testing the next sets of parameters there is a great increase in the resulting illuminance which is tripled compared to the results so far. For this reason, the selected set of parameters is 'Set 18' which has $CV = 1.33\%$ and the average difference with the next set if less than 5%, which is the objective.

To verify that the chosen set of parameters is sufficient, an additional test was conducted. Using the parameters which according to the documentation of Radiance give the most accurate results and the parameters chosen from the convergence test, 5 rounds of simulation for the whole sensor grid (56 sensors) were performed. For each sensor and set of parameters the average illuminance was computed. Following that, the percentage difference for each sensor was computed as well as the average percentage difference which is 2% These results can be found in Table C.2.

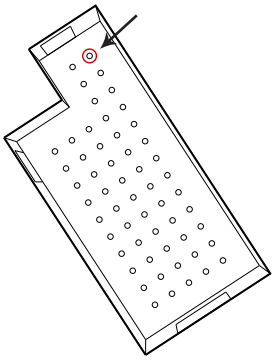

Figure 3.34.: Sensor grid of Room W01050. The sensor in the red circle is used for the convergence test.

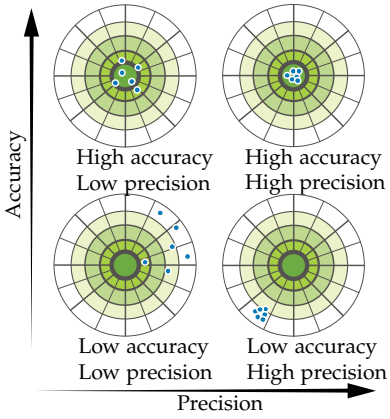

Figure 3.35.: The concept of accuracy versus precision. Adapted from Egon Willighagen, licensed under CC0, via Wikimedia Commons.

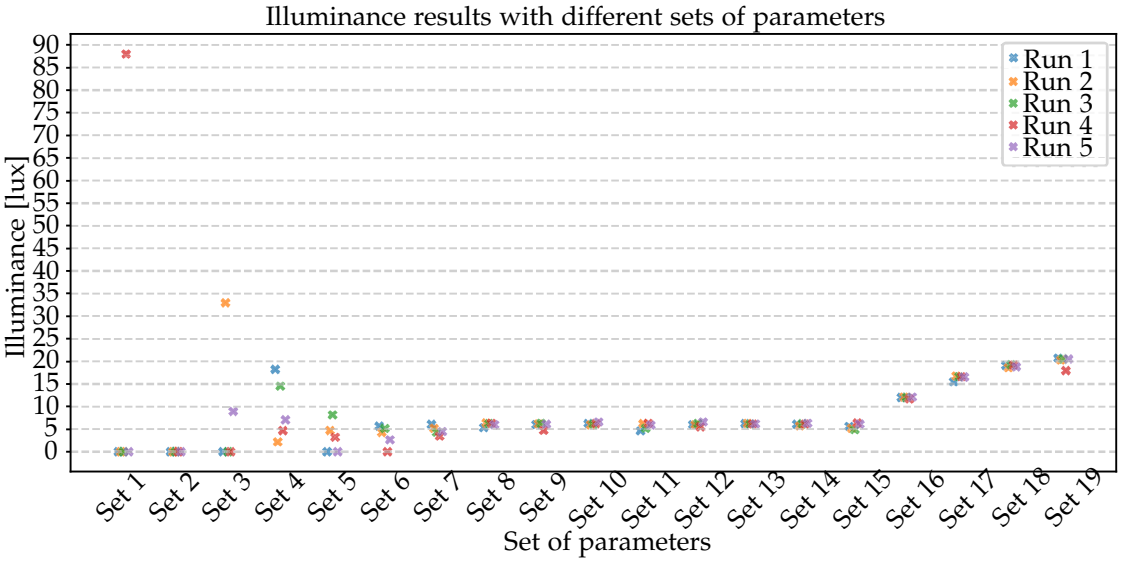

Figure 3.36.: Illuminance results for the 5 runs for each set of parameters. The different 'X's denote the illuminance for the 5 runs for each set. The illuminance values are listed in Table C.1 The five marks for each parameter set are shifted horizontally for better readability.

.

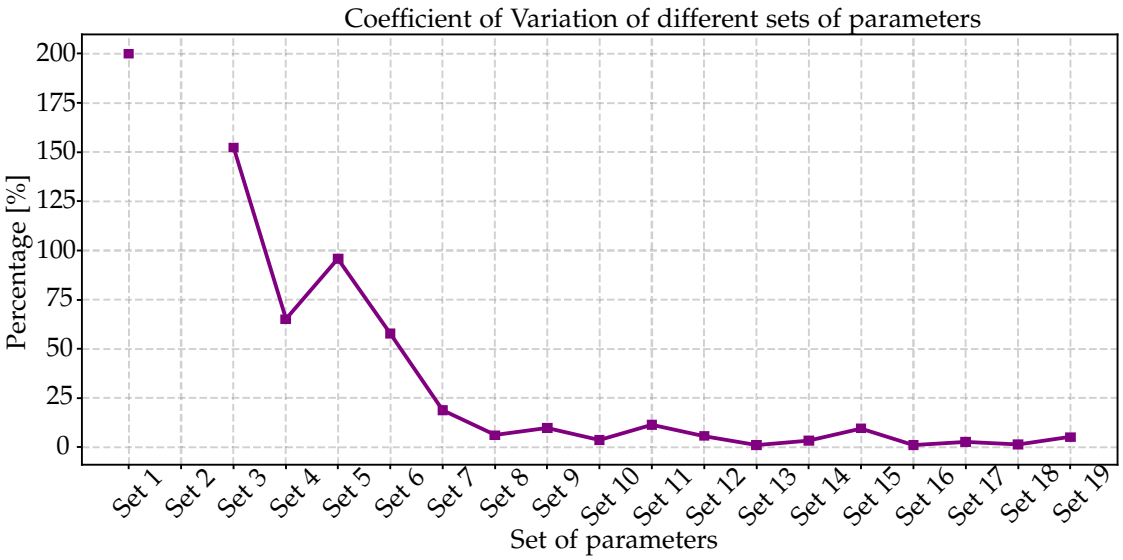

Figure 3.37.: Coefficient of variation of illuminance. The formula is $CV = \frac{\sigma}{\mu} \times 100\%$ For the 2nd Set the Coefficient can not be defined, since all the runs resulted in 0 illuminance (see Table C.1).

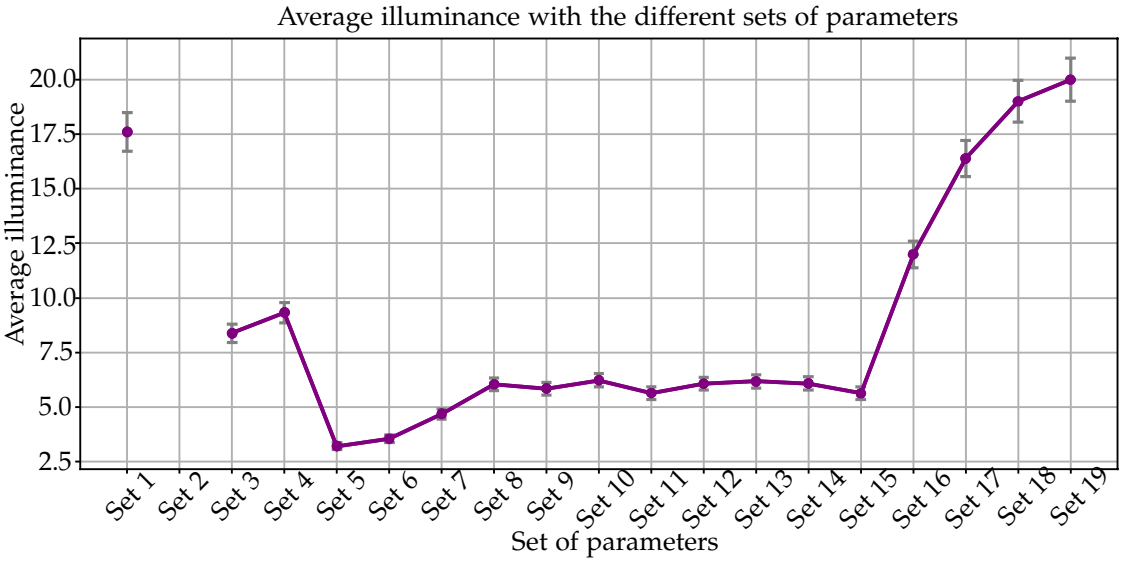

Figure 3.38.: Average illuminance for the different sets of parameters. The error bars denote ±5%.

3.5. Evaluation

This section describes the evaluation of the automatically reconstructed technique which consists of geometric accuracy of the RoomPlan models as well as on how these models perform in daylight simulations compared to the ground truth.

3.5.1. Geometric Comparison

To assess the geometric accuracy of the reconstructed models, two complementary distance metrics were evaluated: the Chamfer distance and the Hausdorff distance. These metrics are used to compare similarity between point clouds. To use them for mesh comparison, 50000 points are uniformly sampled from the meshes.

Given two point sets A and B, the *Chamfer distance(d_C)* is defined as the average of the sum of the squared distance between each point of A and its nearest neighbor in B and vice versa. It is formulated as:

$$d_{\mathrm{CD}}(A,B) = \frac{1}{2} \times \left[\frac{1}{|A|} \sum_{a \in A} \min_{b \in B} \|a-b\|_2^2 \; + \; \frac{1}{|B|} \sum_{b \in B} \min_{a \in A} \|b-a\|_2^2 \right] \tag{3.1}$$

Given two point sets A and B, the *Hausdorff distance (d_H)* is defined as the maximum distance between any pair of nearest neighbors between A and B:

$$d_{\mathrm{H}}(A,B) = \max \left\{ \max_{a \in A} \min_{b \in B} \|a-b\|_2, \; \max_{b \in B} \min_{a \in A} \|b-a\|_2 \right\} \tag{3.2}$$

The Chamfer distance captures the average surface deviation between the meshes, whereas the Hausdorff distance reflects the maximum local discrepancy. In other words, Chamfer describes how close the shapes are on average, while Hausdorff measures the largest deviation occurring anywhere between them.

3.5.2. Daylight Comparison

In this study two types of daylight simulation results are produced: (i) illuminance (lux) heatmaps for the point-in-time grid-based simulations and (ii) luminance (cd/m^2) HDR images which are used to compute DGP. Illuminance quantifies the amount of luminous flux incident on a surface and is commonly used to assess daylight availability at specific locations (e.g., sensors), whereas luminance describes the light emitted or reflected by surfaces in a given direction and is directly related to visual perception and glare. DGP describes the fraction of the occupants of a room or building who are disturbed by glare, ranges from 0 to 1, and is categorized into four classes (see Table 3.3). These types of simulations are commonly performed in practice to evaluate daylight availability as well as occupant perception. To evaluate the results of the simulations, the MAE and the MAPE of the illuminance are computed, as well as the Root Mean Squared Error (RMSE) of the DGP.

$$\mathrm{MAE} = \frac{1}{N} \sum_{i=1}^{N} \left| E_i^{\mathrm{roomplan}} - E_i^{\mathrm{manual}} \right| \qquad \mathrm{MAPE} \; = \frac{100}{N} \sum_{i=1}^{N} \left| \frac{E_i^{\mathrm{roomplan}} - E_i^{\mathrm{manual}}}{E_i^{\mathrm{manual}}} \right|$$

where E_i is the illuminance on sensor i.

$$\text{RMSE} = \sqrt{\frac{1}{N}\sum_{i=1}^{N}\left(\text{DGP}_i^{\text{manual}} - \text{DGP}_i^{\text{roomplan}}\right)^2}$$, where i are the timesteps.

Category	Value
Imperceptible Glare	DGP $<$ 0.35
Perceptible Glare	0.35 $<=$ DGP $<$ 0.4
Disturbing Glare	0.4 $<=$ DGP $<$ 0.45
Intolerable Glare	0.45 $<=$ DGP

Table 3.3.: Daylight Glare Probability Categories

4. Results

4.1. Geometric assessment

The Chamfer and Hausdorff distances are calculated between the Manual and RoomPlan meshes (M–R), the Manual and Not-extruded meshes (M–N), and the RoomPlan and Not-extruded meshes (R–N). Those distances are summarized in Table 4.1 for each of the three Rooms (BGW640, W01050, and GeoInfoLab).

The R-N distances are computed to get a notion of how the results are affected by well-known differences in the models being compared which, in the current case, are only the absence or presence of the extruded window frames. For this reason, in all cases, the Chamfer distance is low (< 0.01).

In addition, the Hausdorff distance is almost equal to the width of the windows' frames, which is expected. Moreover, in all cases the RoomPlan model with extruded frames shows better results than the version without extruded frames when compared to the manual models, which aligns with the expected trend. The wire frames of the Manual and the Roomlan models are illustrated in Figures 4.1, 4.2, and 4.3.

	BGW640			**W01050**			**GeoInfoLab**		
Distance	M–R	M–N	R–N	M–R	M–N	R–N	M–R	M–N	R–N
Chamfer (m^2)	0.1111	0.1171	0.0049	0.0021	0.004	0.0031	0.0092	0.0172	0.0099
Hausdorff (m)	0.8987	0.8983	0.2695	0.2825	0.3457	0.3456	0.4568	0.4568	0.3435

Table 4.1.: M–R = Manual vs RoomPlan, M–N = Manual vs Not extruded, R–N = RoomPlan vs Not extruded.

BGW640 The models of this room exhibit the largest discrepancy. This is caused because the Roomplan model is ≈ 0.9 m shorter than the ground truth. This difference was measured manually, and the Hausdorff distance captures the same difference.

W01050 This room demonstrates significantly reduced overall discrepancy compared to WBG640. The Hausdorff distance points out the different height of the window. Although it was expected that this room would have the best performance due to its smaller size and simpler characteristics, this is not the case. After examining again the data it was found out that the error is caused due to a mistake in the manually reconstructed model which represents the window smaller than it is in reality.

GeoinfoLab This room shows moderate results with average deviation $\approx 10 - 13$ cm. The higher Hausdorff distance compared to W01005 is explained by the absence of a window in the Roomplan model, which was not captured during the scanning process. This is confirmed by the identical M–R and M–N values.

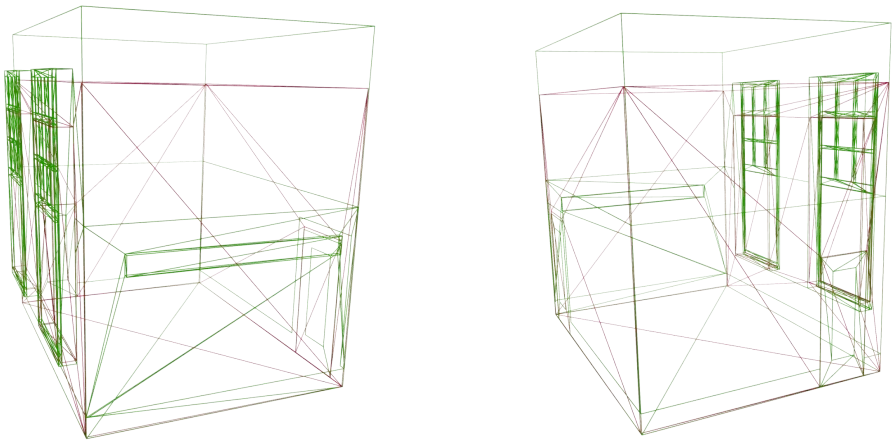

Figure 4.1.: Alignment of 3D models from Manual reconstruction (green) and Roomplan (red) — Room BGW640.

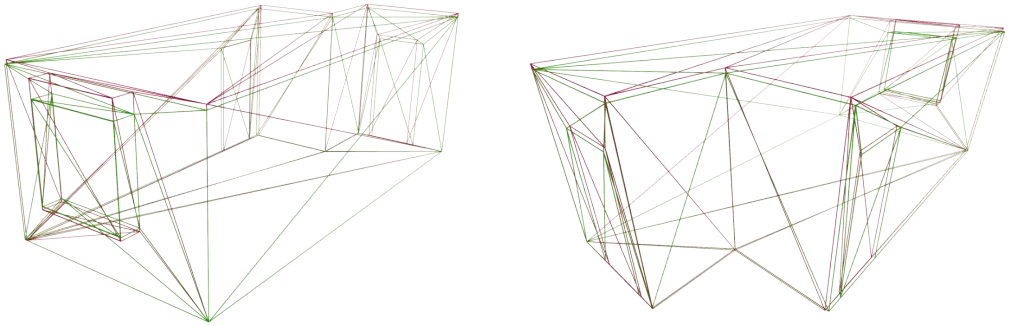

Figure 4.2.: Alignment of 3D models from Manual reconstruction (green) and Roomplan (red) — Room W01050.

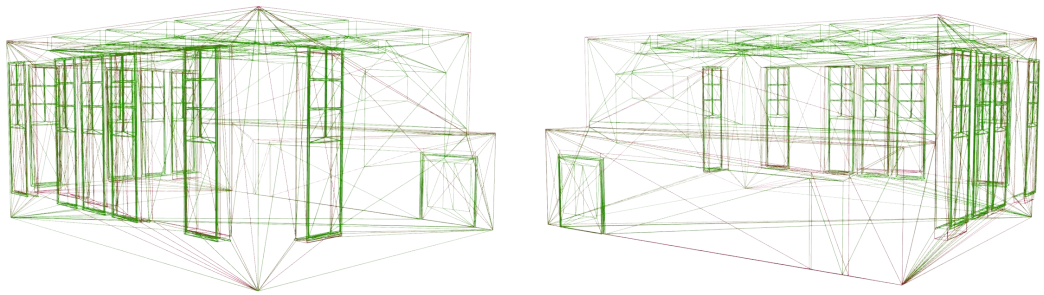

Figure 4.3.: Alignment of 3D models from Manual reconstruction (green) and Roomplan (red) — GeoinfoLab.

4.2. Daylight Simulation results

The results from the daylight simulations are of two types: (1) illuminance heatmaps for the point-in-time Grid-based simulations and (2) HDR images for the point-in-time View-Based. Examples of the results can be found in Figures 4.4, 4.8, and 4.9 for one timestep, while all the results can be found in Appendix E and Appendix D, respectively.

4.2.1. Illuminance maps

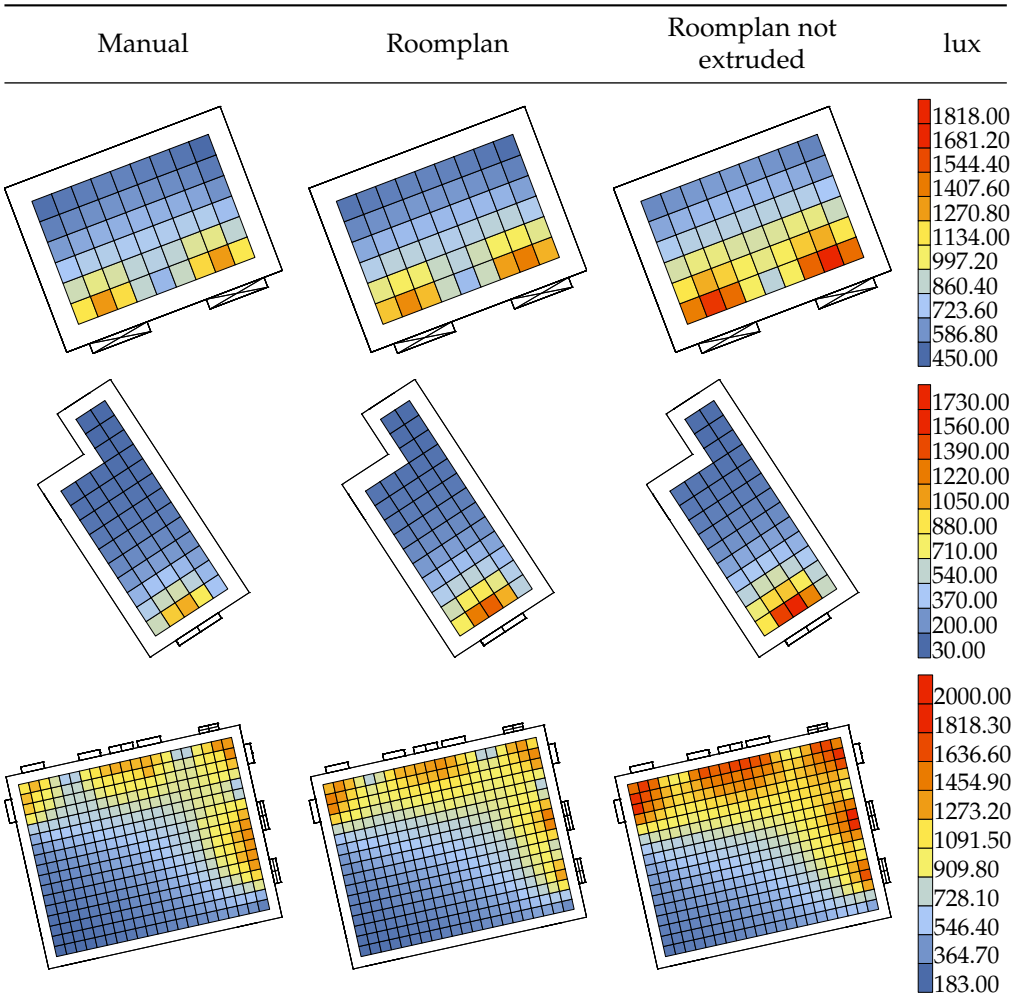

Figure 4.4.: Illuminance heatmaps of the three models on 20 March (Spring Equinox) at 09:00. Each row corresponds to one model (BGW640, W01050, GeoinfoLab). The heatmaps within each row share the same scale.

By observing the heatmaps the most noticeable finding is that Roomplan models without extruded window frames lead to over-prediction of illuminance than the models with extruded

window frames (referred as Roomplan). In Table C.3 the MAE values for each room and timestep are listed. Across all three rooms, Roomplan models have significantly better performance with average MAE of $\approx$ 269 lux along all the time steps, in comparison to not extruded models which have $\approx$ 517 lux, $\approx$ 2 two times more. This can be observed in Figure 4.5, where box of the not extruded model shows a larger spread, indicating lower accuracy. More specifically BGW640 demonstrates the lowest errors with MAE values between 10 and 150 lux excluding the two outliers as shown in Figure 4.6. GeoinfoLab exhibits slightly higher errors in the range of 18 and 200 lux and has only one outlier, while Room W01050 shows the highest variability with a range between 19 and 430 lux. GeoinfoLab has the lowest Average error $\approx$ 161 lux, followed by W01050 with 277 lux and BGW640 with $\approx$ 369 lux.

Except for the MAE also the MAPE was calculated to make results easier to comprehend (see Figure 4.7 and Table C.4). BGW640 exhibits the lowest errors, with RoomPlan achieving average error of 6% across all timesteps and standard deviation of 2.3% indicating good agreement with the manual geometry. GeoinfoLab shows moderate deviations, with average MAPE between 10 and 12% and a single peak at 22%. The W01050 room shows the largest errors, with average MAPE of 42%. For BGW640 and W01050, the highest error occurs on the 21st of June at 12:00. Across all cases, RoomPlan substantially outperforms the not-extruded model, which has 2-5 times higher errors depending on the room. This shows the importance of modeling the window extrusions for daylight applications. However, it was only after the execution of the simulations it was discovered that there is a mistake in the model of Room W01050. In the manual model, the window is smaller than in reality, while in the Roomplan model the window has the correct dimensions. This explains the unexpected illuminance error for this model. Since the more complicated models have significantly better performance, it is expected that also this model will produce more accurate results if it is modeled correctly. Unfortunately, there was no time available to account for this mistake.

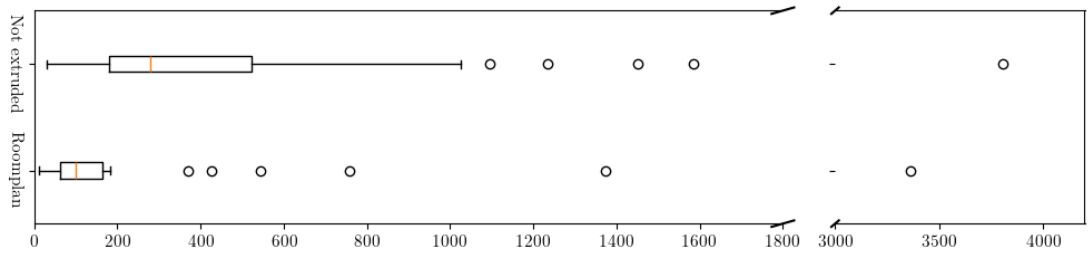

Figure 4.5.: MAE for Roomplan and Roomplan not extruded models

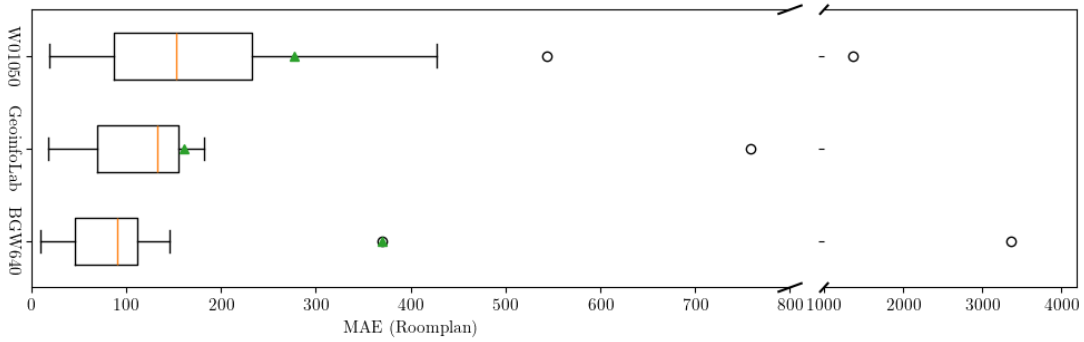

Figure 4.6.: Per room MAE of the illuminance (lux) for Roomplan models. The green triangles indicate the average.

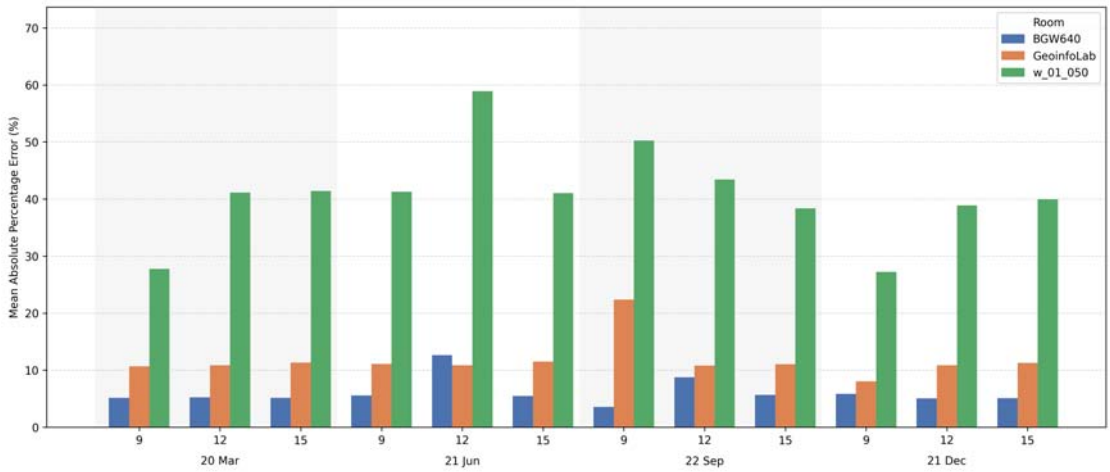

Figure 4.7.: MAPE of illuminance (lux) for the Roomplan models.

4.2.2. HDR renders

To evaluate the impact of geometric accuracy on visual comfort, HDR renderings and Daylight Glare Probability (DGP) values were generated for all three rooms using both the manual and RoomPlan-based models. Some examples of the outputs are illustrated in Figure 4.8 and Figure 4.9 for the 20th of March at 09:00, while the renders for all the timesteps can be found in Appendix D.

Across all three rooms, the DGP results show a very high degree of agreement between the RoomPlan and manual geometries. As it can be also observed visually in the renders the results are very close, almost indistinguishable to the eye. In the majority of the timesteps the difference is bellow 0.01 for RoomPlan and below 0.03 for the not-extruded model. The RMSE values are small with values below 0.001 for Roomplan. BGW640 RoomPlan reproduces the correct glare category in 35 out of 36 cases, with only one borderline classification shift for Room W01050 on September 22nd at 09:00 where the absolute difference between Manual and Roomplan is 0.04. The not-extruded geometries produces two category mismatches, on June 21 at 12:00 for BGW640 and on September 22 at 09:00 for W01050.

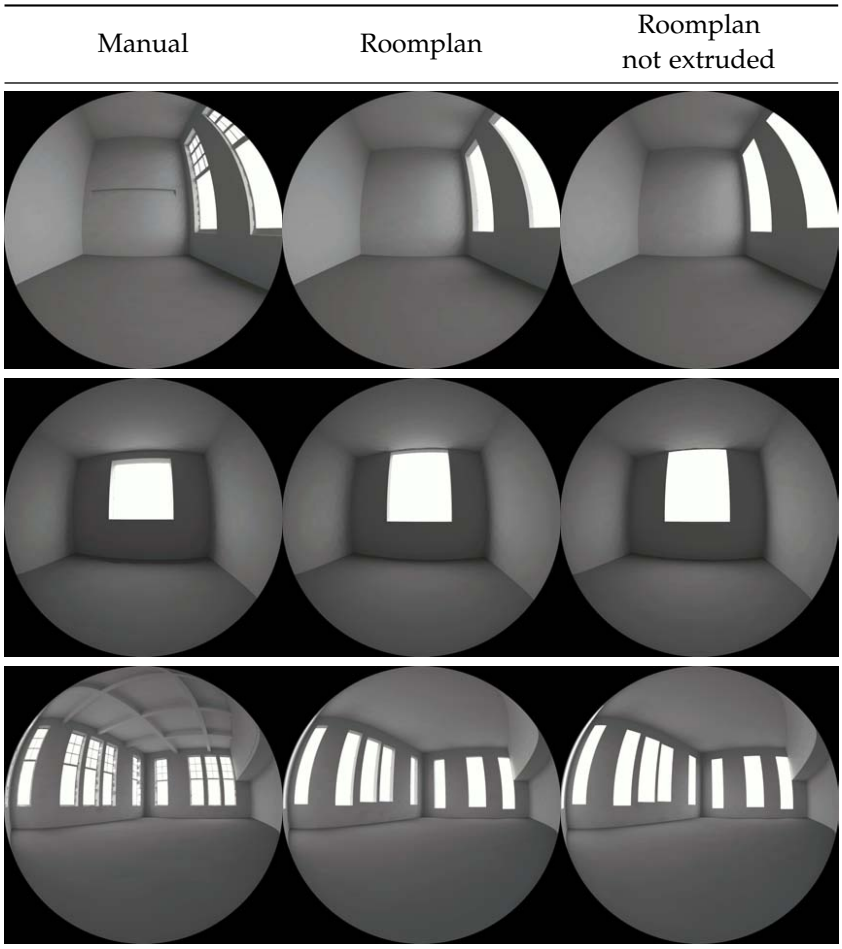

Figure 4.8.: Grayscale renderings of the three models on 20 March (Spring Equinox) at 09:00. Each row corresponds to one model (BGW640, W01050, GeoinfoLab).

	RMSE	
	Roomplan	Not extruded
BGW640	0.0044	0.019
W01050	0.0155	0.024
GeoinfoLab	0.0053	0.019

Table 4.2.: DGP RMSE

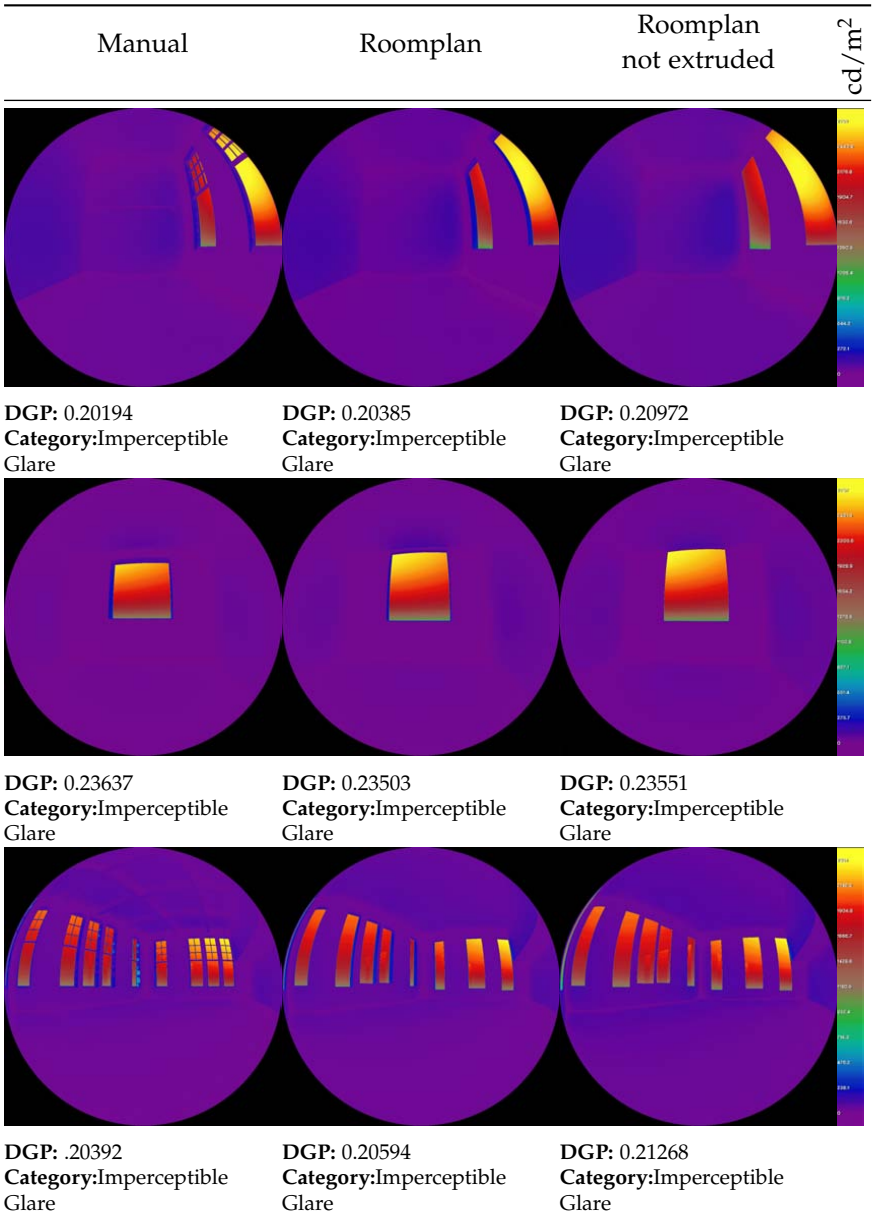

Figure 4.9.: False-color renderings of the three models on 20 March (Spring Equinox) at 09:00. Each row corresponds to one model (BGW640, W01050, GeoinfoLab). The images within each row share the same scale.

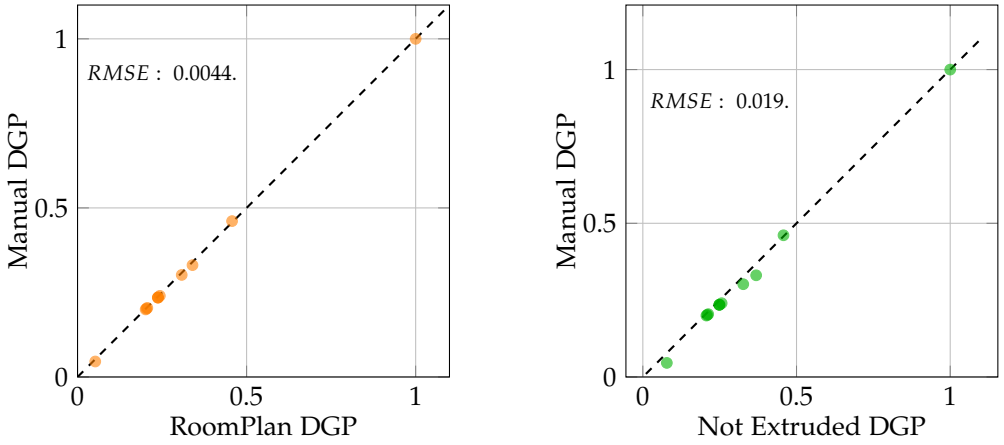

Figure 4.10.: DGP comparison for Room BGW640.

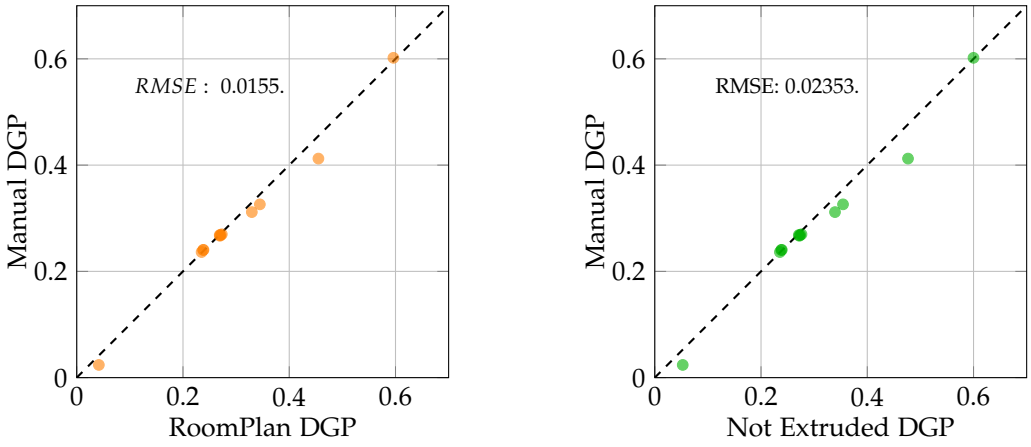

Figure 4.11.: DGP Comparison for Room W01050.

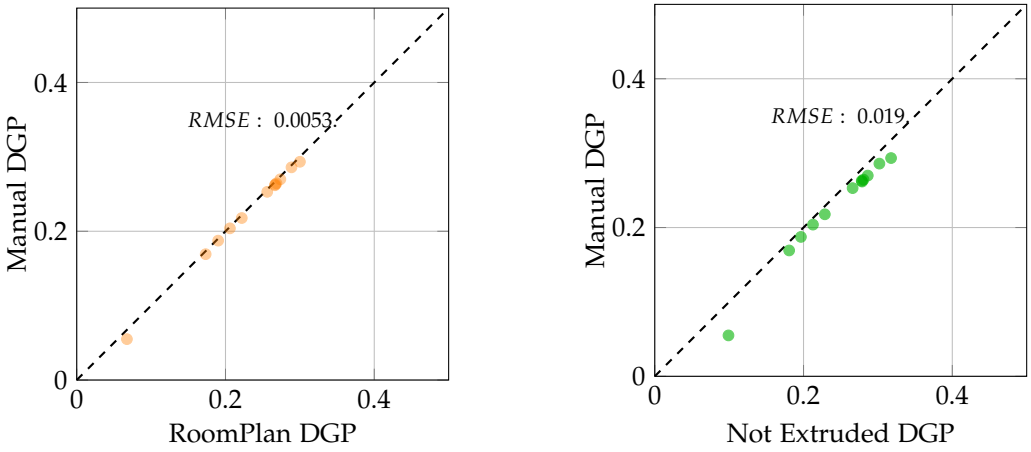

Figure 4.12.: DGP Comparison for GeoinfoLab.

5. Conclusions

This study evaluated whether RoomPlan-generated 3D geometry can be used as a substitute for manually reconstructed models in daylight simulation workflows. The main contribution is the development of a Python-based software which automatically converts a Roomplan scan to Honeybee Model, after reconstructing the ceiling and the window frames, which can directly be used in Grasshopper for daylight simulations, reducing significantly the required time. The evaluation was based on the geometrical accuracy of Roomplan models in comparison with manually reconstructed models as well as on the comparison of the results of grid-based and view-based daylight simulation performed on these models. For this purpose 3 rooms were modeled using TLS (Leica P40) and manually reconstructed based on the point clouds. The manual reconstruction was not part of the current thesis, but the models were provided. The same 3 rooms were captured using Roompla API on an iPhone 12 Pro.

A key aspect of this study concerns the geometry acquisition process itself. RoomPlan offers an alternative to traditional modeling workflows such as manual reconstruction, LiDAR scanning, or photogrammetry, each of which differs substantially in acquisition time, required expertise, and reconstruction fidelity. RoomPlan provides a fast and intuitive method for capturing indoor geometry compared to the other methods. In addition, it produces a clean representation rather than a raw point cloud or mesh that demands extensive post-processing. This makes it useful for users who lack experience with geometric data cleaning. However, Roomplan is inherently limited by they way it works. which simplifies the geometries significantly. However comparing the time it takes to scan a room with Roomplan (about 5 minutes for BGW640) with the time it takes to scan and postprocess the same room to get a 3D Mesh (about 15 hours) highlights the trade-off between acquisition speed and geometric fidelity. Considering its speed Roomplan does an impressive job in 3D reconstruction.

The developed software successfully complements Roomplan API and reconstructs the missing elements of the geometries. In addition to that, the most significant contribution is the direct conversion to Honeybee Model, allowing users to proceed directly from scanning to simulation. In addition it is not bounded to Roomplan API because it works based on USD files. Therefore any USD file with semantic information can be converted to Honeybee Model. Another important aspect is that Honeybee is part of the Ladybug Tools. Based on that and by developing a dedicated application which uses Roomplan API the capabilities of the software can be expanded to utilize the whole Ladybug Tools ecosystem for all kind of simulations it offers.

Geometric accuracy was assessed using Chamfer and Hausdorff distances between meshes derived from the manual and automatically generated models. One of the 3 examined models scored low values in both metrics while the other two higher. One thing that was not expected is that these results do not correlate with the simulations' results. However, after conducting the analysis it was discovered that the ground truth model for Room W01050 was not correct. More precisely, the window was smaller that in reality, while RoomPlan's model had the right dimensions.

The grid-based illuminance results demonstrated clear differences between rooms. As mentioned before it is unexpected that the accuracy in illuminance do not correlate with the geometric accuracy. This is because the model with the most accurate geometry has the worst accuracy in the illuminance simulations. The other two models with relatively worst geometry accuracy had more accurate simulation results. In contrast to illuminance, DGP results were practically identical to the ground truth with minor differences except for 3 cases.

The selected timesteps covered a range of solar positions, including early morning (9AM), midday, and late afternoon (15PM) for four representative dates of the year (2 Equinox and 2 Solstices). This ensures that different lighting conditions were studied. In rooms where no intolerable glare occurred in the manual model, such as BGW640 and GeoinfoLab, all geometries produced similar DGP behavior. In contrast, rooms with higher glare potential, such as W01050 where the manual DGP reached values above 0.40 and 0.60 in certain conditions.

Despite the promising results, this work is subject to several limitations. Only three rooms were evaluated, which restricts generalization. Moreover, only two types of daylight simulations were performed. It would be interesting to test the geometries in annual daylight simulations to examine if the inaccurate geometry propagates in the results or not. In addition, it is recommended to evaluate the geometrical accuracy in a more detailed way, and for instance compare the aperture areas in the manual and the RoomPlan models, because the metrics used for the geometric evaluation account for the whole rooms and do not focus on the windows which are the most important think in daylight simulations.

5.1. Answering the research questions

This section answers, based on the finding of the project, the research questions stated at the beginning of the current project and form the research direction. Initially, the subquestion are answered first and then the main research question.

> How feasible and accurate is the use of iPhone for generating 3D indoor models suitable for daylight simulation?

Sub-questions

1. What are the possibilities of using the RoomPlan API and accessing data from iPhone's sensors for daylight simulations?
2. How can the RoomPlan API's model be transformed into a format compatible with daylight simulation tools?
3. How do RoomPlan generated models perform compared to manually reconstructed models with respect to geometrical accuracy and daylight simulations results?

What are the possibilities of using the RoomPlan API and accessing data from iPhone's sensors?

RoomPlan reconstructs 3D models which include the permanent structures of a room, as well as the furniture. In addition, the furniture depending on the user's options can be represented as bounding boxes or as triangular meshes of furniture form a library with furniture models.

The iPhone is equipped with compass and barometer sensors. Unfortunately, due to lack of experience with developing iPhone applications and using Swift programming language accessing data from these sensors was not tested. If accessed, those sensors can give info and assist with orienting the model with respect to the north as well as set the altitude of the room. This is relevant in case the surrounding environment (neighboring buildings) is used in the simulation. Another aspect that needs to be examined is whether RoomPlan automatically orients the models using data from the compass. Moreover, another suggestion for future work is to test the ability of RoomPlan to capture multiple rooms and add a functionality to the developed tool to read USDZ files with more than one room.

How can the RoomPlan API's 3D model be transformed into a format compatible with daylight simulation tools?

RoomPlan offers 3 different export options for the models each one with different representation of the geometry, namely: (i) Parametric; (ii) Mesh; and (iii) Model. In the proposed methodology, the Model option is chosen because it gives the possibility to acquire furniture models, instead of bounding boxes, in addition to the structural components. Nevertheless, the furniture were not used in the simulations and the part of the script that reads them need correction. In addition, it was decided to HoneyBee as the simulation software because it widely used by practitioners. To achieve the transformation to a format compatible with simulation tools the first objective was to create a watertight 3D model and first and foremost to create the ceiling which is not modeled in RoomPlan. The steps for this are the following:

1. Isolation of the interior faces of the walls.
2. Creation of faces without holes or cavities.
3. Creation of windows' frames.
4. Creation of the floor and the ceiling.
5. Creation of HoneyBee Model.

How do RoomPlan generated models perform compared to manually reconstructed models with respect to geometrical accuracy and daylight simulations results?

In the current work, RoomPlan's output was used to create watertight 3D models and perform daylight simulations. The models concern three rooms with different geometrical characteristics. The processed geometries were compared to manually reconstructed 3D models of the same rooms. In addition, the automatically reconstructed and the manually reconstructed models were used to perform and compare the results of illuminance and luminance based daylight simulations.

RoomPlan exhibits relatively high accuracy, taking into account the short duration of the capture process. Nevertheless, each model based on its characteristics displays certain inaccuracies. Based on the acquired scans, RoomPlan appears to have difficulty in identifying multiple windows when they are located close to each other (e.g., see Figure 3.29). In addition, it appears that when there are structures that obstruct the view to the ceiling the estimation of the ceiling's height is not correct. For instance, in Room BGW640, there are light installments which extend almost from wall to wall located at a height of 4.88 meters, which is the height of the walls in the RoomPlan model. In addition to the lights there are also ducts on about the same height. Therefore, it can be said that these structures which reduce the visibility to the ceiling confuse RoomPlan. However, the cause of this needs to be verified because another

fact that needs to be taken into account is that by design (Section 2.3.1) RoomPlan is capable to model ceilings up to 3.6 meters. Contrary to that though, RoomPlan managed to capture with 10 cm error a wall 5.77 meters tall (GeoinfoLab). It is recommended to scan other types of rooms, with different characteristics, as well as perform multiple scans of the same room to compare how it performs between the different scans and evaluate what is the best method to scan with RoomPlan and what it is capable of scanning accurately.

When compared to the ground truth, the results show that the RoomPlan models exhibit poorer performance in illuminance simulations, while the luminance simulation results are in close agreement with the ground truth. The MAE for the illuminance simulation is $\approx$ 269 lux. Considering daylight provision standards such as NEN-EN 17037 and WELL this error value is rather high. For instance, NEN-EN 17037 considers as minimum level of daylight provision a range between 100 and 300 lux [Royal Netherlands Standardization Institute (NEN)]. Having such a great error makes Roomplan models not suitable for illuminance daylight simulations. On the other hand, the results for the DGP are far more accurate with RMSE less than 0.01 for the RoomPlan models with extruded window frames and only 1 wrong glare category in 36 cases. Therefore it can be said that for luminance and visual comfort studies RoomPlan models are suitable.

One important aspect that needs to be explored is how RoomPlan models perform in annual daylight analysis. It is recommended to perform annual simulations, to explore the suitability of RoomPlan for this kind of simulations, sine it is possible that the over and underexposure caused by geometry inaccuracies are smoothened out.

Appendices

A. Reproducibility self-assessment

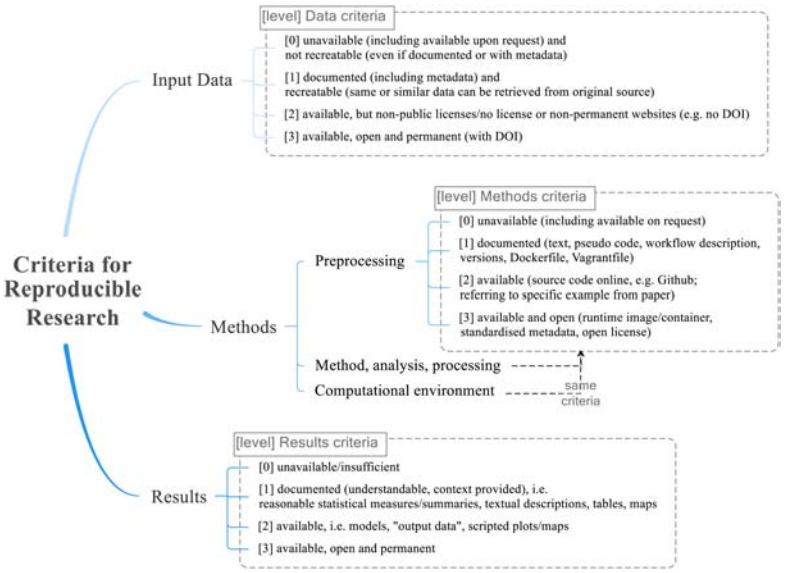

Figure A.1.: Reproducibility criteria

A.1. Marks for each of the criteria

Grade for each criterion:

- input data: 2
- preprocessing: 2
- methods: 1
- computational environment: 2
- result: 1

B. 3D Models

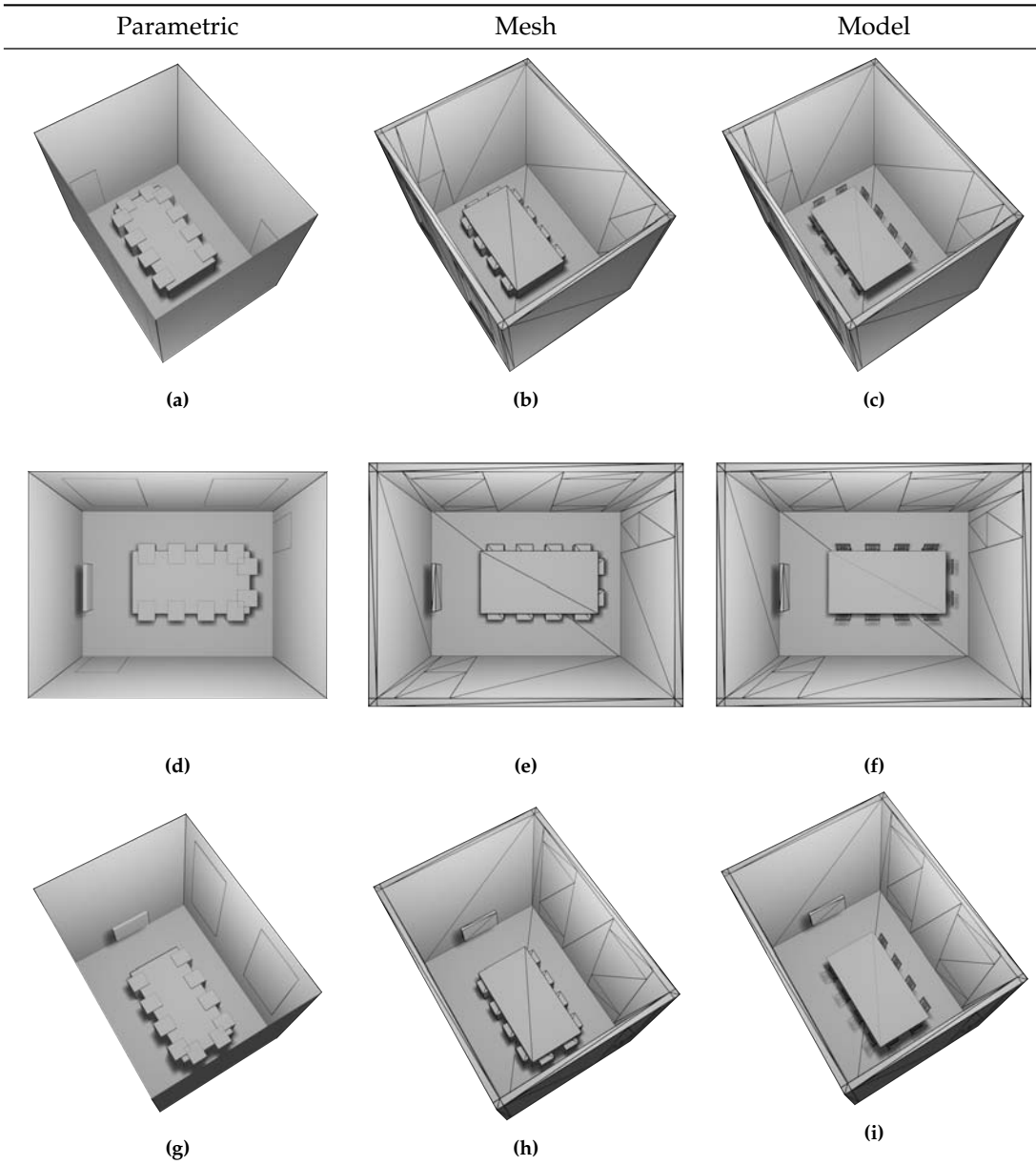

Figure B.1.: RoomPlan's output in USD format for Room BGW640.

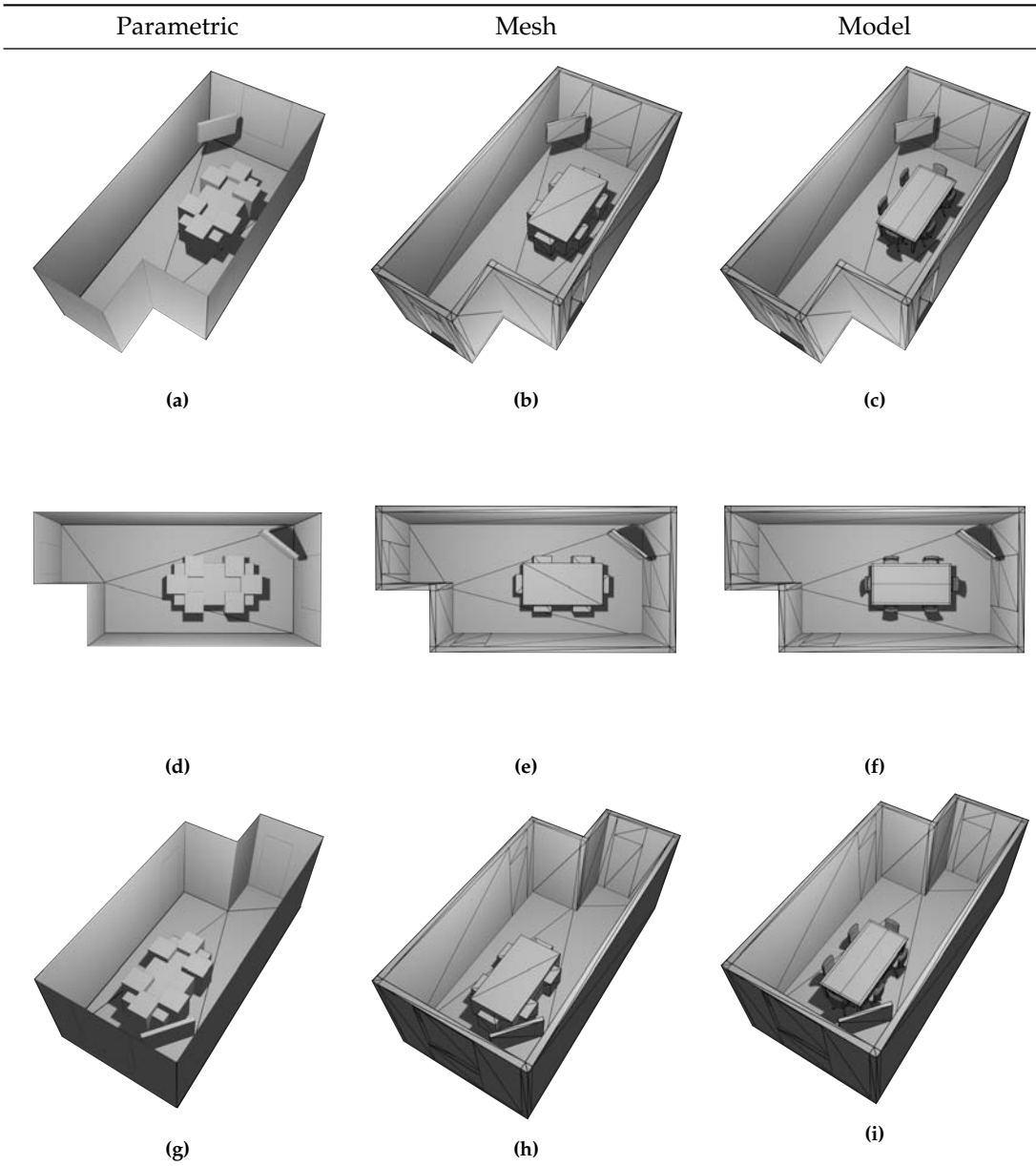

Figure B.2.: RoomPlan's output in USD format for Room W01050.

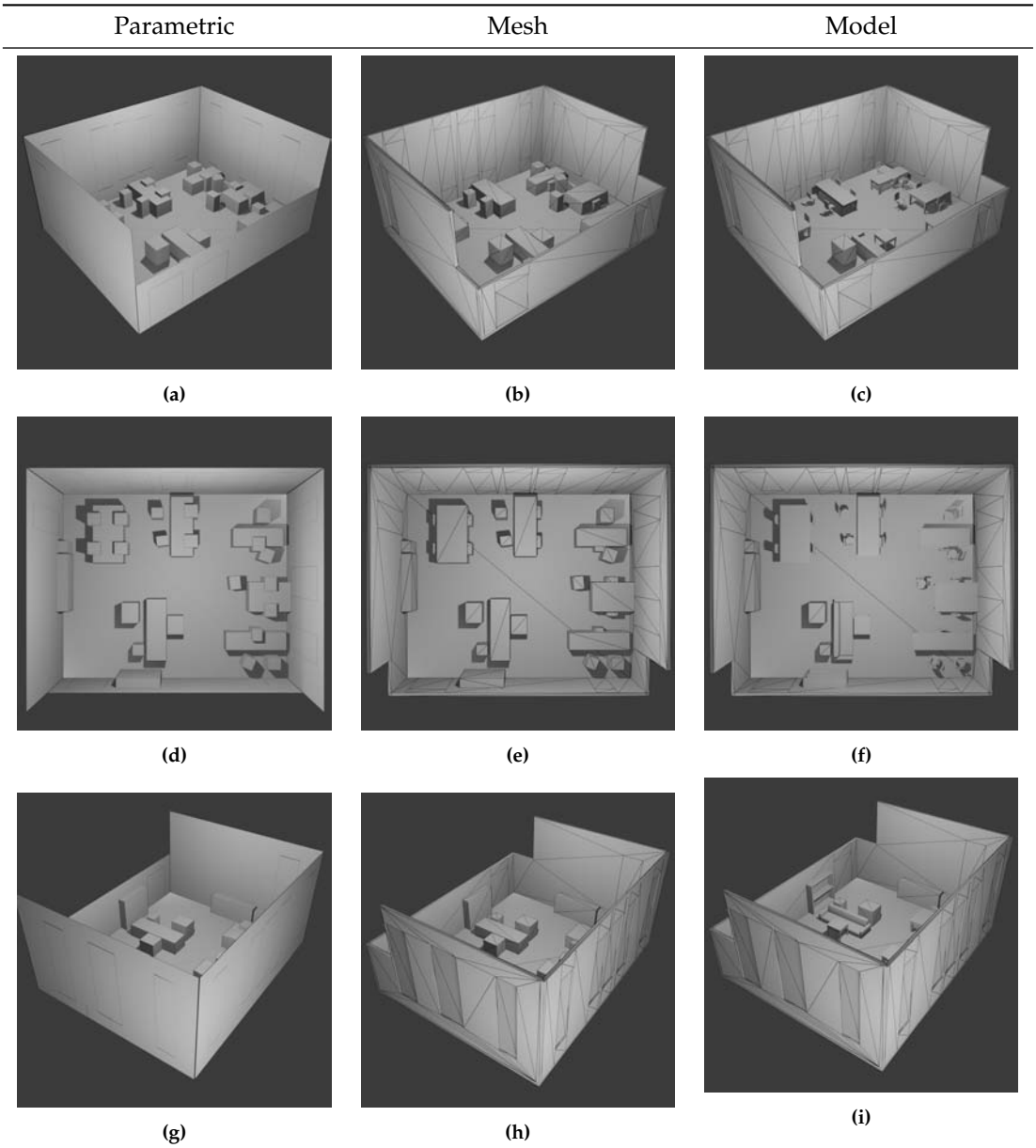

Figure B.3.: RoomPlan's output in USD format for GeoinfoLab.

C. Tables

	Runs				
	Run 1	Run 2	Run 3	Run 4	Run 5
Set 1	0	0	0	87.99	0
Set 2	0	0	0	0	0
Set 3	0	32.96	0	0	8.94
Set 4	18.23	2.18	14.53	4.67	7.05
Set 5	0	4.68	8.16	3.21	0
Set 6	5.69	4.28	5.15	0	2.64
Set 7	6.06	5.2	4.29	3.44	4.48
Set 8	5.35	6.36	6.22	6.3	5.98
Set 9	6.02	6.16	6.31	4.71	6.07
Set 10	6.26	5.95	6.09	6.24	6.62
Set 11	4.62	6.23	5.16	6.28	5.89
Set 12	6.01	5.99	6.26	5.52	6.58
Set 13	6.21	6.29	6.11	6.13	6.16
Set 14	6.08	5.70	6.21	6.11	6.31
Set 15	5.60	5.20	4.90	6.34	6.11
Set 16	12.01	12.10	12.02	11.73	12.10
Set 17	15.47	16.73	16.59	16.59	16.54
Set 18	19.09	18.61	19.30	19.18	18.81
Set 19	20.69	20.28	20.52	17.95	20.51

Table C.1.: Convergence test illuminance results.

	Chosen Parameters						Maximum Parameters						
Sensor	**Run 1**	**Run 2**	**Run 3**	**Run 4**	**Run 5**	**Avg.**	**Run 1**	**Run 2**	**Run 3**	**Run 4**	**Run 5**	**Avg.**	**Diff.**
#1	289.71	290.29	290.70	289.10	289.99	290.0	292.0399	292.8379	293.1655	293.913	291.316235	292.7	-1%
#2	568.03	561.96	560.43	561.74	561.21	562.7	563.393	563.591	564.7334	563.8294	564.848462	564.1	0%
#3	657.23	657.90	657.87	660.86	661.01	659.0	662.2468	662.0363	659.1956	662.5705	662.292482	661.7	0%
#4	560.76	565.80	566.23	562.76	566.78	564.5	563.1623	564.7282	565.0046	565.7784	566.970149	565.1	0%
#5	316.99	318.25	321.98	320.32	320.60	319.6	324.0126	322.7993	326.143	323.6316	322.403344	323.8	-1%
#6	249.31	248.68	250.83	247.16	250.37	249.3	251.6214	250.8277	251.2138	251.7118	251.041772	251.3	-1%
#7	353.57	351.97	352.14	352.67	350.71	352.2	355.281	354.8279	355.179	350.5316	354.293089	354.0	-1%
#8	384.85	381.65	385.64	388.99	381.49	384.5	388.795	386.5564	386.7336	389.6261	387.904635	387.9	-1%
#9	344.95	343.36	344.10	341.68	344.48	343.7	347.0735	346.5282	346.1405	345.7539	347.280943	346.6	-1%
#10	245.47	246.33	248.74	247.17	245.06	246.6	248.0335	247.1777	248.1448	247.6805	247.601034	247.7	0%
#11	183.67	185.57	184.09	181.59	183.24	183.6	186.192	187.1015	186.1185	186.0997	187.192651	186.5	-2%
#12	224.59	224.31	223.20	223.14	224.06	223.9	226.9711	224.5942	226.4434	227.434	225.665837	226.2	-1%
#13	233.83	233.95	233.78	233.73	234.75	234.0	236.7839	237.6361	236.7692	238.8164	237.842133	237.6	-1%
#14	215.97	215.60	214.66	217.52	217.33	216.2	218.0565	218.7989	217.2231	218.0238	219.303282	218.3	-1%
#15	175.01	175.97	174.46	175.61	176.50	175.5	177.0087	177.8251	176.5627	176.9685	175.570575	176.8	-1%
#16	130.99	132.32	131.91	131.98	132.54	131.9	134.2641	135.2432	134.7527	135.1527	134.757626	134.8	-2%
#17	150.36	150.66	149.04	149.63	149.09	149.8	150.9976	152.4143	151.5488	151.4094	152.378565	151.7	-1%
#18	154.19	153.42	153.26	153.40	152.87	153.4	155.7273	154.4542	154.786	156.5031	155.613793	155.4	-1%
#19	144.22	144.10	145.72	143.90	144.82	144.6	146.4467	145.1386	146.7501	146.018	146.327953	146.1	-1%
#20	124.66	125.04	125.24	124.41	124.87	124.8	125.8311	127.8111	127.2756	127.006	127.448573	127.1	-2%
#21	96.75	98.14	96.92	97.64	97.12	97.3	98.34072	99.62089	99.52592	100.0324	100.078291	99.5	-2%
#22	103.67	104.07	105.54	104.26	104.33	104.4	106.3088	107.6442	107.3359	105.8015	108.069424	107.0	-2%
#23	104.08	106.57	106.39	106.65	105.85	105.9	108.5618	107.2987	107.612	108.2822	107.778585	107.9	-2%
#24	100.66	99.98	100.69	101.38	101.85	100.9	103.32	102.8649	103.3276	103.0992	104.132677	103.3	-2%
#25	91.26	91.32	90.20	92.19	91.06	91.2	93.60245	93.9268	92.99786	92.60252	94.670988	93.6	-3%
#26	71.86	72.58	72.36	72.47	72.56	72.4	74.14536	74.93801	74.3286	74.46559	74.672983	74.5	-3%
#27	75.52	76.63	75.58	76.32	75.89	76.0	78.59437	78.91111	78.25239	78.49578	79.500451	78.8	-4%
#28	75.82	76.61	77.61	76.63	77.15	76.8	78.86439	79.02621	78.39883	77.15965	79.077349	78.5	-2%
#29	73.20	73.60	74.03	73.58	74.54	73.8	76.43296	76.66724	76.43418	76.93628	76.29236	76.6	-4%
#30	68.70	69.55	68.77	68.39	68.57	68.8	70.89456	70.87002	71.03477	70.65257	70.75163	70.8	-3%
#31	55.32	55.48	55.66	55.61	55.10	55.4	57.65629	57.76926	57.26378	57.95309	57.665011	57.7	-4%
#32	57.15	57.77	58.16	57.78	57.22	57.6	59.63813	60.12932	60.27863	59.50783	59.486515	59.8	-4%
#33	57.84	58.04	57.52	56.97	58.24	57.7	59.30449	59.89322	60.49219	59.97982	59.846806	59.9	-4%
#34	56.54	56.36	55.55	55.75	56.01	56.0	57.89096	58.61015	57.92975	58.00814	58.919622	58.3	-4%
#35	52.93	53.51	53.39	53.02	53.54	53.3	55.40789	55.39898	55.11059	55.2062	55.502602	55.3	-4%
#36	43.71	44.00	43.53	43.36	43.54	43.6	45.67312	45.9167	45.72981	45.71315	45.273414	45.7	-4%
#37	44.79	45.09	45.16	44.11	44.58	44.7	47.04956	47.25065	46.70226	46.46901	47.26862	46.9	-5%
#38	45.28	44.92	45.09	45.72	44.80	45.2	47.4703	47.05072	47.44459	47.54467	47.426265	47.4	-5%
#39	44.62	44.70	43.99	44.15	44.59	44.4	46.33236	46.42118	46.76008	46.38767	46.737795	46.5	-5%
#40	42.35	42.56	42.96	42.23	42.59	42.5	44.73462	44.84883	45.30019	44.68452	44.938594	44.9	-5%
#41	34.81	34.98	34.30	35.41	35.19	34.9	36.96769	37.39722	37.02812	37.22355	36.747537	37.1	-6%
#42	36.44	36.05	36.48	36.18	36.12	36.3	37.66744	37.76739	38.13305	38.09005	37.999373	37.9	-4%
#43	36.60	36.66	37.52	36.75	36.36	36.8	38.88426	38.53104	38.81592	38.57892	38.658648	38.7	-5%
#44	36.95	36.57	36.58	36.47	36.63	36.6	38.6499	38.66717	38.50807	39.00841	38.992966	38.8	-5%
#45	35.28	35.55	36.07	36.12	35.56	35.7	37.30349	37.24967	37.56036	37.83673	37.873071	37.6	-5%
#46	28.88	28.76	28.74	28.69	28.38	28.7	30.74223	30.0089	30.58535	30.29246	29.984594	30.3	-5%
#47	29.35	29.92	28.84	29.87	29.89	29.6	31.66694	31.78661	31.76683	31.79858	31.652319	31.7	-7%
#48	31.04	31.28	31.20	31.29	30.93	31.1	33.34976	33.17078	33.33716	33.32384	33.242412	33.3	-6%
#49	32.35	32.54	33.11	32.63	32.51	32.6	33.99262	34.28178	34.56678	34.42306	34.451629	34.3	-5%
#50	31.59	31.87	31.94	31.94	31.70	31.8	33.71991	33.91438	33.07743	33.77082	34.010519	33.7	-6%
#51	24.15	23.98	24.25	23.72	23.90	24.0	25.56378	25.6152	25.28819	25.46962	25.688594	25.5	-6%
#52	24.64	24.14	24.90	24.56	24.51	24.5	26.48618	26.6644	26.44331	26.38673	26.597753	26.5	-7%
#53	20.97	20.53	20.71	21.01	20.47	20.7	22.43702	22.26774	21.6261	22.28887	22.023462	22.1	-6%
#54	20.64	20.37	20.35	20.07	20.59	20.4	22.30356	22.26189	20.95344	22.03853	21.845017	21.9	-7%
#55	19.28	19.28	19.35	19.51	19.45	19.4	20.66492	20.73883	19.93033	19.82083	20.073919	20.2	-4%
#56	19.37	18.18	18.57	19.11	18.34	18.7	20.3699	20.36743	20.63424	20.25731	19.876787	20.3	-8%

Table C.2.: Results of illuminance simulation for Room W01050 using Radiance Parameters of Set 18 and Maximum Parameters.

	Date	Time	Roomplan	Roomplan not extruded
BGW640	20 Mar	09:00	43.08294	189.0236
	20 Mar	12:00	89.28864	363.5438
	20 Mar	15:00	53.227	233.3065
	21 Jun	09:00	91.8318	374.0498
	21 Jun	12:00	3362.689	3806.754
	21 Jun	15:00	90.8507	380.847
	22 Sep	09:00	145.4636	1234.732
	22 Sep	12:00	369.8415	1026.623
	22 Sep	15:00	100.7593	528.5917
	21 Dec	09:00	32.76983	90.73293
	21 Dec	12:00	46.60537	194.239
	21 Dec	15:00	10.20549	45.11611
GeoinfoLab	20 Mar	09:00	72.91568	230.2818
	20 Mar	12:00	128.6349	421.3849
	20 Mar	15:00	93.16367	292.2368
	21 Jun	09:00	152.9276	475.4556
	21 Jun	12:00	182.7138	601.4691
	21 Jun	15:00	162.6933	519.4609
	22 Sep	09:00	758.8283	1449.973
	22 Sep	12:00	138.0826	455.2064
	22 Sep	15:00	141.1568	451.4311
	21 Dec	09:00	21.10233	76.82742
	21 Dec	12:00	61.71139	198.1419
	21 Dec	15:00	18.14687	57.8308
W01050	20 Mar	09:00	83.14159	133.6986
	20 Mar	12:00	162.7572	258.0136
	20 Mar	15:00	97.27115	156.0645
	21 Jun	09:00	167.9223	267.9233
	21 Jun	12:00	1372.307	1586.106
	21 Jun	15:00	160.6897	259.0989
	22 Sep	09:00	543.1925	1095.033
	22 Sep	12:00	427.1016	670.8976
	22 Sep	15:00	144.0207	235.4983
	21 Dec	09:00	58.80034	83.97942
	21 Dec	12:00	88.26095	140.6973
	21 Dec	15:00	19.06152	30.83331
		AVG	269.3	517.1
		MIN	10.2	30.8
		MAX	3362.7	3806.8

Table C.3.: MAE of Illuminance [lx].

	Date	Time	Roomplan	Roomplan not extruded	Statistics
BGW640	20 Mar	09:00	5.1%	23.8%	
	20 Mar	12:00	5.2%	22.8%	
	20 Mar	15:00	5.2%	24.3%	
	21 Jun	09:00	5.6%	24.1%	**Roomplan**
	21 Jun	12:00	12.7%	24.5%	**AVG** **MIN** **MAX**
	21 Jun	15:00	5.5%	24.4%	6.1% 3.6% 12.7%
	22 Sep	09:00	3.6%	29.0%	**Not extruded**
	22 Sep	12:00	8.8%	24.7%	**AVG** **MIN** **MAX**
	22 Sep	15:00	5.7%	28.8%	24% 16.2% 29.0%
	21 Dec	09:00	5.8%	16.2%	
	21 Dec	12:00	5.1%	22.0%	
	21 Dec	15:00	5.1%	23.8%	
GeoinfoLab	20 Mar	09:00	10.7%	34.3%	
	20 Mar	12:00	10.9%	35.5%	
	20 Mar	15:00	11.3%	35.6%	
	21 Jun	09:00	11.1%	34.8%	**Roomplan**
	21 Jun	12:00	10.9%	34.2%	**AVG** **MIN** **MAX**
	21 Jun	15:00	11.5%	36.5%	11.7% 8.1% 22.4%
	22 Sep	09:00	22.4%	56.4%	**Not extruded**
	22 Sep	12:00	10.8%	34.5%	**AVG** **MIN** **MAX**
	22 Sep	15:00	11.1%	34.2%	36.3% 29.2% 56.4%
	21 Dec	09:00	8.1%	29.2%	
	21 Dec	12:00	10.9%	34.6%	
	21 Dec	15:00	11.3%	35.5%	
W01050	20 Mar	09:00	27.7%	60.6%	
	20 Mar	12:00	41.1%	60.6%	
	20 Mar	15:00	41.4%	61.0%	
	21 Jun	09:00	41.3%	60.7%	**Roomplan**
	21 Jun	12:00	58.9%	76.0%	**AVG** **MIN** **MAX**
	21 Jun	15:00	41.0%	61.2%	41.9% 27.2% 58.9%
	22 Sep	09:00	50.3%	95.8%	**Not extruded**
	22 Sep	12:00	43.4%	63.3%	**AVG** **MIN** **MAX**
	22 Sep	15:00	38.4%	57.7%	62.7% 38.0% 95.8%
	21 Dec	09:00	27.2%	38.0%	
	21 Dec	12:00	38.9%	57.7%	
	21 Dec	15:00	40.0%	59.4%	

Table C.4.: MAPE of Illuminance (%).

D. Renders

D.1. Black&White

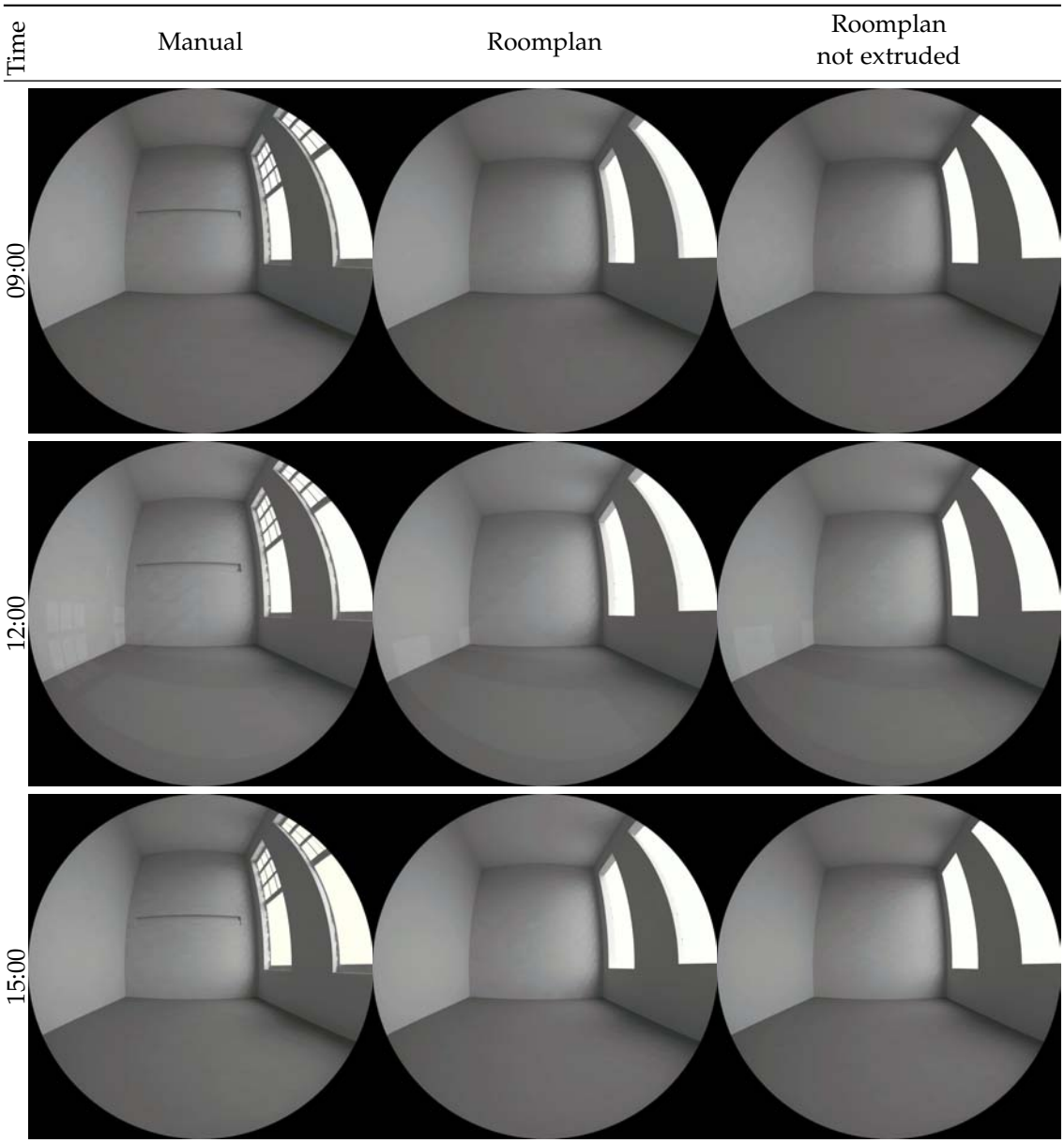

Figure D.1.: Black and white renderings of Room BGW640 on 20 March (Spring Equinox)

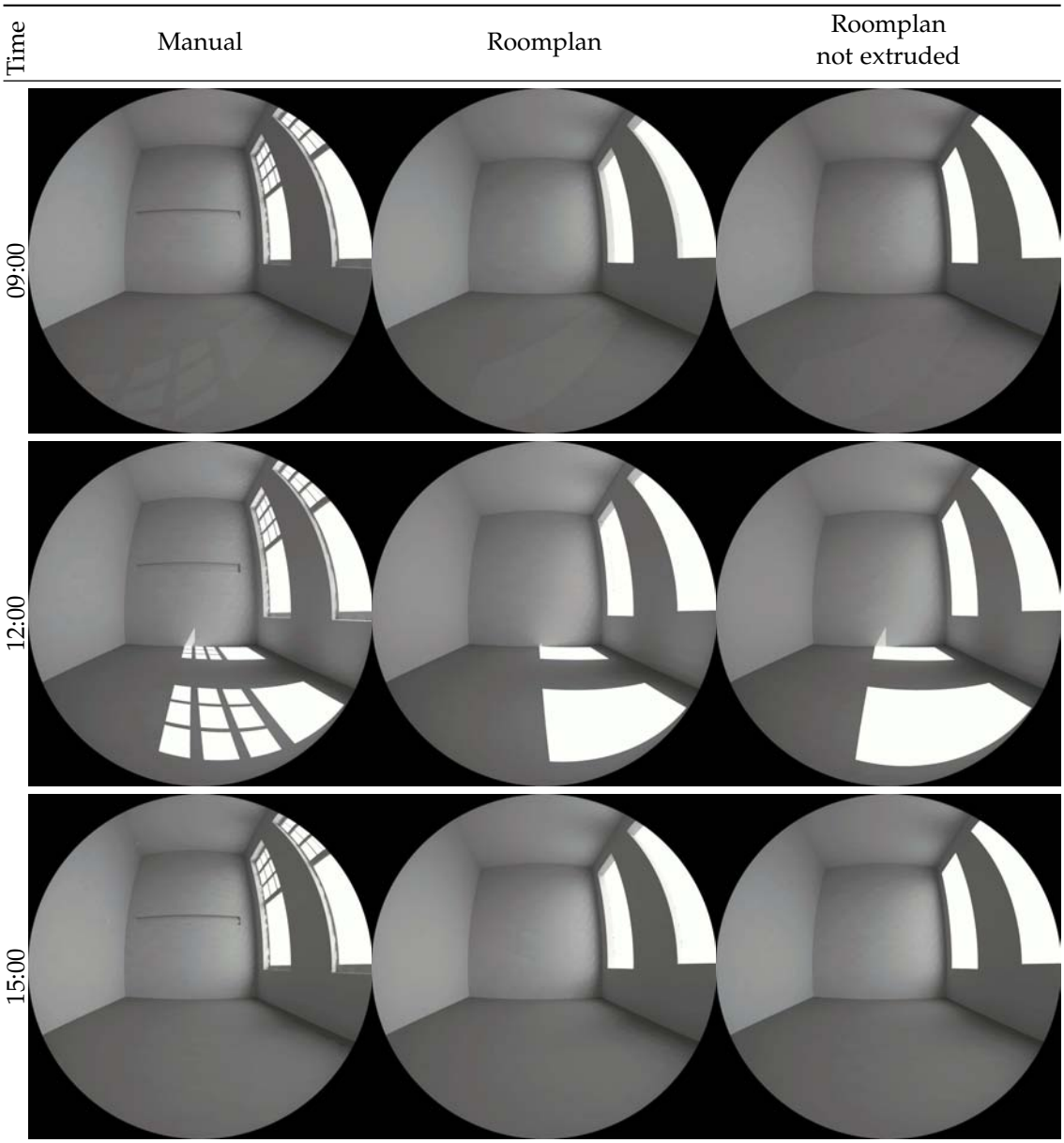

Figure D.2.: Black and white renderings of Room BGW 640 on 21 June (Summer Solstice).

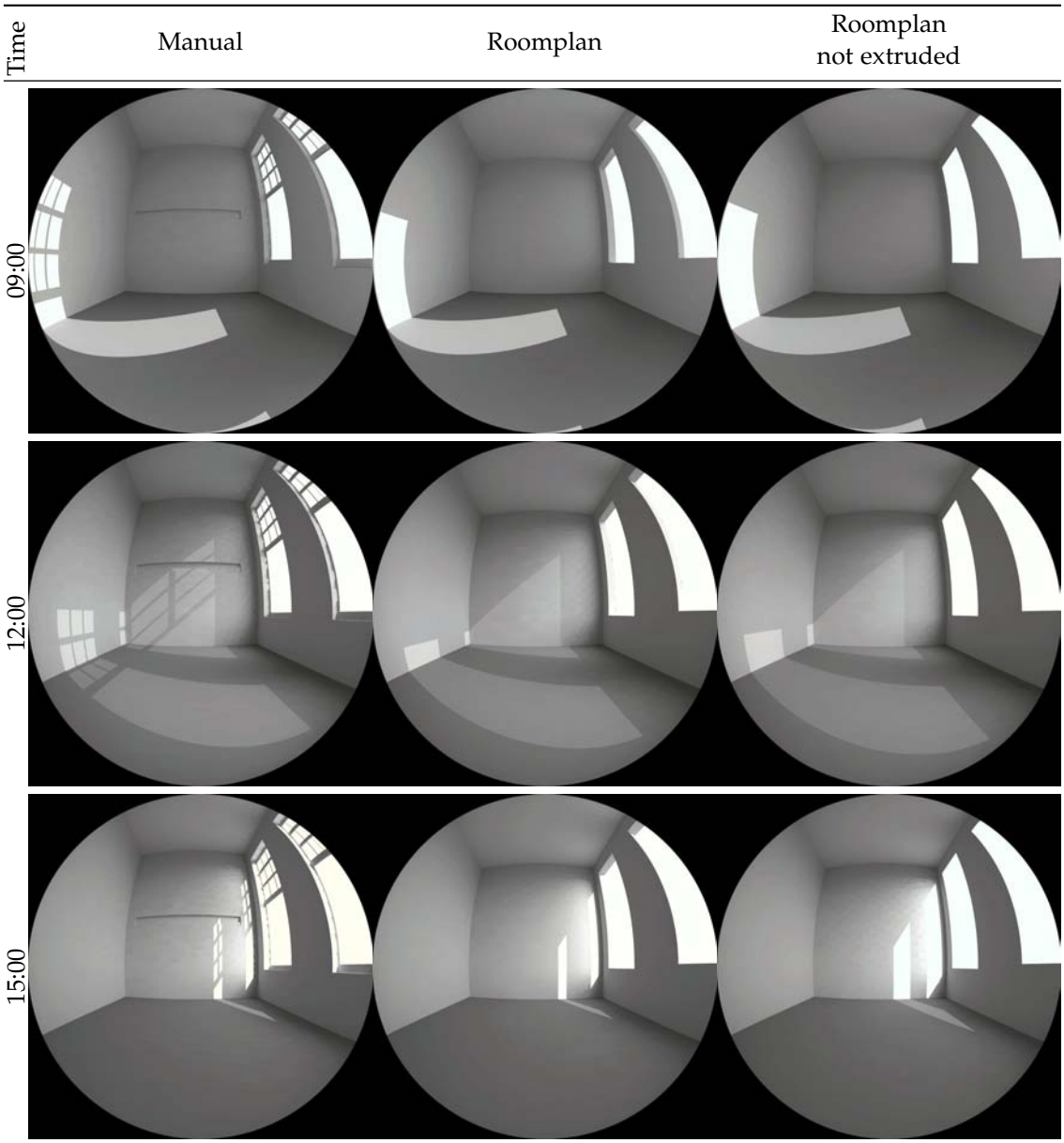

Figure D.3.: Black and white renderings of Room BGW 640 on 22 September (Autumn Equinox).

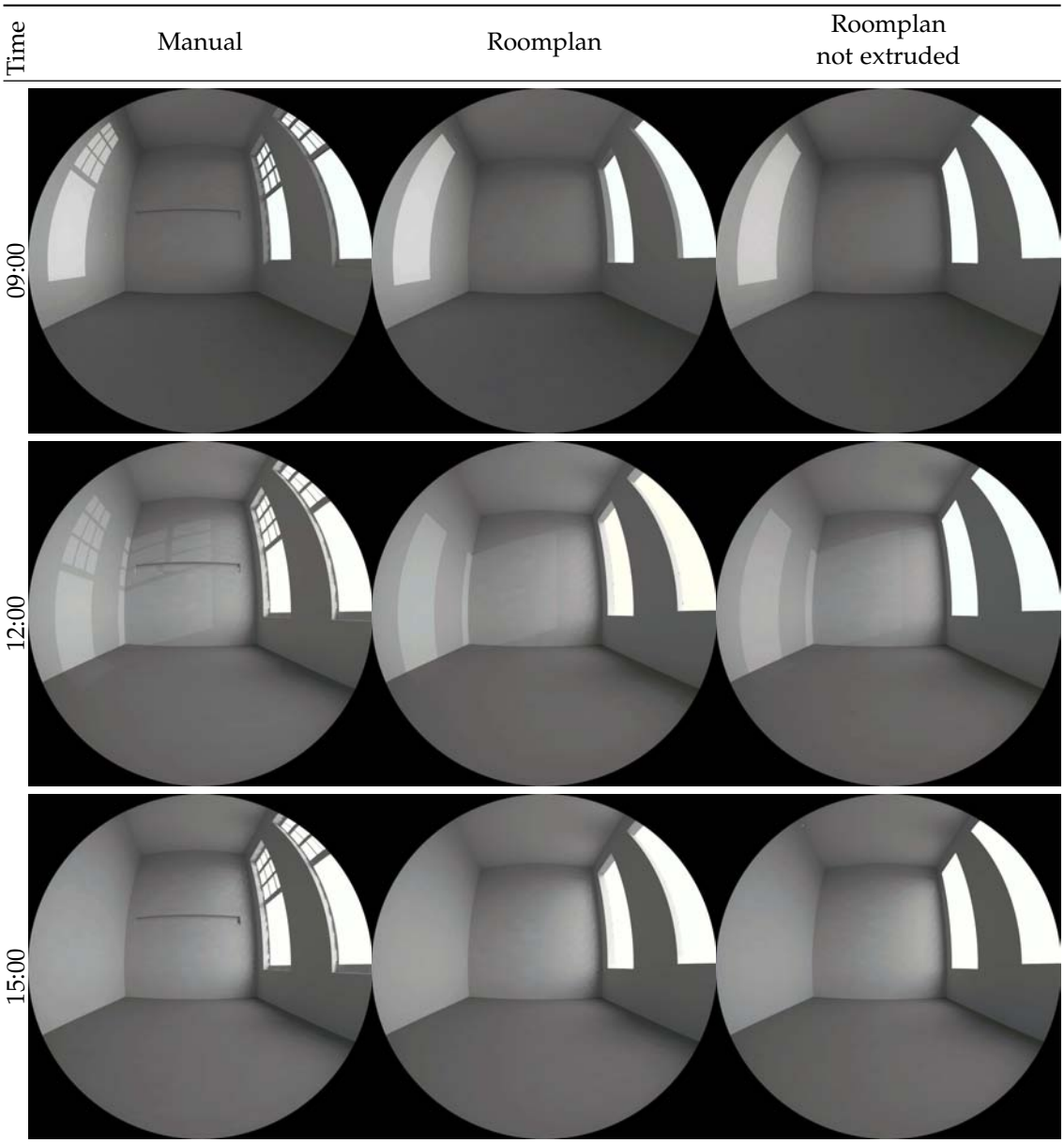

Figure D.4.: Black and white renderings of Room BGW 640 on 21 December (Winter Solstice).

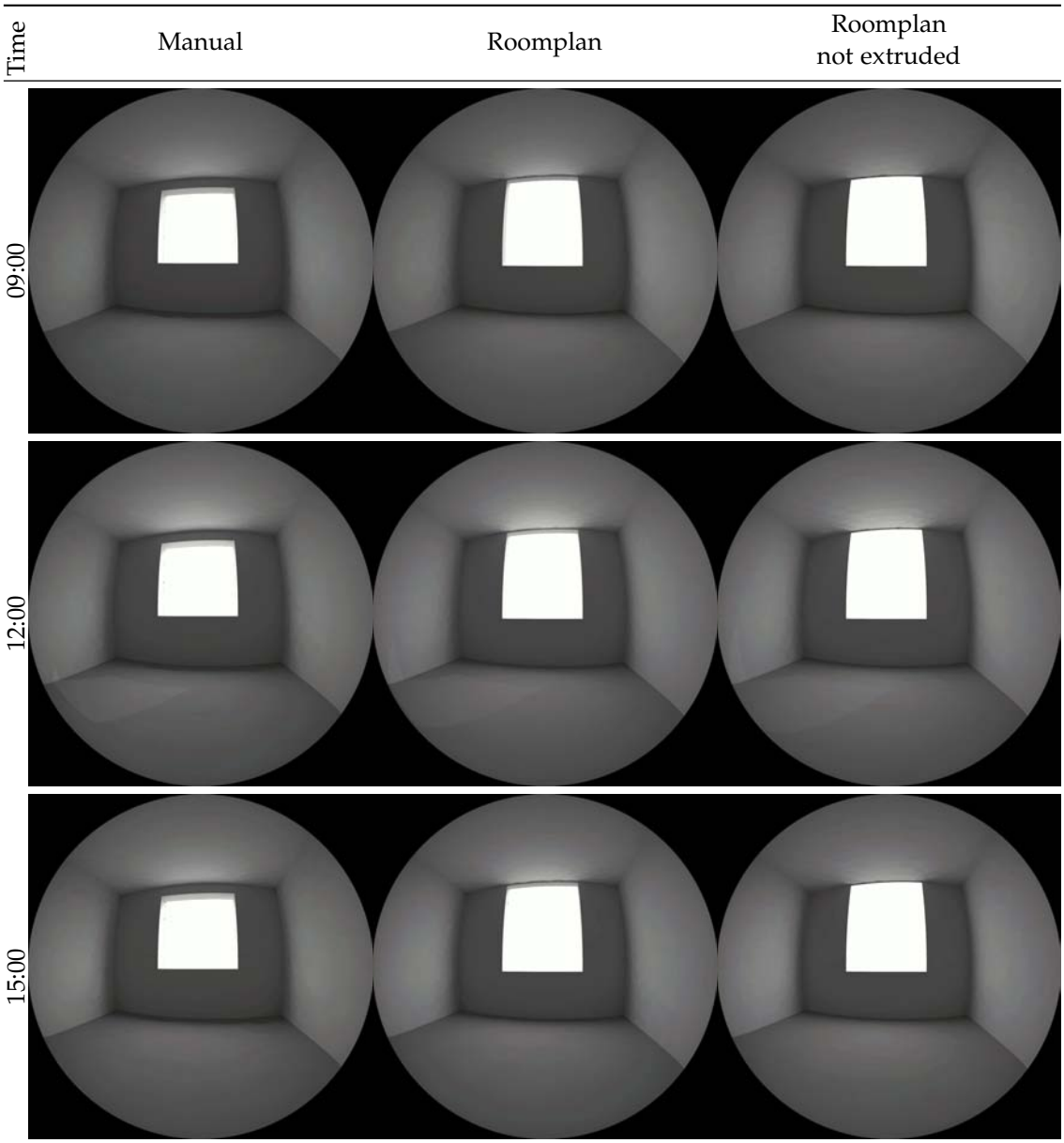

Figure D.5.: Black and white renderings of Room W01050 on 20 March (Spring Equinox)

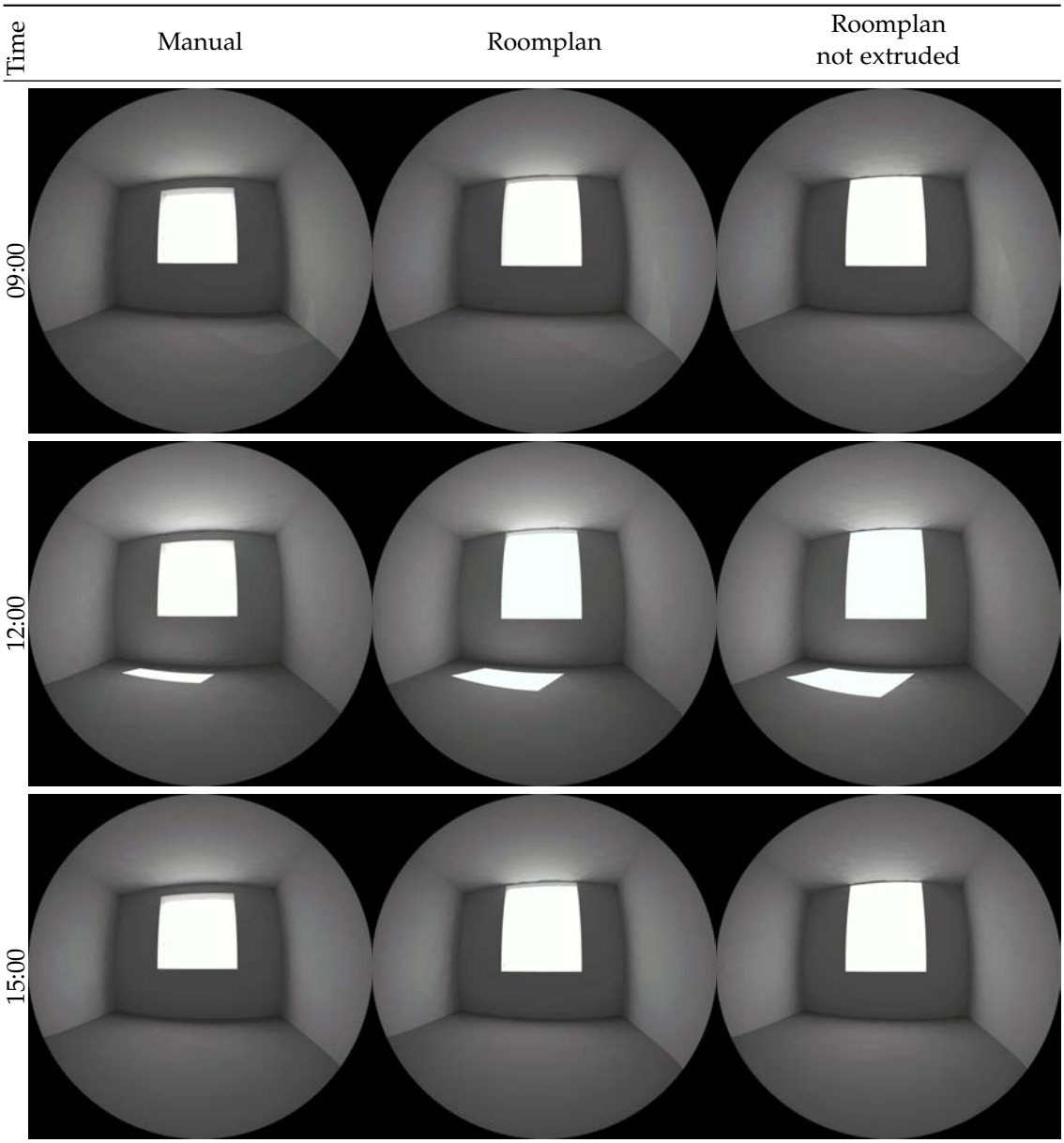

Figure D.6.: Black and white renderings of Room W01050 on 21 June (Summer Solstice)

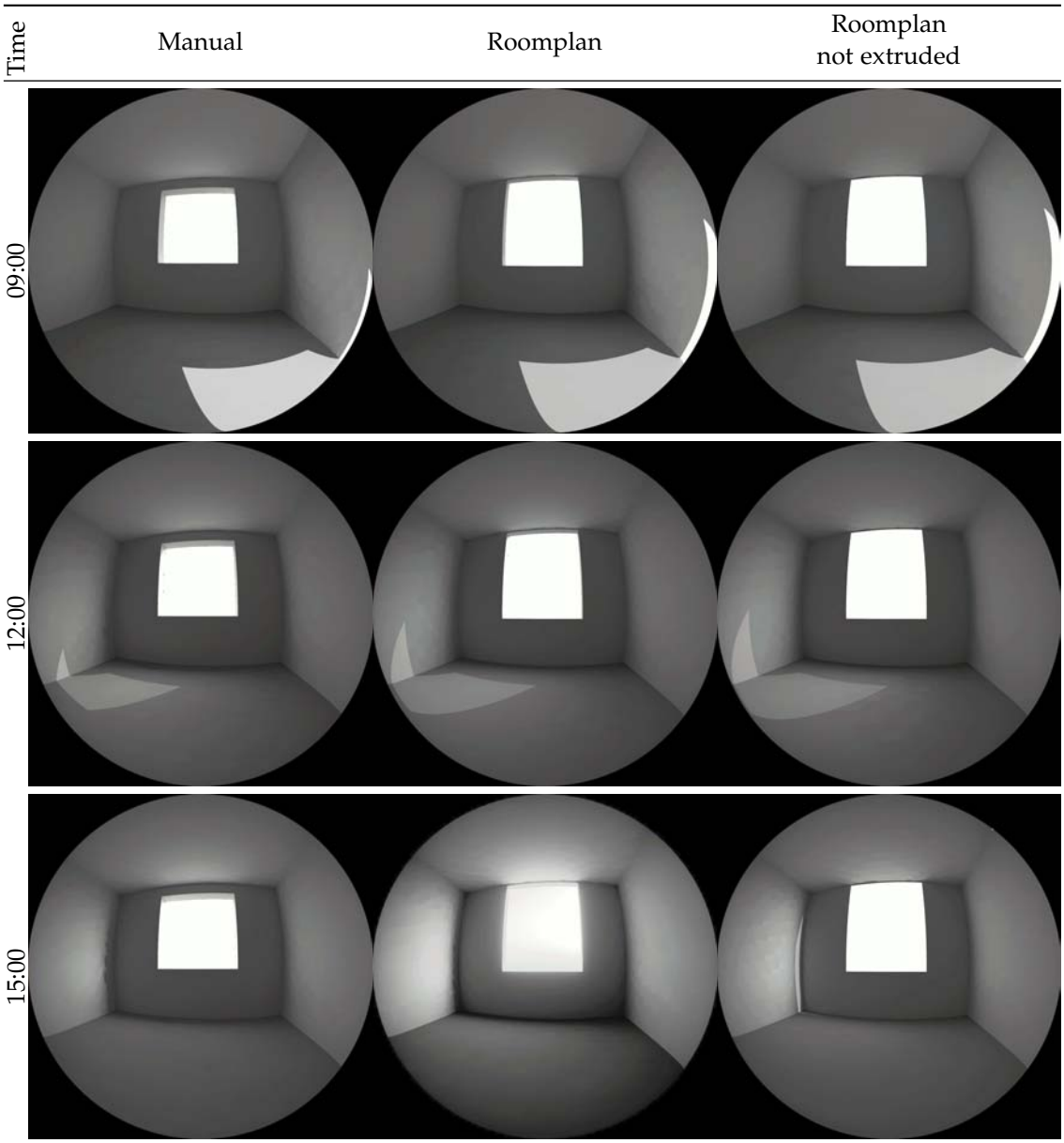

Figure D.7.: Black and white renderings of Room W01050 on 22 Semptember (Autumn Equinox)

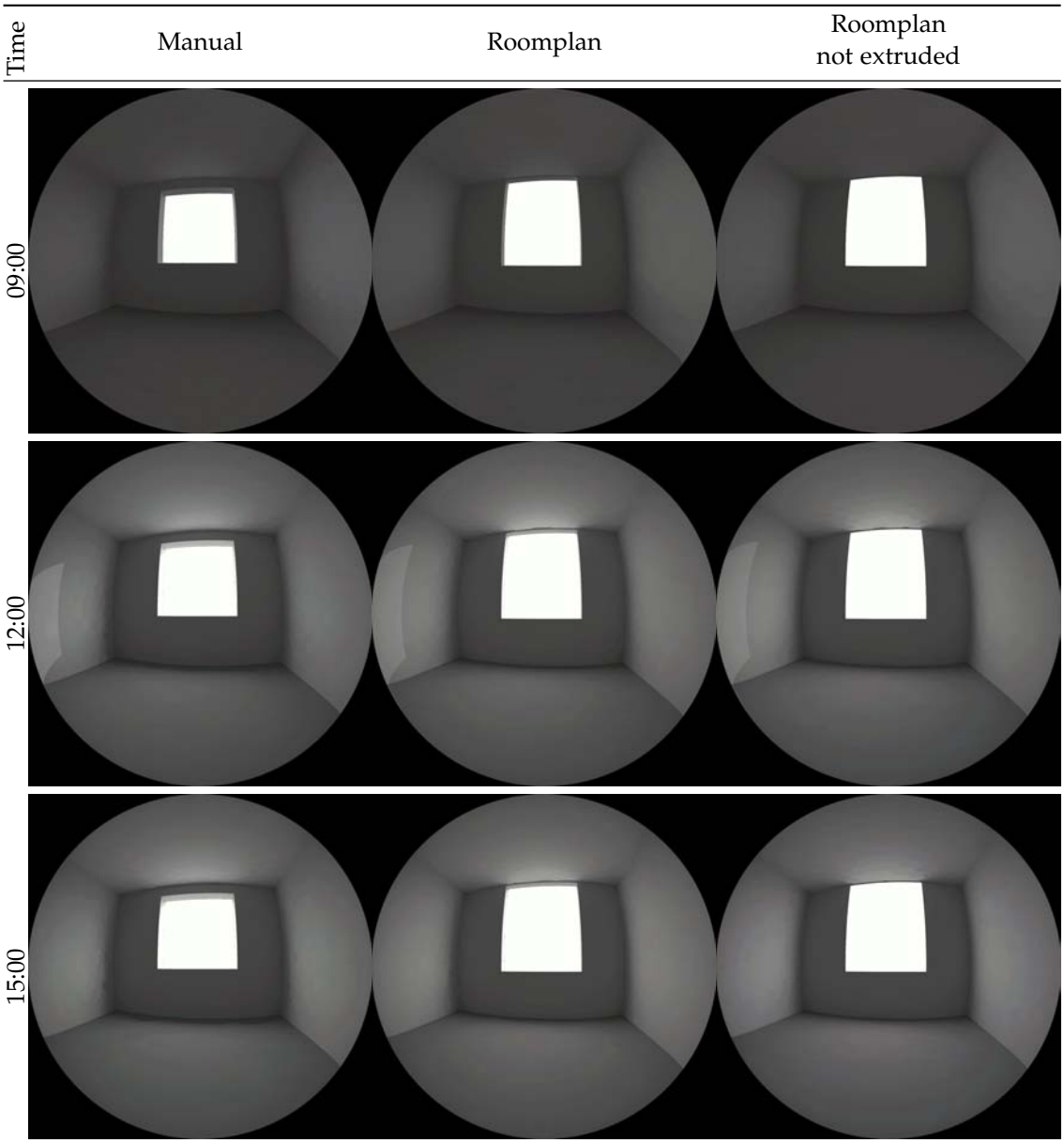

Figure D.8.: Black and white renderings of Room W01050 on 21 Dcember (Winter Solstice)

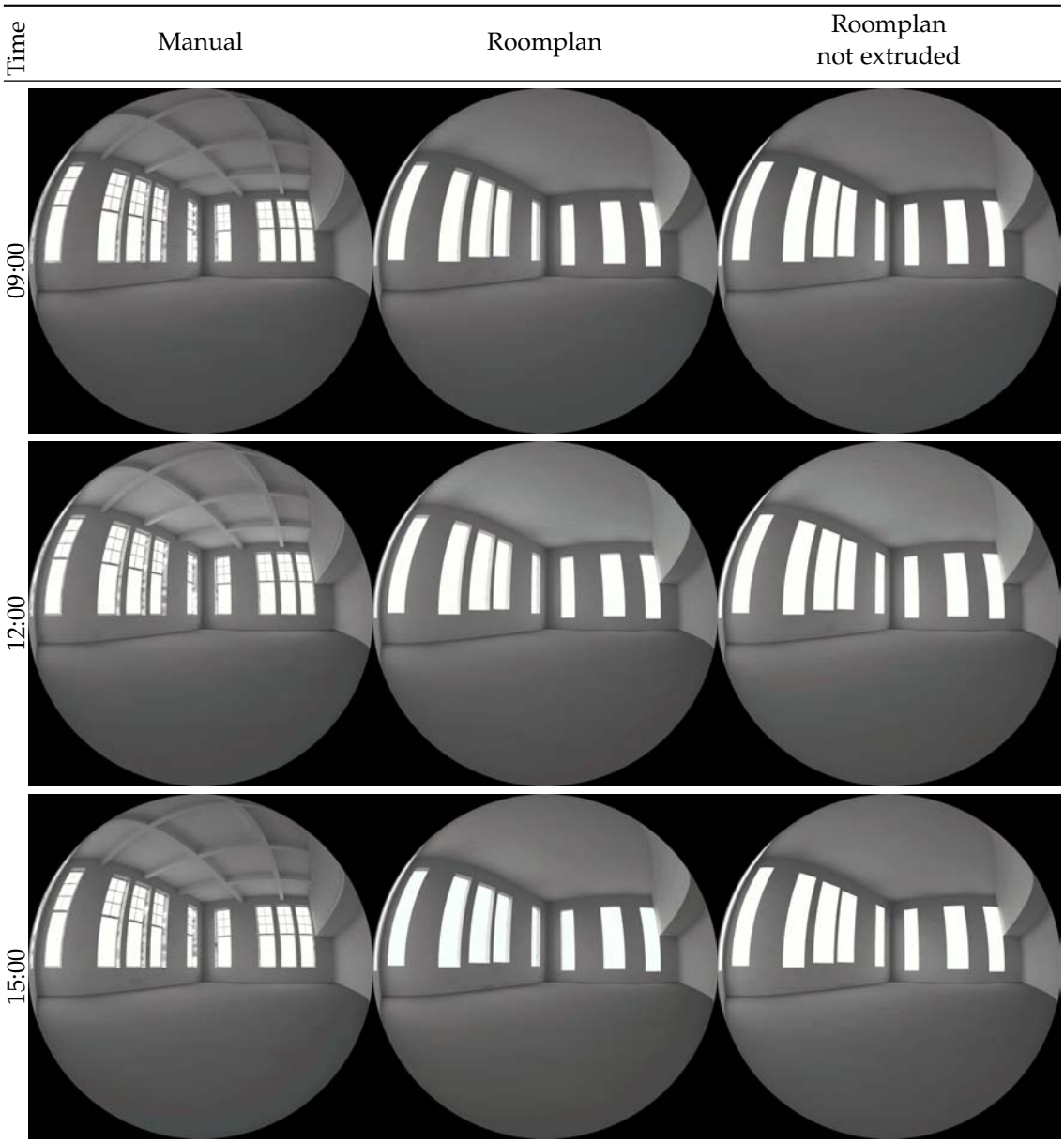

Figure D.9.: Black and white renderings of Room BGW640 on 20 March (Spring Equinox)

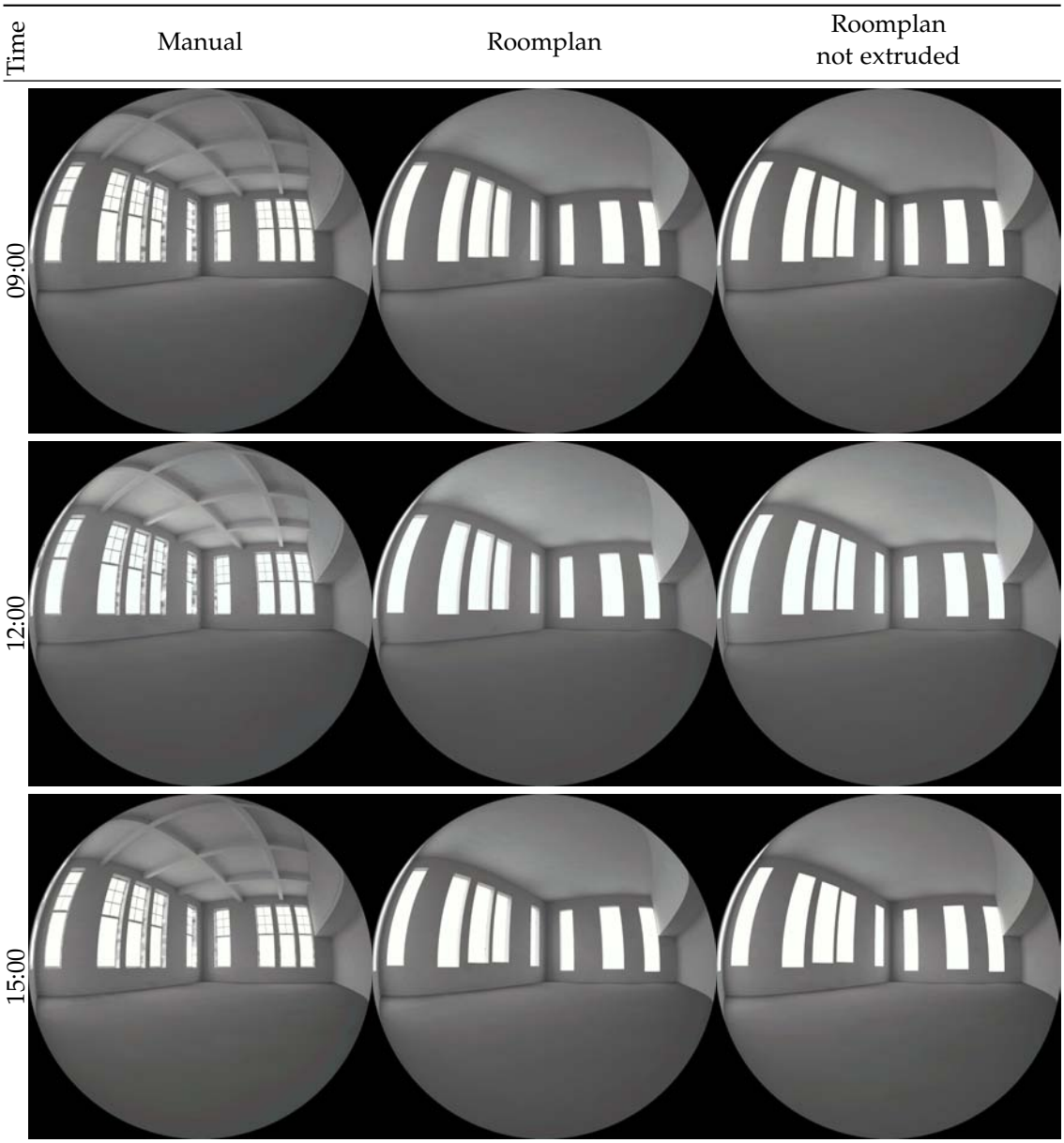

Figure D.10.: Black and white renderings of GeoinfoLab on 21 June (Summer Solstice)

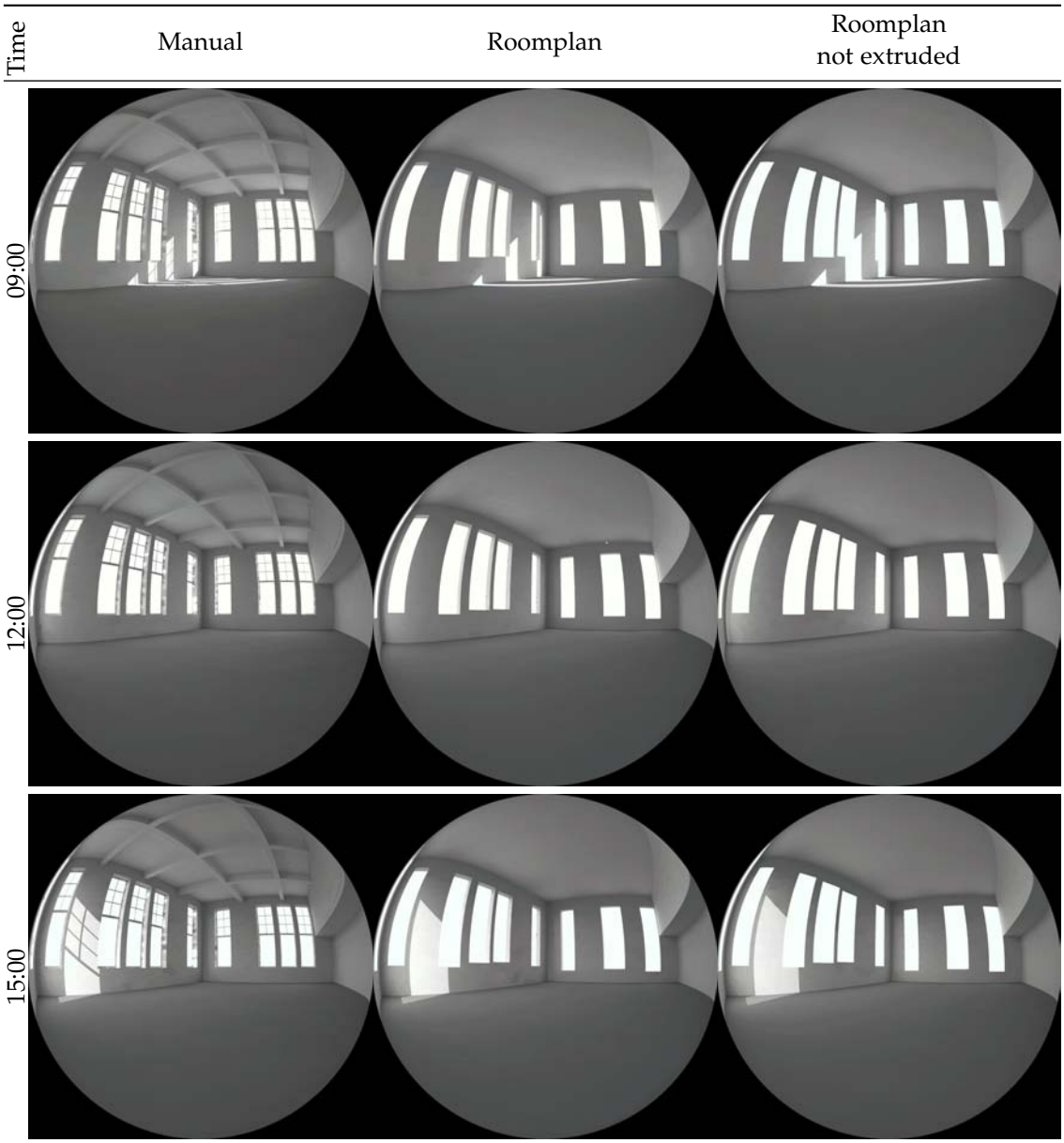

Figure D.11.: Black and white renderings of GeoinfoLab on 22 september (Autumn Equinox)

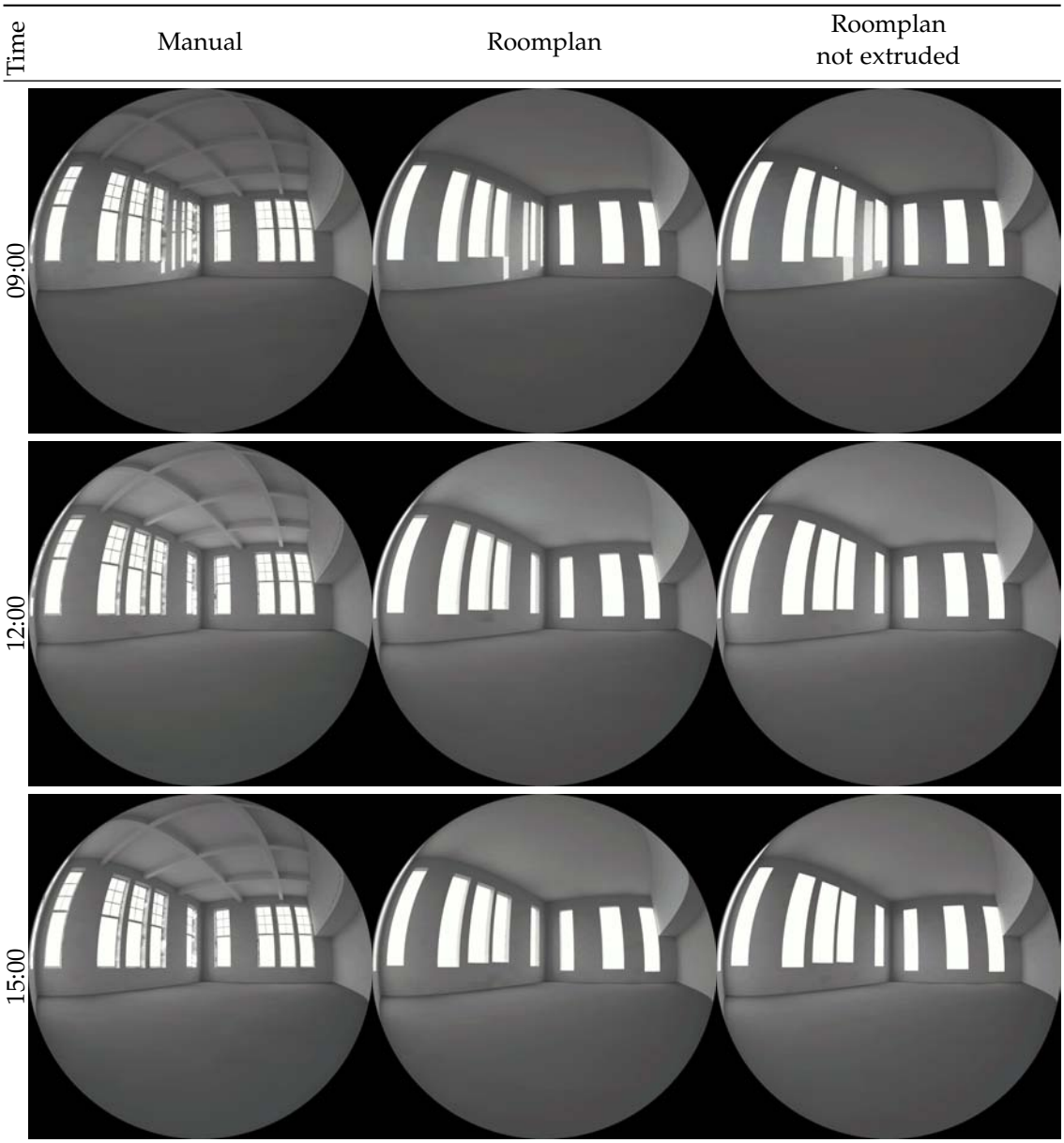

Figure D.12.: Black and white renderings of GeoinfoLab on 21 December (Winter Solstice)

D.2. Falsecolor

Time	Manual	Roomplan	Roomplan not extruded	cd/m^2
09:00	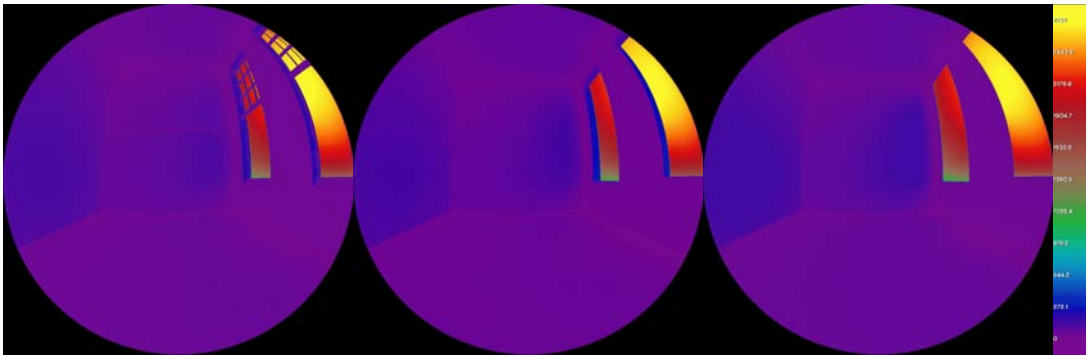			
	DGP: 0.20194 **Category:** Imperceptible Glare	**DGP:** 0.20385 **Category:** Imperceptible Glare	**DGP:** 0.20972 **Category:** Imperceptible Glare	2721
12:00	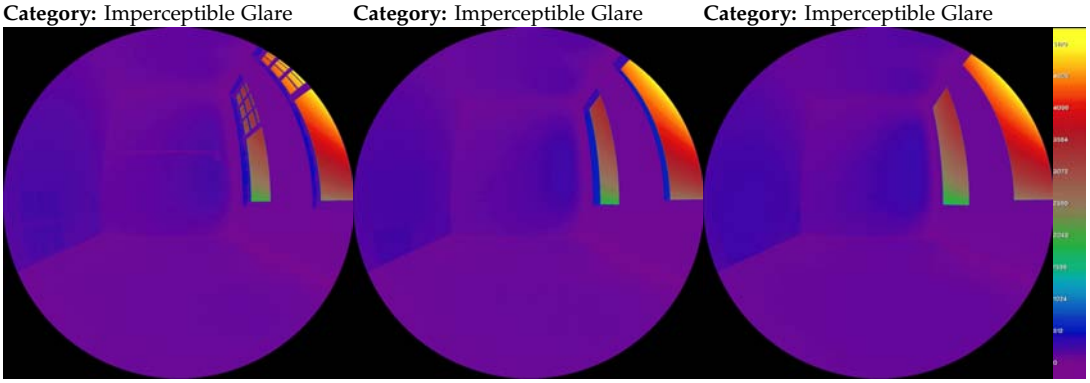			
	DGP: 0.23458 **Category:** Imperceptible Glare	**DGP:** 0.23740 **Category:** Imperceptible Glare	**DGP:** 0.24867 **Category:** Imperceptible Glare	5120
15:00	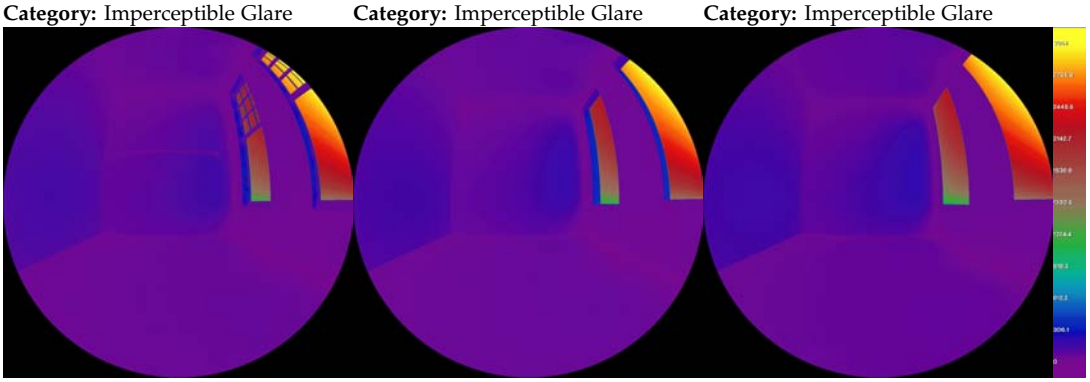			
	DGP: 0.20438 **Category:** Imperceptible Glare	**DGP:** 0.20636 **Category:** Imperceptible Glare	**DGP:** 0.21272 **Category:** Imperceptible Glare	3061

Figure D.13.: False-color renders of Room BGW 640 on the 20th of March (Spring Equinox)

Time	Manual	Roomplan	Roomplan not extruded	cd/m^2
09:00	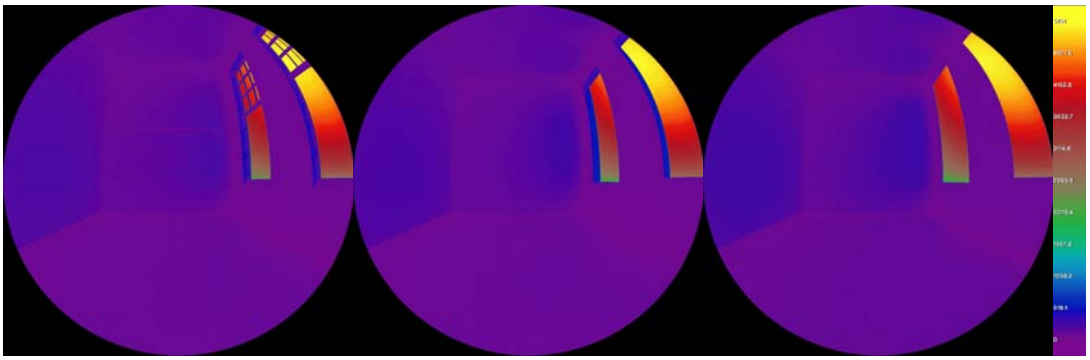			
	DGP: 0.24001 **Category:** Imperceptible Glare	**DGP:** 0.24342 **Category:** Imperceptible Glare	**DGP:** 0.25645 **Category:** Imperceptible Glare	5191
12:00	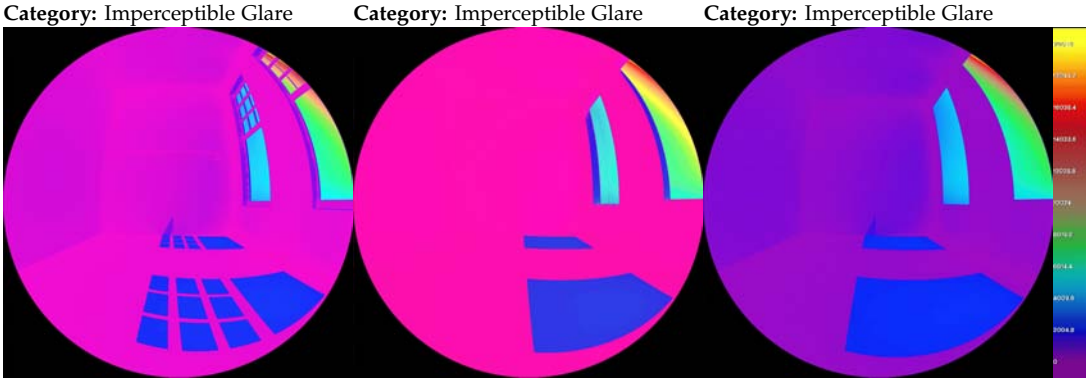			
	DGP: 0.33077 **Category:** Imperceptible Glare	**DGP:** 0.34003 **Category:** Imperceptible Glare	**DGP:** 0.36874 **Category:** Perceptible Glare	20048
15:00	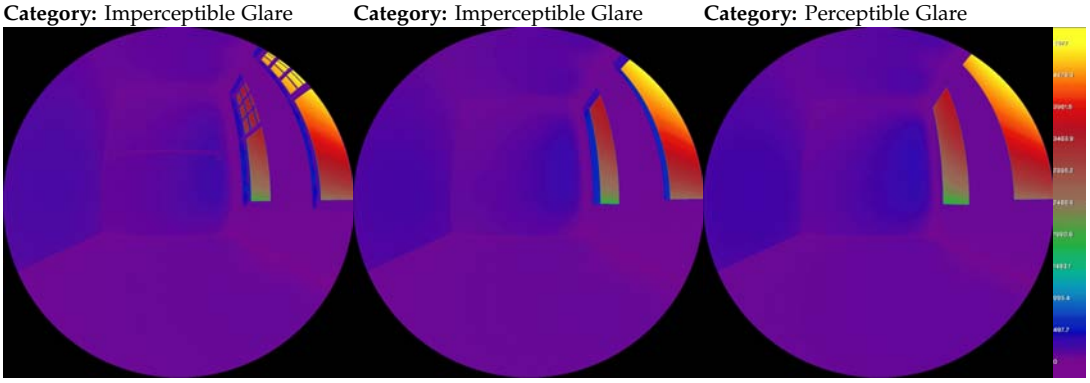			
	DGP: 0.23508 **Category:** Imperceptible Glare	**DGP:** 0.23799 **Category:** Imperceptible Glare	**DGP:** 0.24961 **Category:** Imperceptible Glare	4977

Figure D.14.: False-color renders of Room BGW 640 on the 21st of June (Summer Solstice)

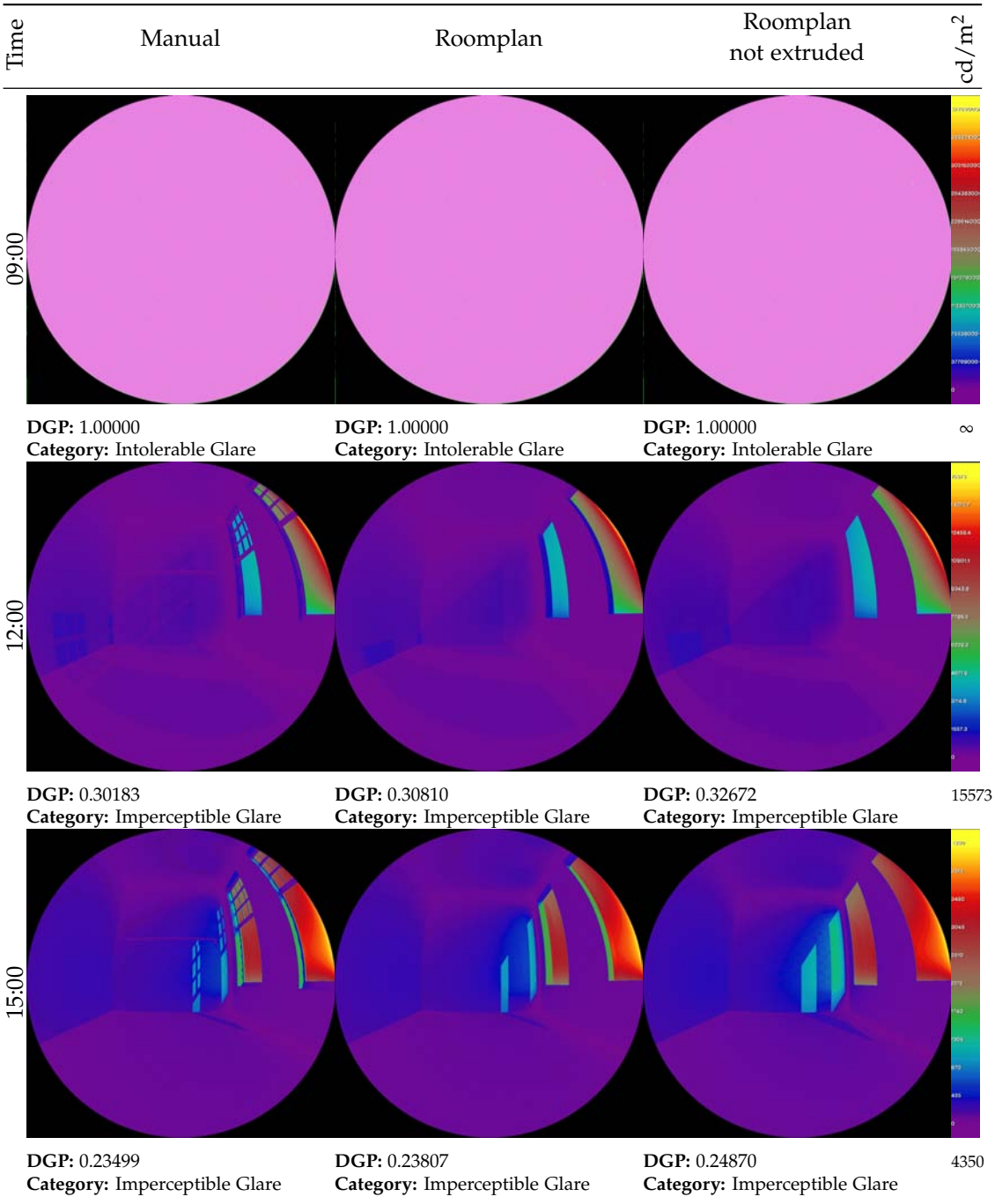

Figure D.15.: False-color renders of Room BGW 640 on the 22nd of September (Autumn Equinox)

Time	Manual	Roomplan	Roomplan not extruded	cd/m^2
09:00	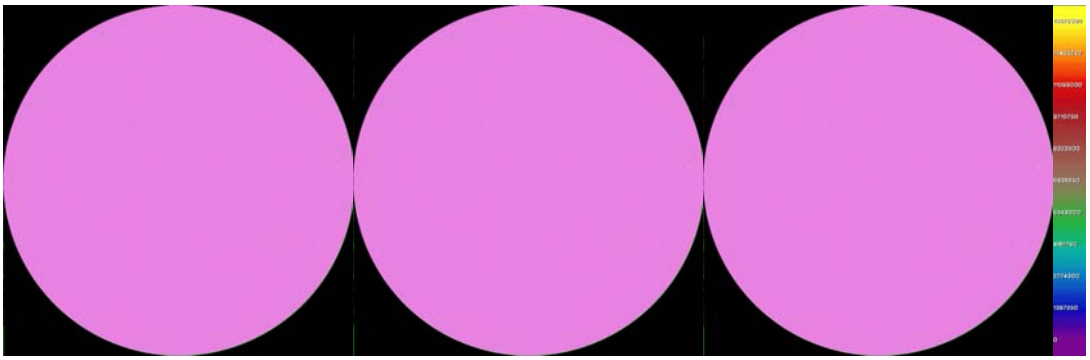			
	DGP: 0.46101 **Category:** Intolerable Glare	**DGP:** 0.45703 **Category:** Intolerable Glare	**DGP:** 0.45762 **Category:** Intolerable Glare	
12:00	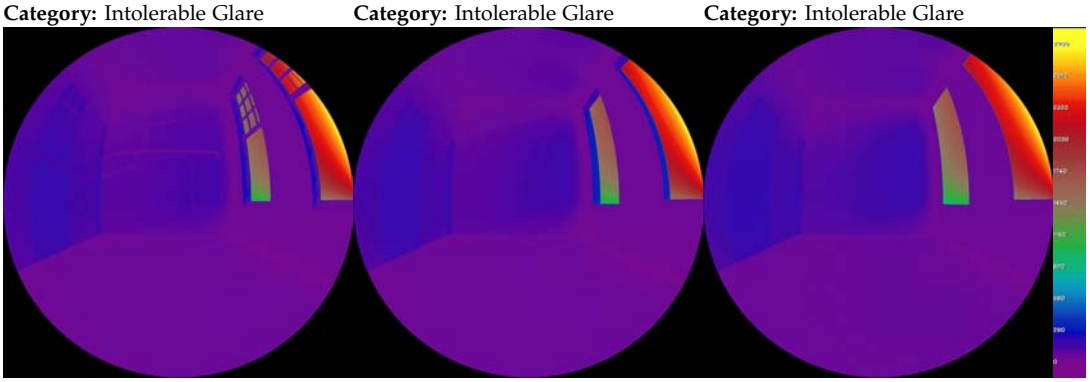			
	DGP: 0.19983 **Category:** Imperceptible Glare	**DGP:** 0.20142 **Category:** Imperceptible Glare	**DGP:** 0.20681 **Category:** Imperceptible Glare	2900
15:00	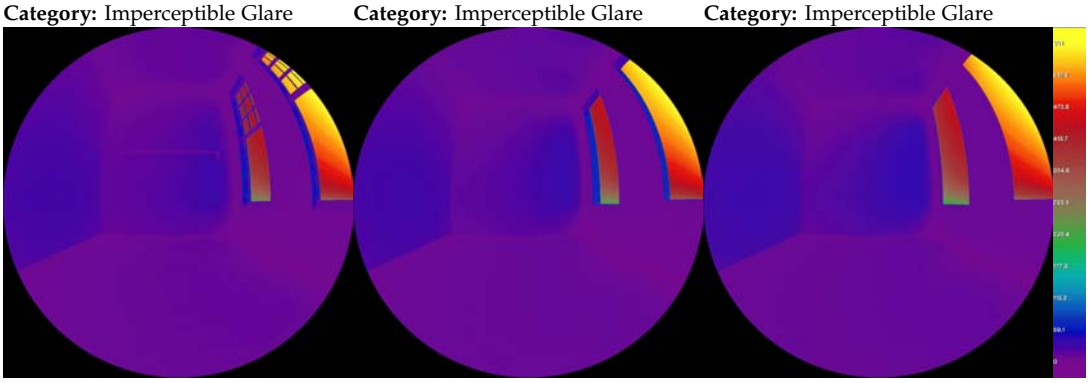			
	DGP: 0.04585 **Category:** Imperceptible Glare	**DGP:** 0.05235 **Category:** Imperceptible Glare	**DGP:** 0.07814 **Category:** Imperceptible Glare	591

Figure D.16.: False-color renders of Room BGW 640 on the 21st of December (Winter Solstice)

Time	Manual	Roomplan	Roomplan not extruded	cd/m^2
09:00	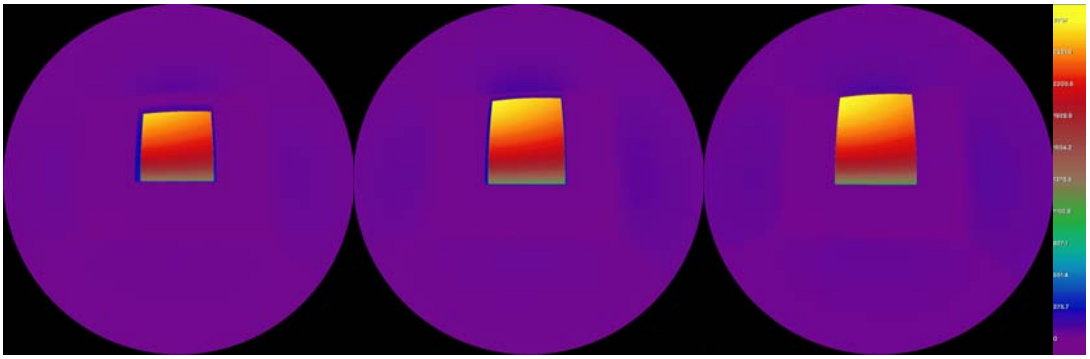			
	DGP: 0.23637 **Category:** Imperceptible Glare	**DGP:** 0.23503 **Category:** Imperceptible Glare	**DGP:** 0.23551 **Category:** Imperceptible Glare	2757
12:00	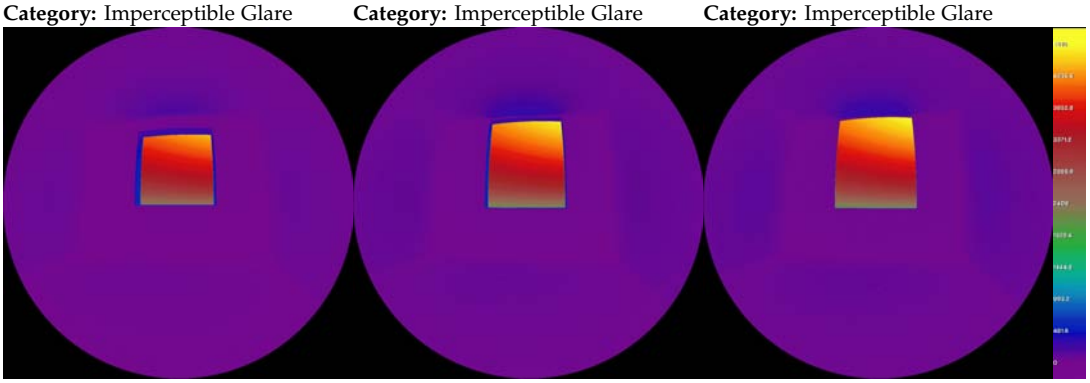			
	DGP: 0.26832 **Category:** Imperceptible Glare	**DGP:** 0.27099 **Category:** Imperceptible Glare	**DGP:** 0.27370 **Category:** Imperceptible Glare	4816
15:00	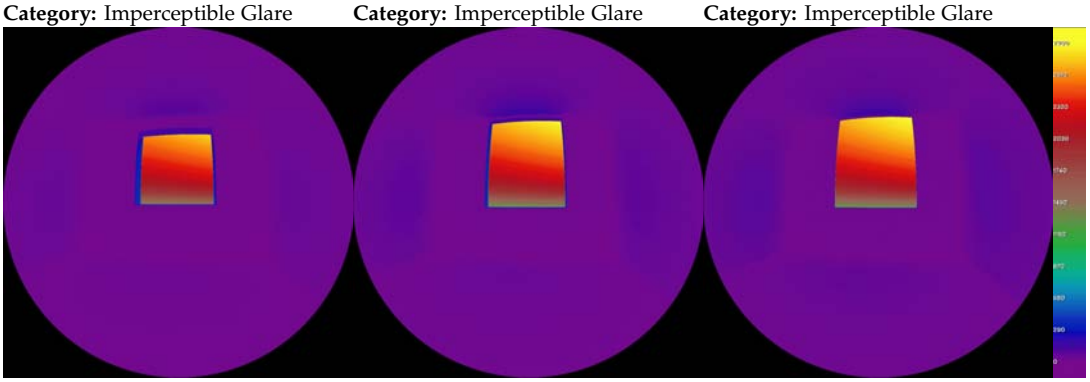			
	DGP: 0.24053 **Category:** Imperceptible Glare	**DGP:** 0.23863 **Category:** Imperceptible Glare	**DGP:** 0.23910 **Category:** Imperceptible Glare	2900

Figure D.17.: False-color renders of Room W01050 on the 20th of March (Spring Equinox)

Time	Manual	Roomplan	Roomplan not extruded	cd/m^2
09:00	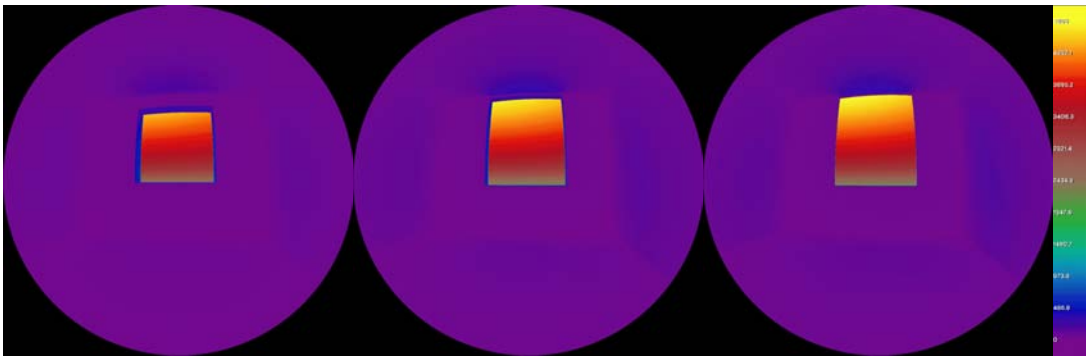			
	DGP: 0.26985 **Category:** Imperceptible Glare	**DGP:** 0.27309 **Category:** Imperceptible Glare	**DGP:** 0.27614 **Category:** Imperceptible Glare	4869
12:00	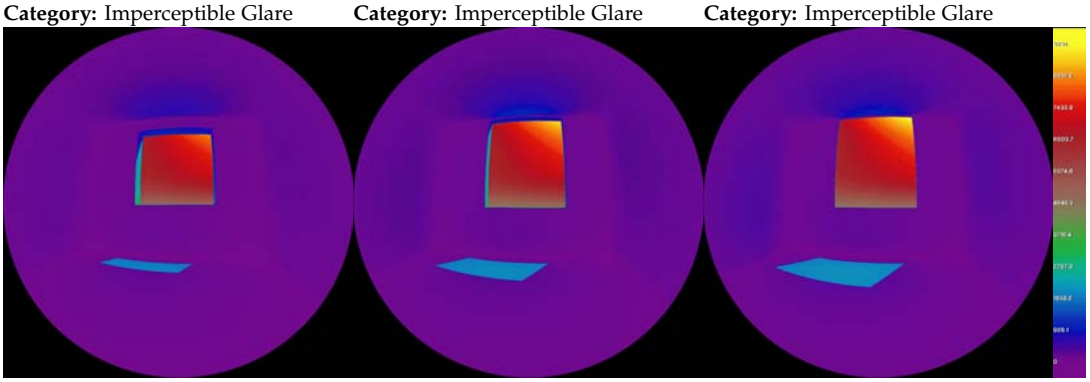			
	DGP: 0.31155 **Category:** Imperceptible Glare	**DGP:** 0.32956 **Category:** Imperceptible Glare	**DGP:** 0.33924 **Category:** Imperceptible Glare	9291
15:00	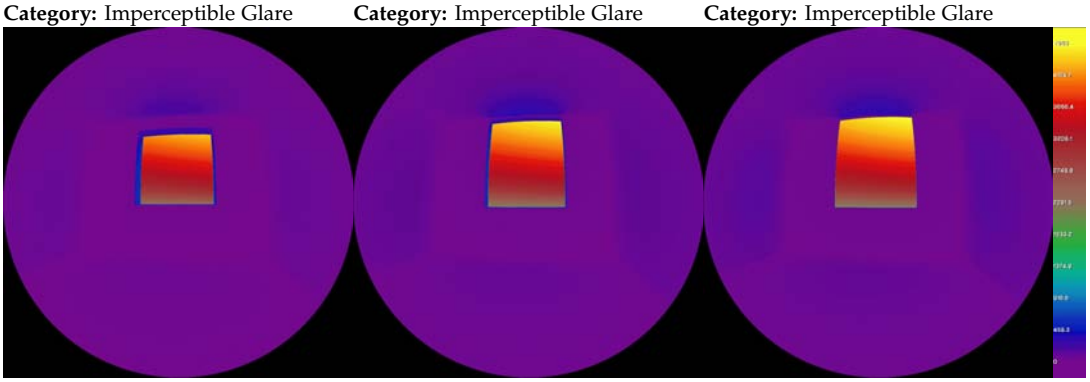			
	DGP: 0.26696 **Category:** Imperceptible Glare	**DGP:** 0.26952 **Category:** Imperceptible Glare	**DGP:** 0.27219 **Category:** Imperceptible Glare	4583

Figure D.18.: False-color renders of Room W01050 on the 21st of June (Summer Solstice)

Time	Manual	Roomplan	Roomplan not extruded	cd/m^2
09:00	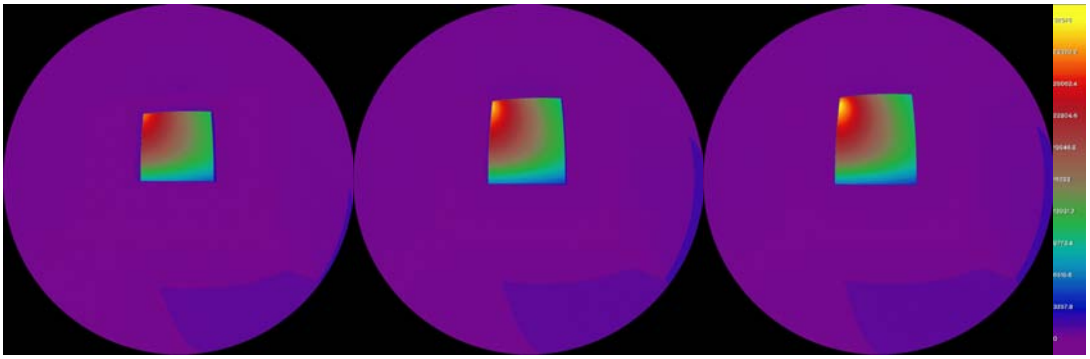			
	DGP: 0.41230 **Category:** Disturbing Glare	**DGP:** 0.45491 **Category:** Intolerable Glare	**DGP:** 0.47668 **Category:** Intolerable Glare	32578
12:00	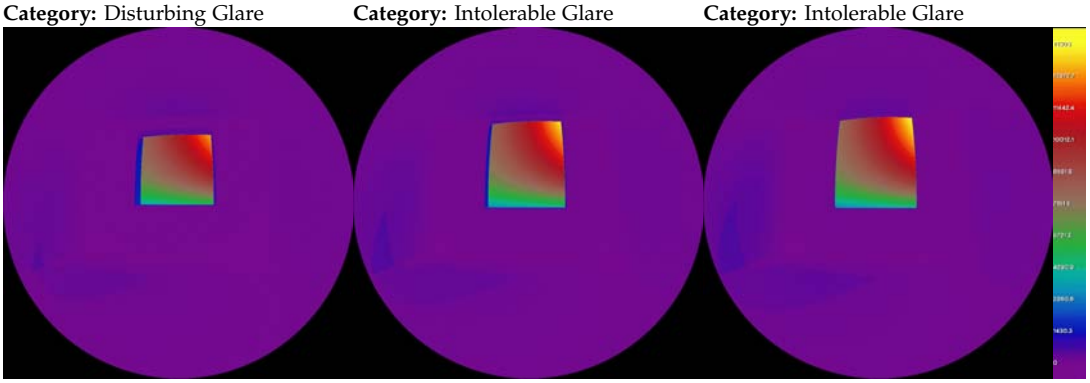			
	DGP: 0.32615 **Category:** Imperceptible Glare	**DGP:** 0.34468 **Category:** Imperceptible Glare	**DGP:** 0.35433 **Category:** Perceptible Glare	14303
15:00	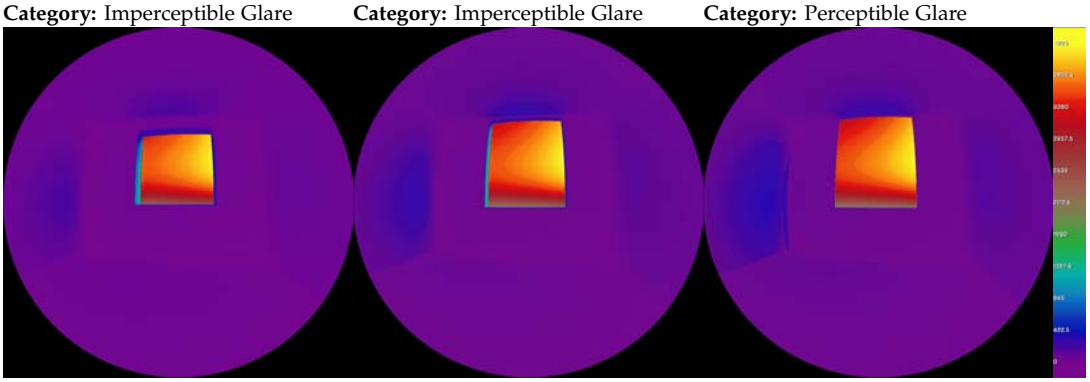			
	DGP: 0.26840 **Category:** Imperceptible Glare	**DGP:** 0.26914 **Category:** Imperceptible Glare	**DGP:** 0.27111 **Category:** Imperceptible Glare	4225

Figure D.19.: False-color renders of Room W01050 on the 22nd of September (Autumn Equinox)

Time	Manual	Roomplan	Roomplan not extruded	cd/m^2
09:00	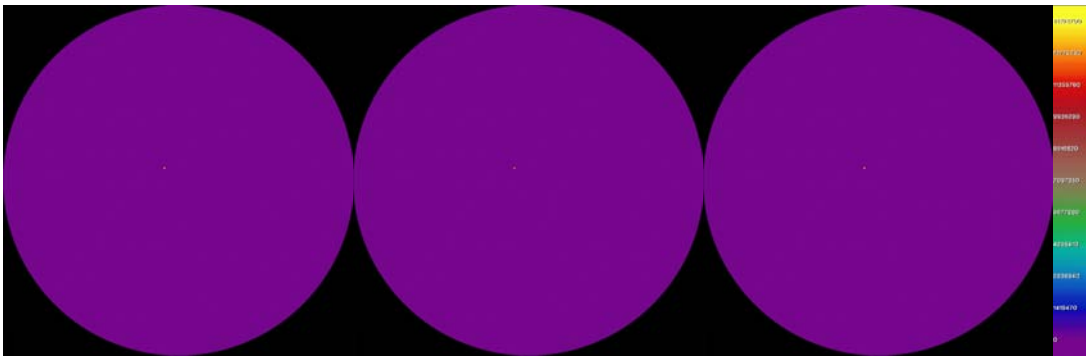			
	DGP: 0.60192 **Category:** Intolerable Glare	**DGP:** 0.59605 **Category:** Intolerable Glare	**DGP:** 0.59992 **Category:** Intolerable Glare	∞
12:00	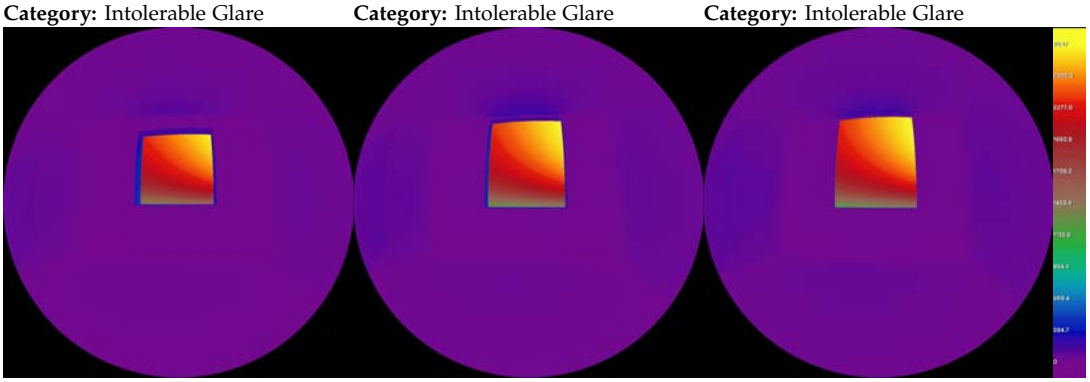			
	DGP: 0.24025 **Category:** Imperceptible Glare	**DGP:** 0.23789 **Category:** Imperceptible Glare	**DGP:** 0.23803 **Category:** Imperceptible Glare	2847
15:00	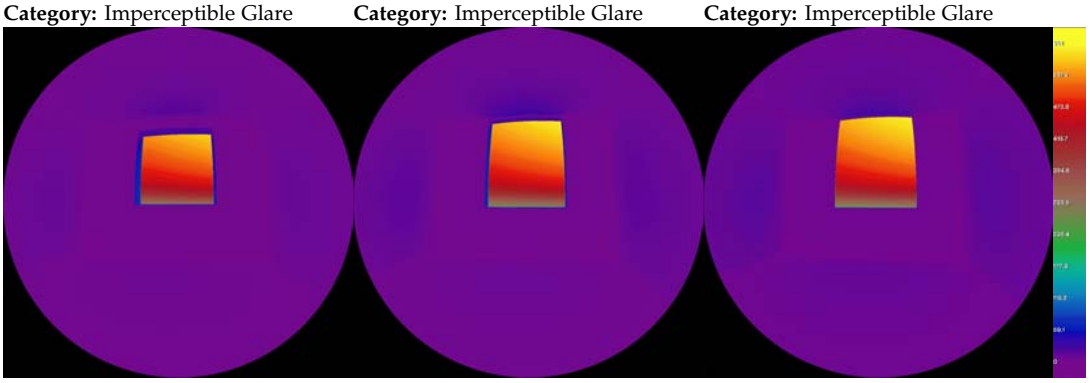			
	DGP: 0.02390 **Category:** Imperceptible Glare	**DGP:** 0.04161 **Category:** Imperceptible Glare	**DGP:** 0.05264 **Category:** Imperceptible Glare	591

Figure D.20.: False-color renders of Room W01050 on the 21st of December (Winter Solstice)

Time	Manual	Roomplan	Roomplan not extruded	cd/m^2
09:00	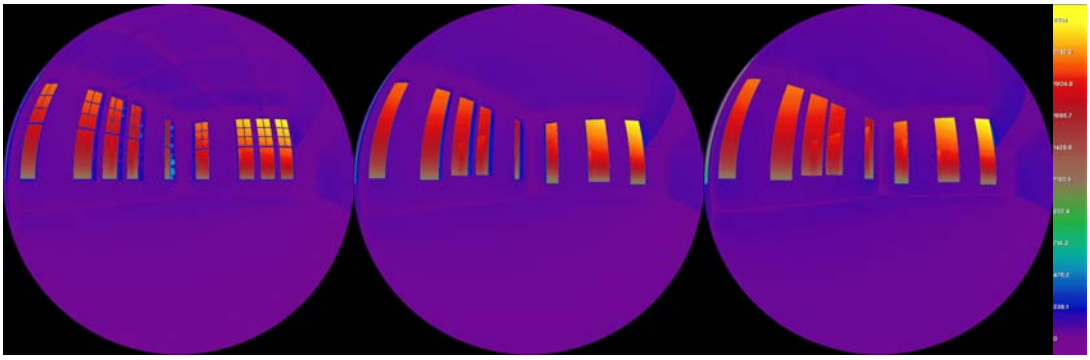			
	DGP: 0.20392 **Category:** Imperceptible Glare	**DGP:** 0.20595 **Category:** Imperceptible Glare	**DGP:** 0.21268 **Category:** Imperceptible Glare	2381
12:00	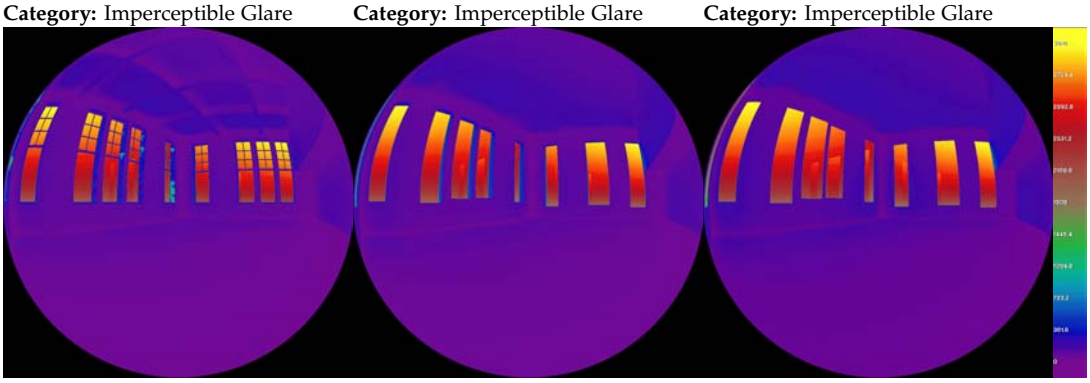			
	DGP: 0.25298 **Category:** Imperceptible Glare	**DGP:** 0.25613 **Category:** Imperceptible Glare	**DGP:** 0.26601 **Category:** Imperceptible Glare	3616
15:00	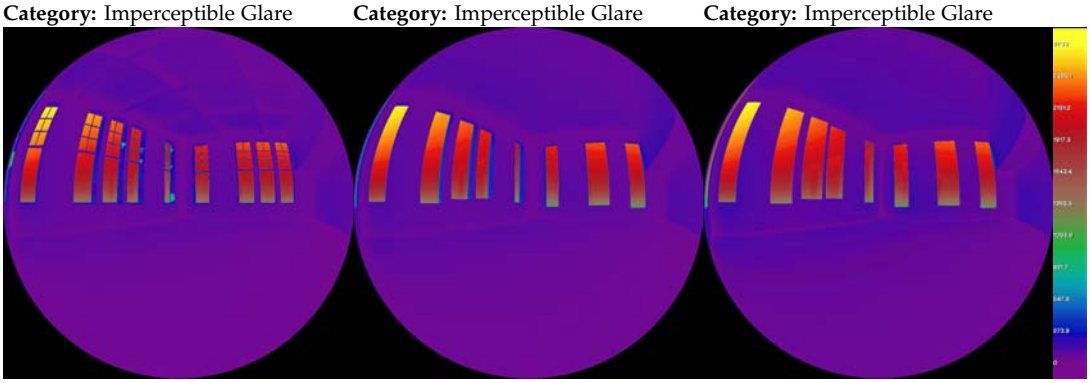			
	DGP: 0.21779 **Category:** Imperceptible Glare	**DGP:** 0.22189 **Category:** Imperceptible Glare	**DGP:** 0.22865 **Category:** Imperceptible Glare	2739

Figure D.21.: False-color renders of Room GeoinfoLab on the 20th of March (Spring Equinox)591.5302pt418.25368pt

Time	Manual	Roomplan	Roomplan not extruded	cd/m^2
09:00	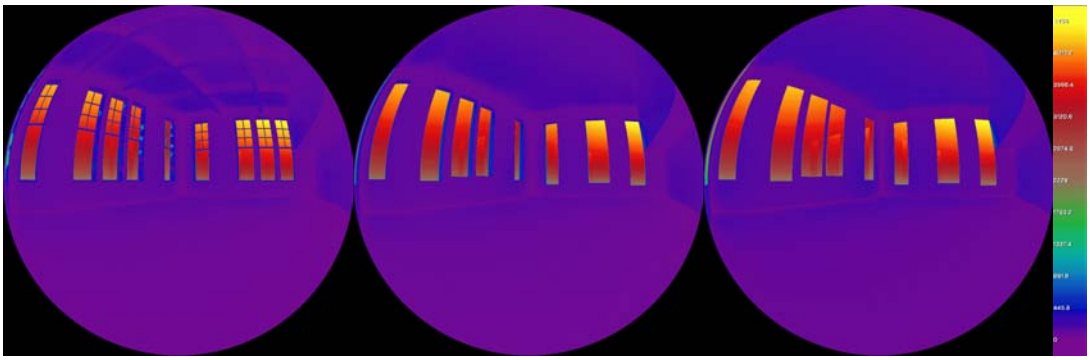			
	DGP: 0.26441 **Category:** Imperceptible Glare	**DGP:** 0.26846 **Category:** Imperceptible Glare	**DGP:** 0.28061 **Category:** Imperceptible Glare	4458
12:00	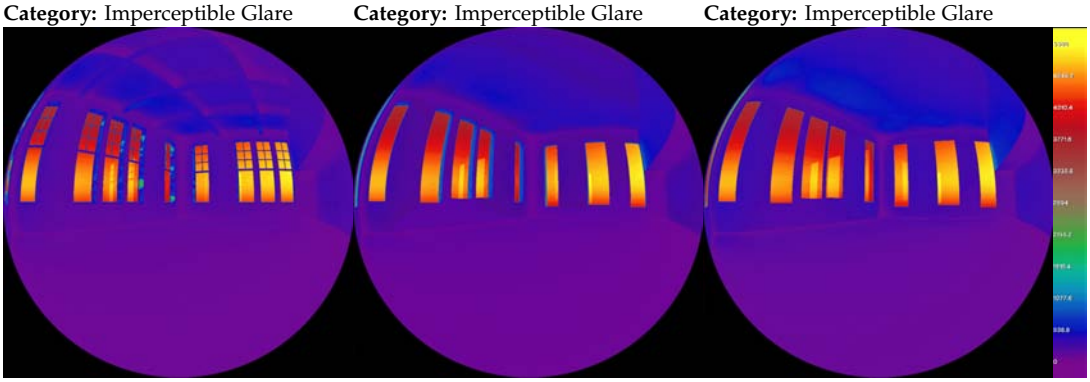			
	DGP: 0.29340 **Category:** Imperceptible Glare	**DGP:** 0.30007 **Category:** Imperceptible Glare	**DGP:** 0.31770 **Category:** Imperceptible Glare	5388
15:00	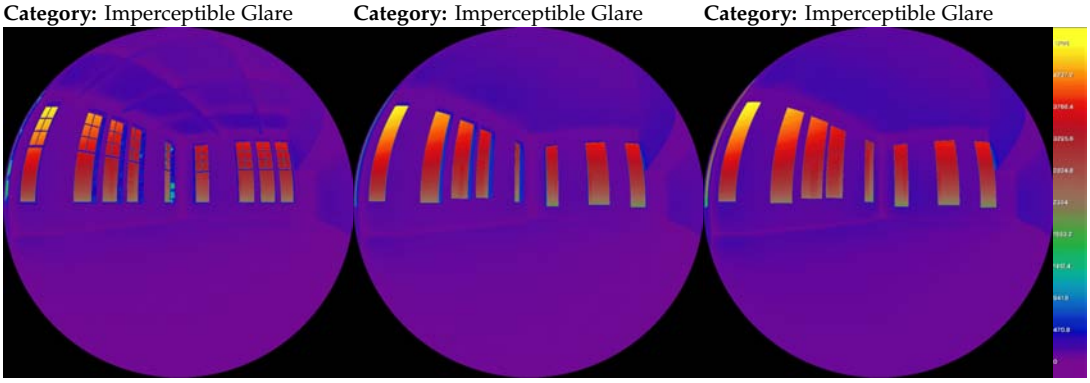			
	DGP: 0.26178 **Category:** Imperceptible Glare	**DGP:** 0.26645 **Category:** Imperceptible Glare	**DGP:** 0.27877 **Category:** Imperceptible Glare	4708

Figure D.22.: False-color renders of Room GeoinfoLab on the 21st of June (Summer Solstice)

Time	Manual	Roomplan	Roomplan not extruded	cd/m^2
09:00	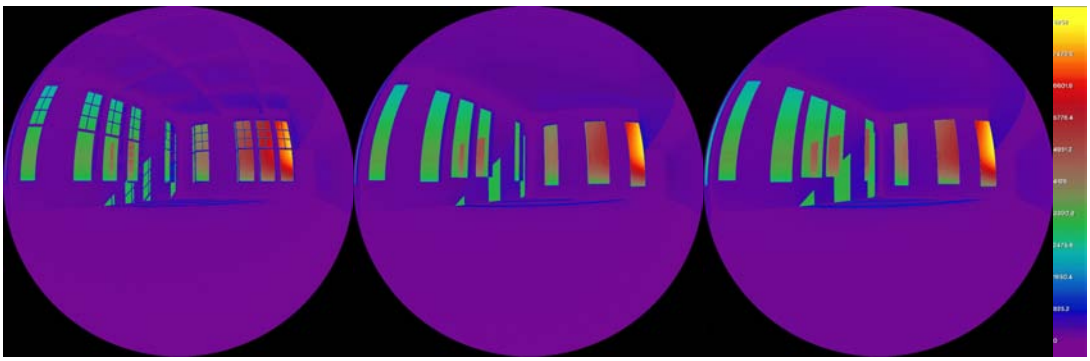			
	DGP: 0.28591 **Category:** Imperceptible Glare	**DGP:** 0.28872 **Category:** Imperceptible Glare	**DGP:** 0.30198 **Category:** Imperceptible Glare	8252
12:00	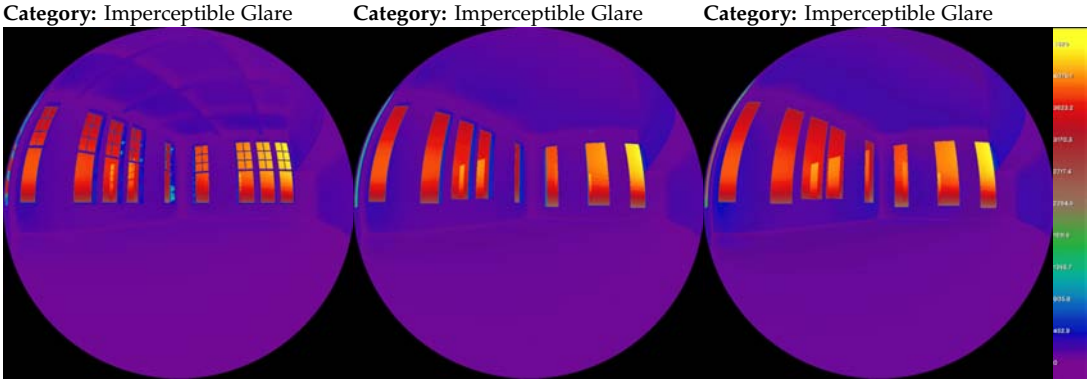			
	DGP: 0.26986 **Category:** Imperceptible Glare	**DGP:** 0.27376 **Category:** Imperceptible Glare	**DGP:** 0.28639 **Category:** Imperceptible Glare	4529
15:00	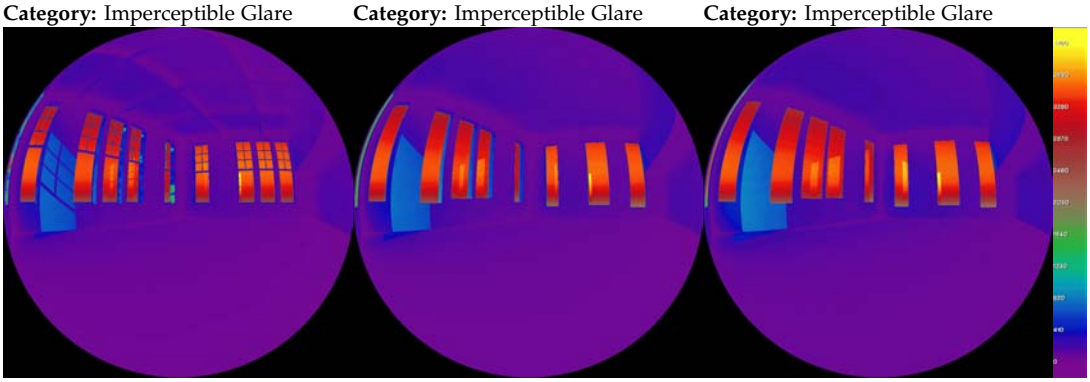			
	DGP: 0.26287 **Category:** Imperceptible Glare	**DGP:** 0.26695 **Category:** Imperceptible Glare	**DGP:** 0.27821 **Category:** Imperceptible Glare	4100

Figure D.23.: False-color renders of Room GeoinfoLab on the 22nd of September (Autumn Equinox)

Time	Manual	Roomplan	Roomplan not extruded	cd/m^2
09:00	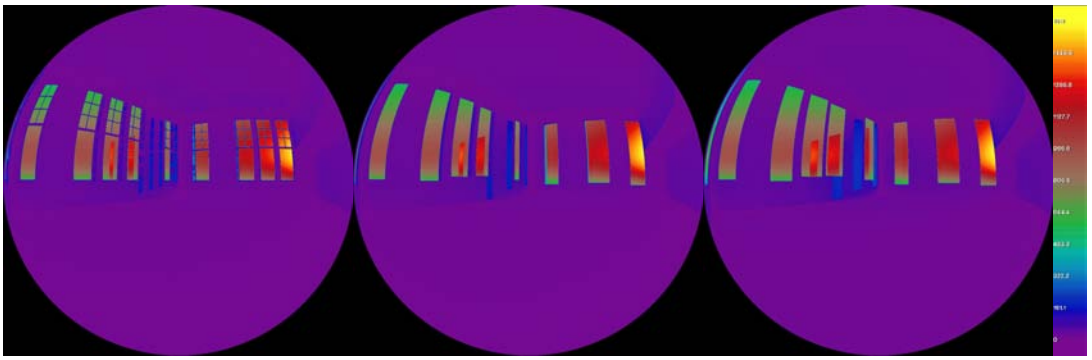			
	DGP: 0.16919 **Category:** Imperceptible Glare	**DGP:** 0.17334 **Category:** Imperceptible Glare	**DGP:** 0.18069 **Category:** Imperceptible Glare	1611
12:00	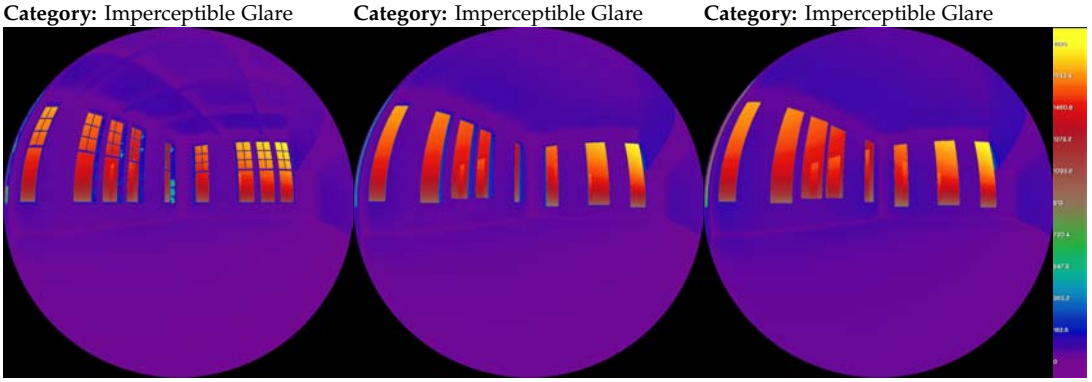			
	DGP: 0.18739 **Category:** Imperceptible Glare	**DGP:** 0.19015 **Category:** Imperceptible Glare	**DGP:** 0.19649 **Category:** Imperceptible Glare	1826
15:00	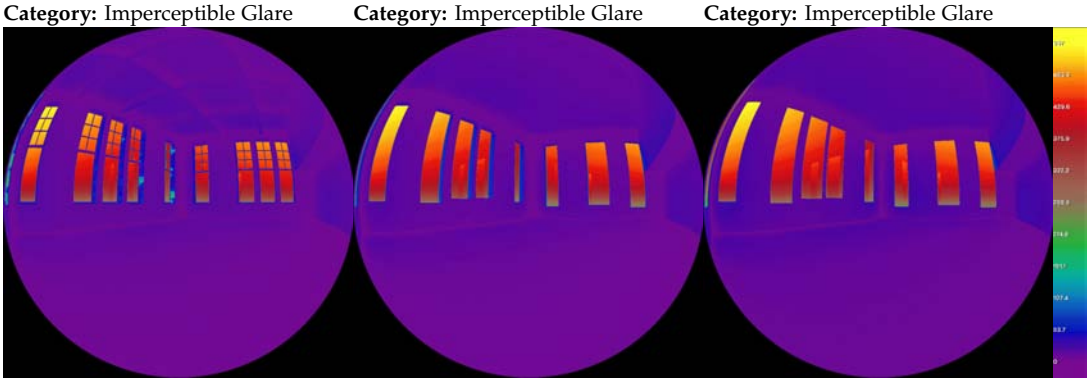			
	DGP: 0.05498 **Category:** Imperceptible Glare	**DGP:** 0.06748 **Category:** Imperceptible Glare	**DGP:** 0.09910 **Category:** Imperceptible Glare	537

Figure D.24.: False-color renders of Room GeoinfoLab on the 21st of December (Winter Solstice)

E. Heatmaps

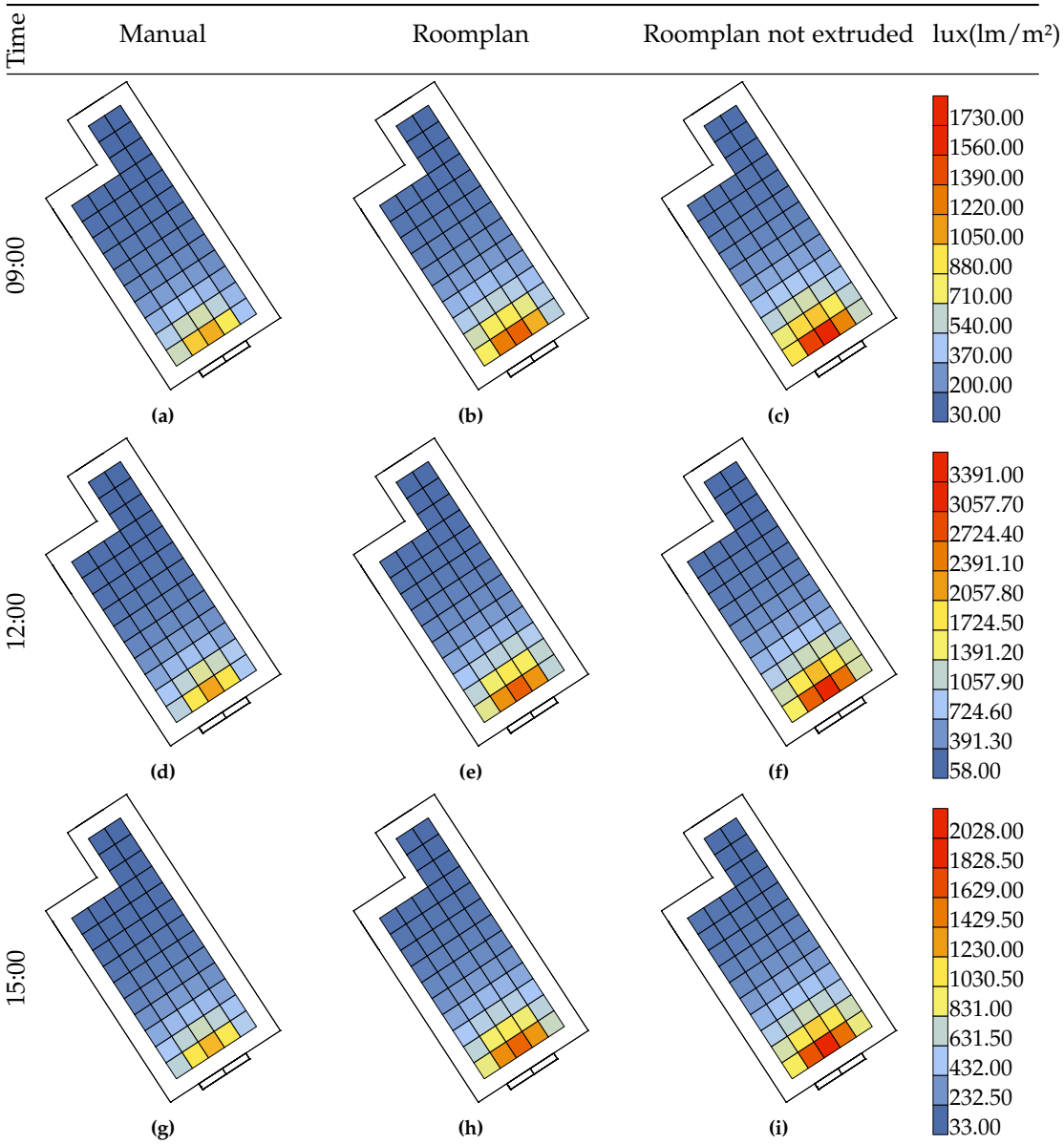

Figure E.1.: Heatmaps of illuminance for the 20th of March (Spring Equinox) for W01050. 418.25368pt-0.56833pt35.28255pt

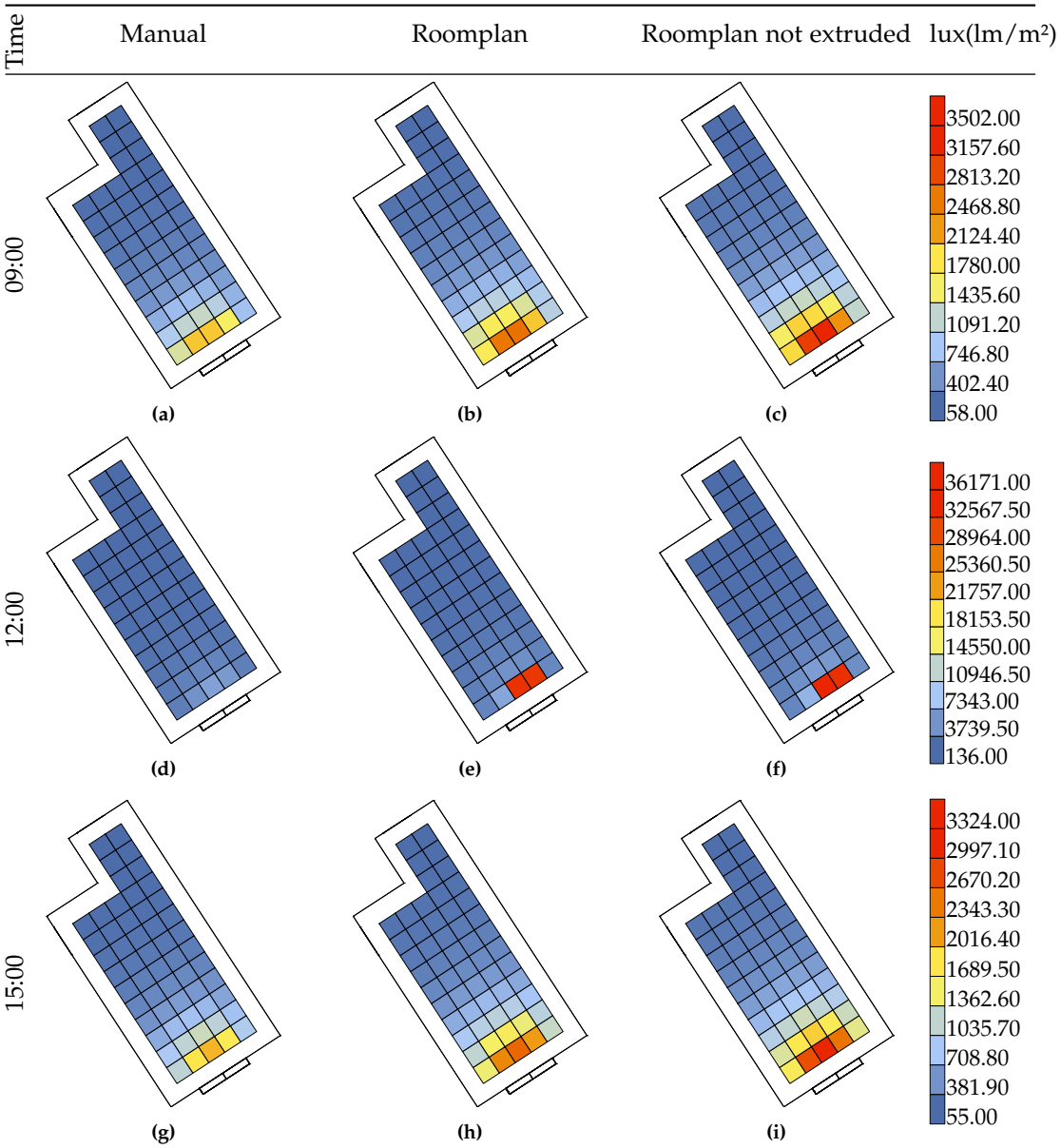

Figure E.2.: Heatmaps of illuminance for the 21st of June (Summer Solstice) for Room BGW640.

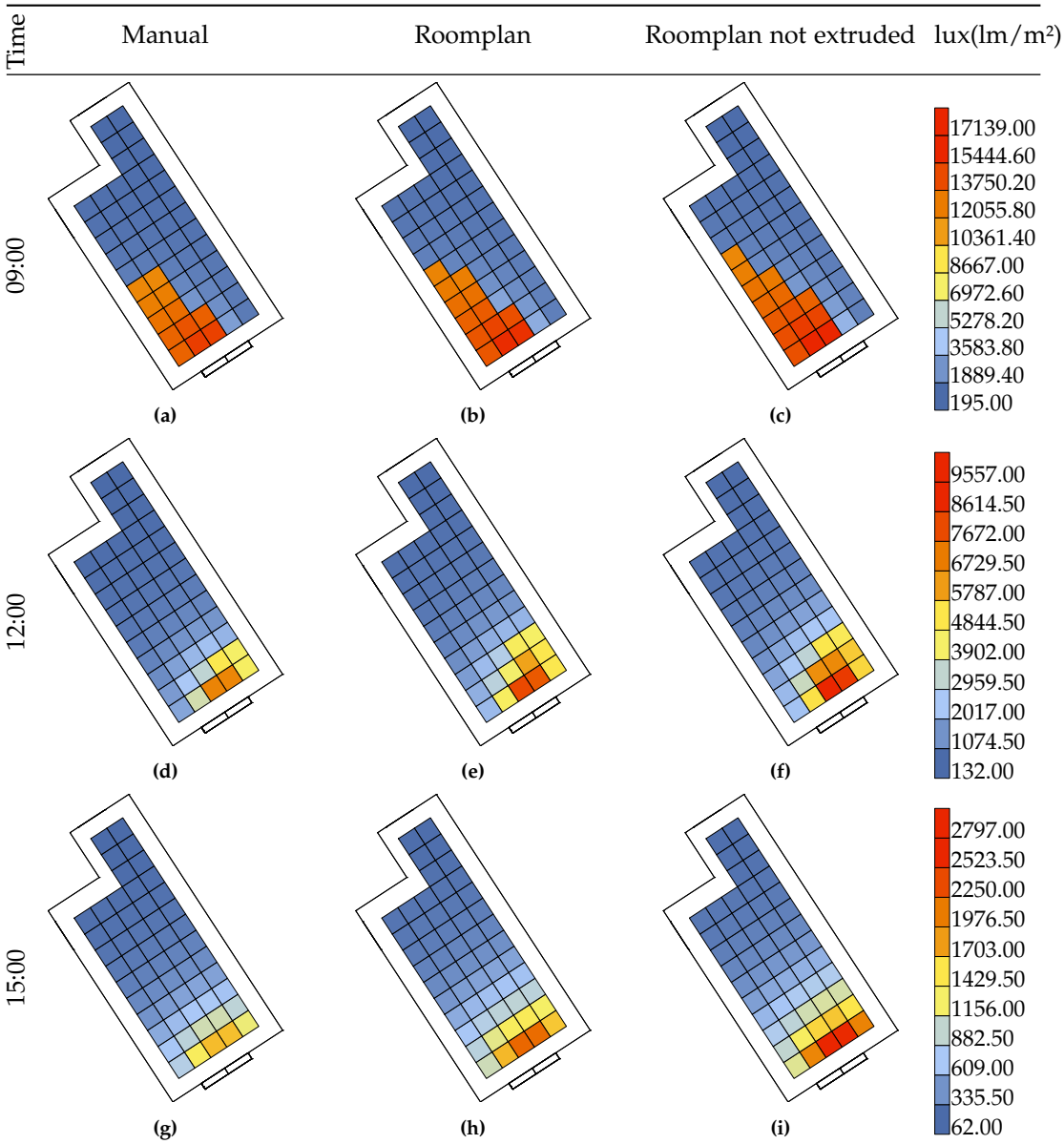

Figure E.3.: Heatmaps of illuminance for the 22nd of September (Autumn Equinox) for GeoinfoLab.

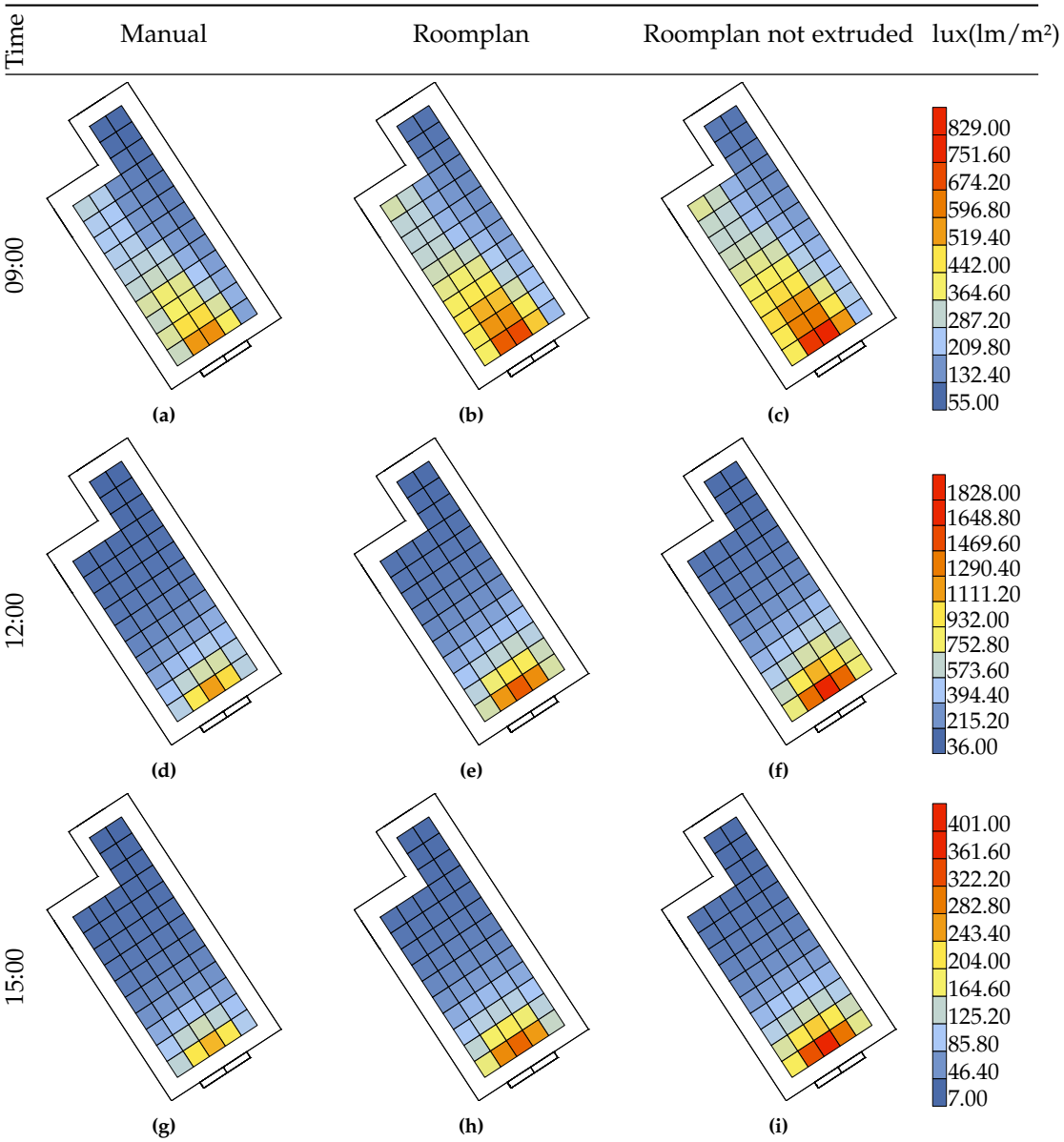

Figure E.4.: Heatmaps of illuminance for the 21st of December (Winter Solstice) for Room BGW640.

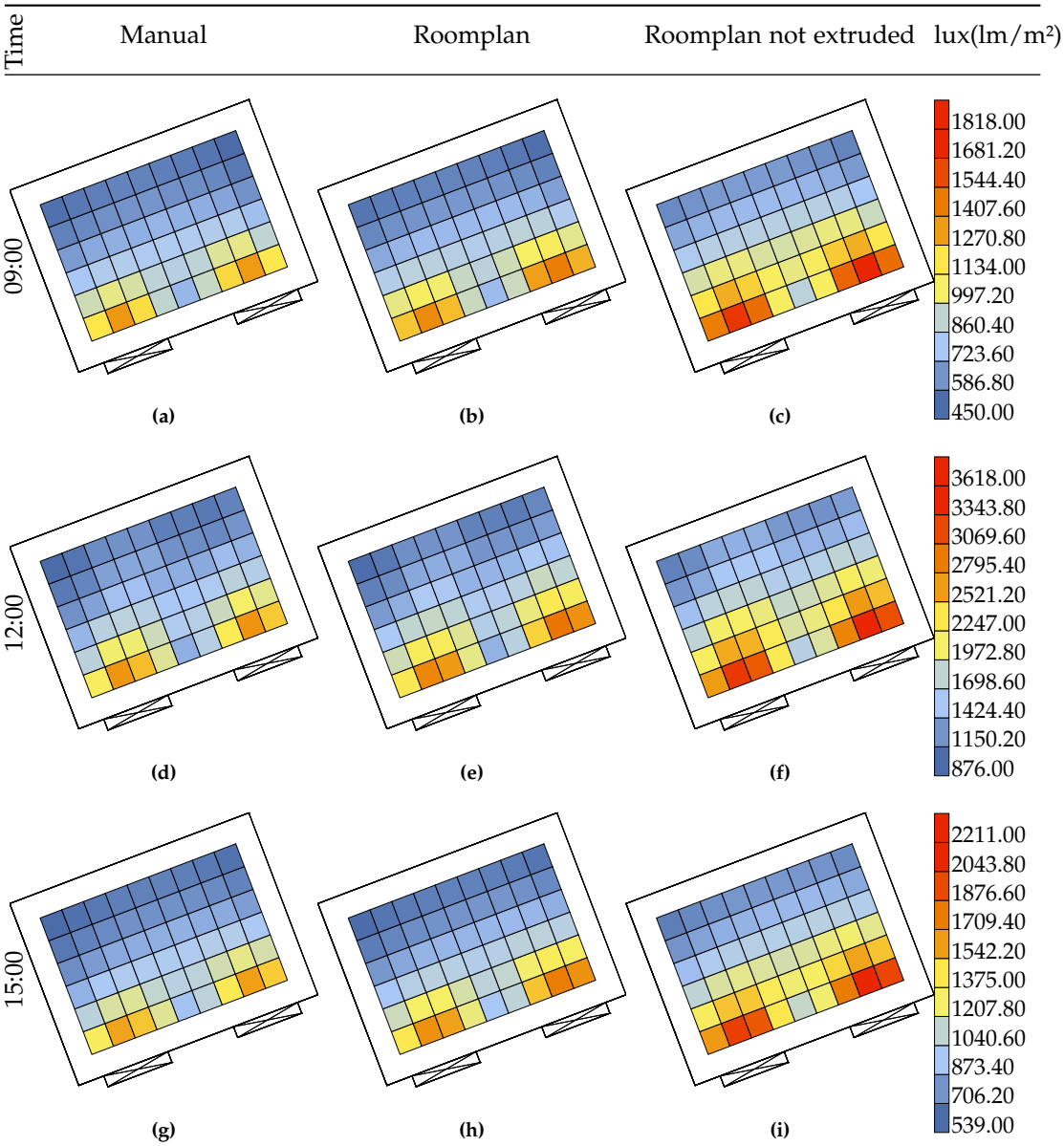

Figure E.5.: Heatmaps of illuminance for the 20th of March (Spring Equinox) for Room BGW640.

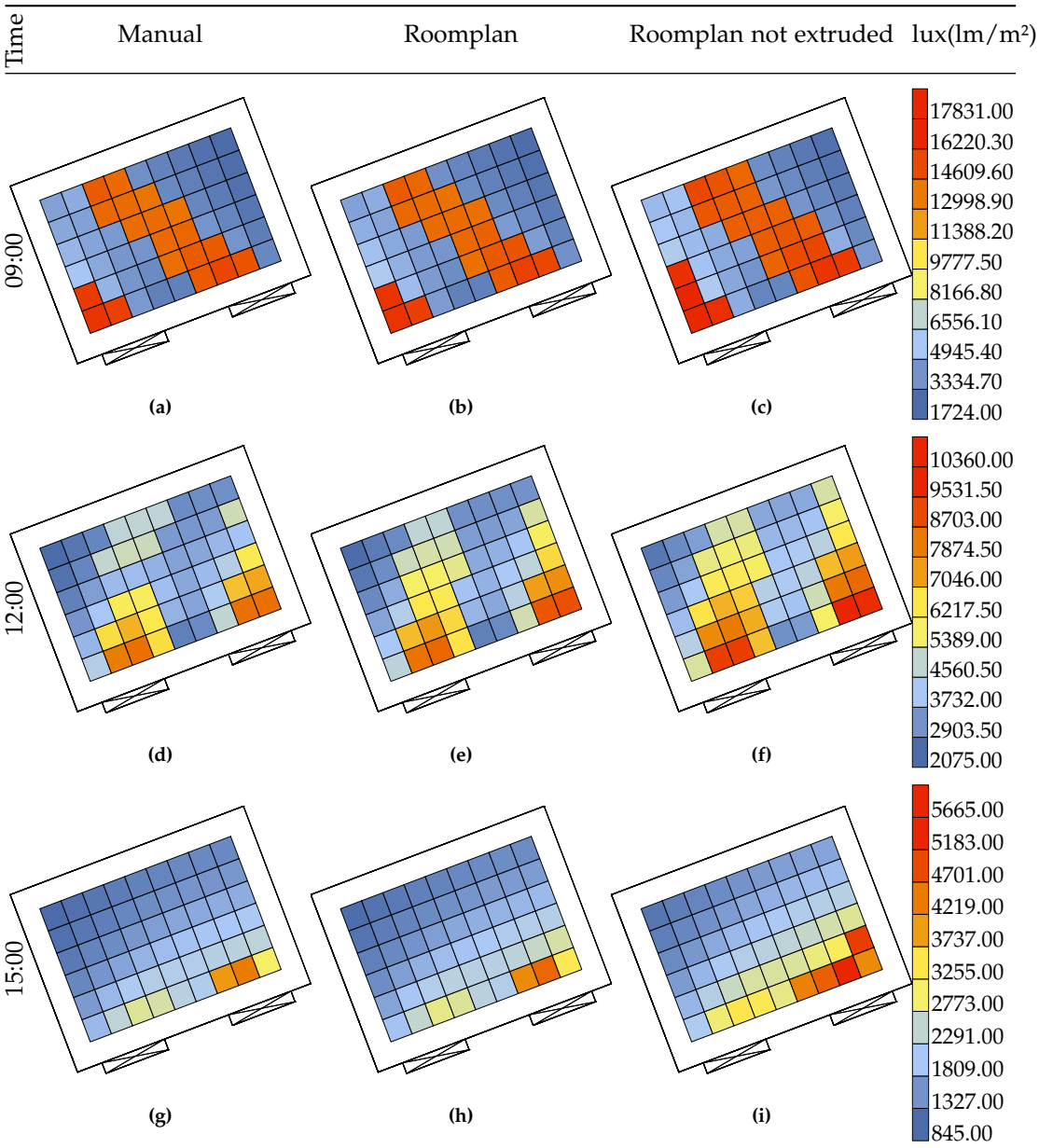

Figure E.6.: Heatmaps of illuminance for the 22nd of September (Autumn Equinox) for Room BGW640.

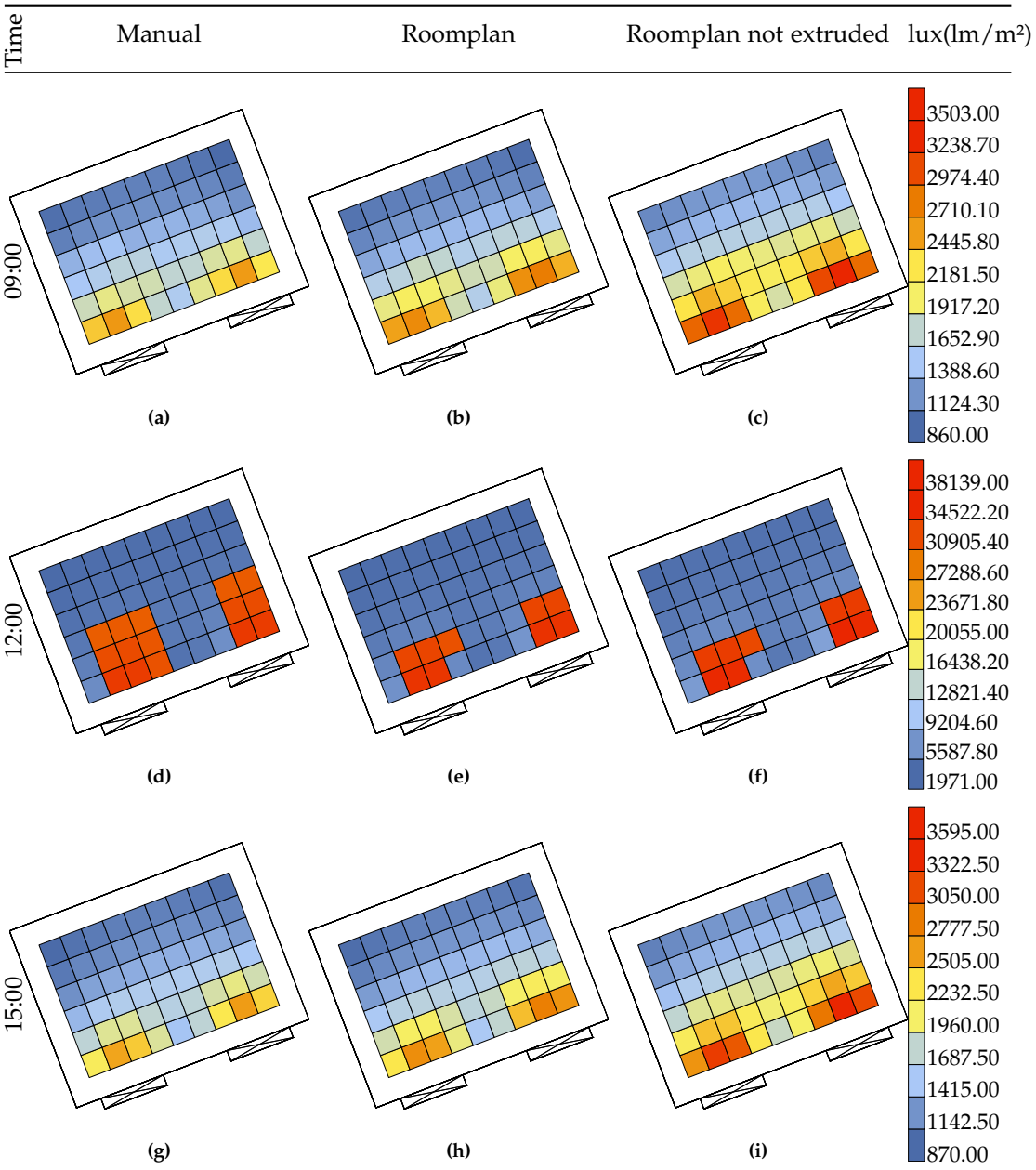

Figure E.7.: Heatmaps of illuminance for the 21st of June (Summer Solstice) for Room BGW640.

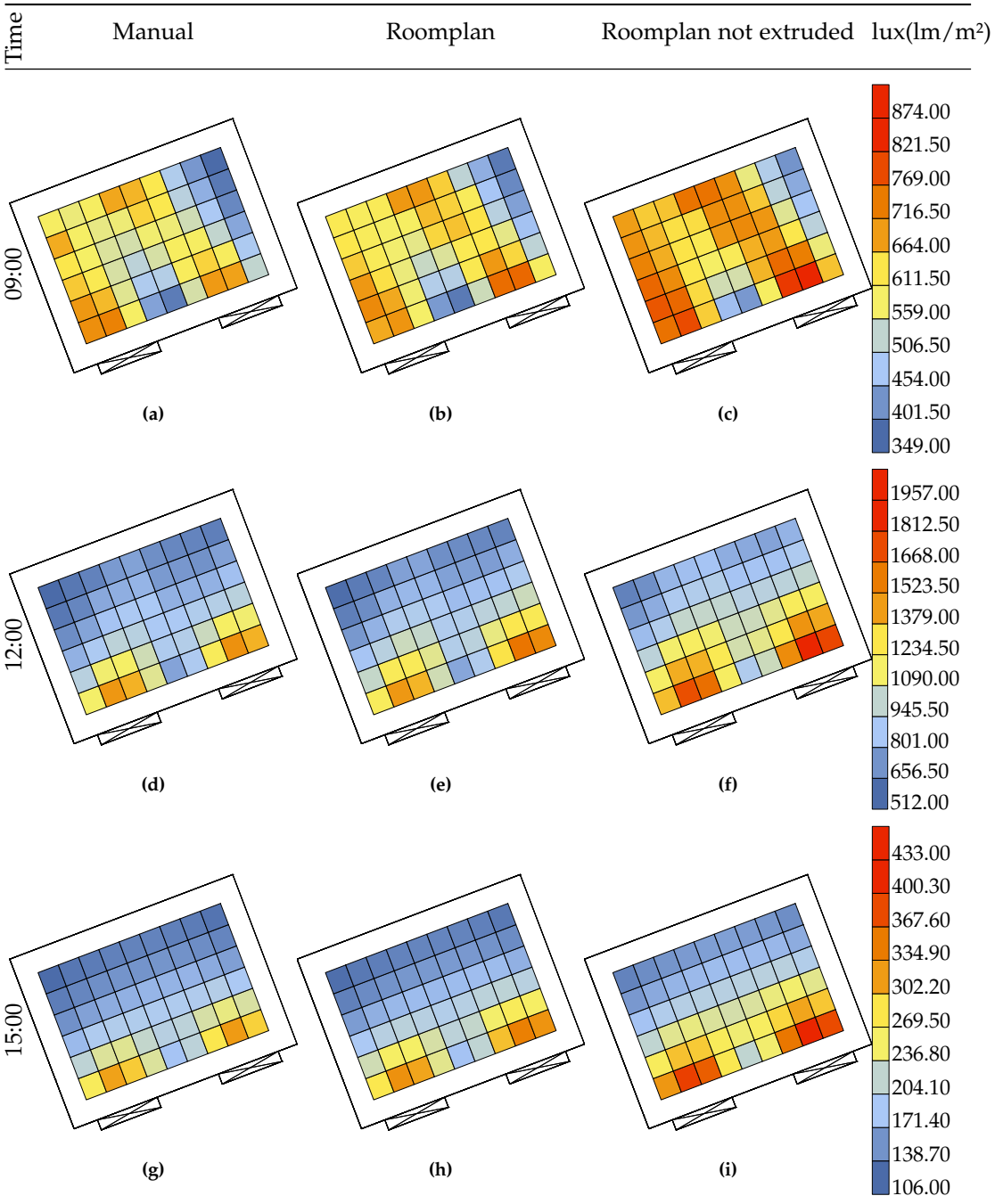

Figure E.8.: Heatmaps of illuminance for the 21st of December (Winter Solstice) for Room BGW640.

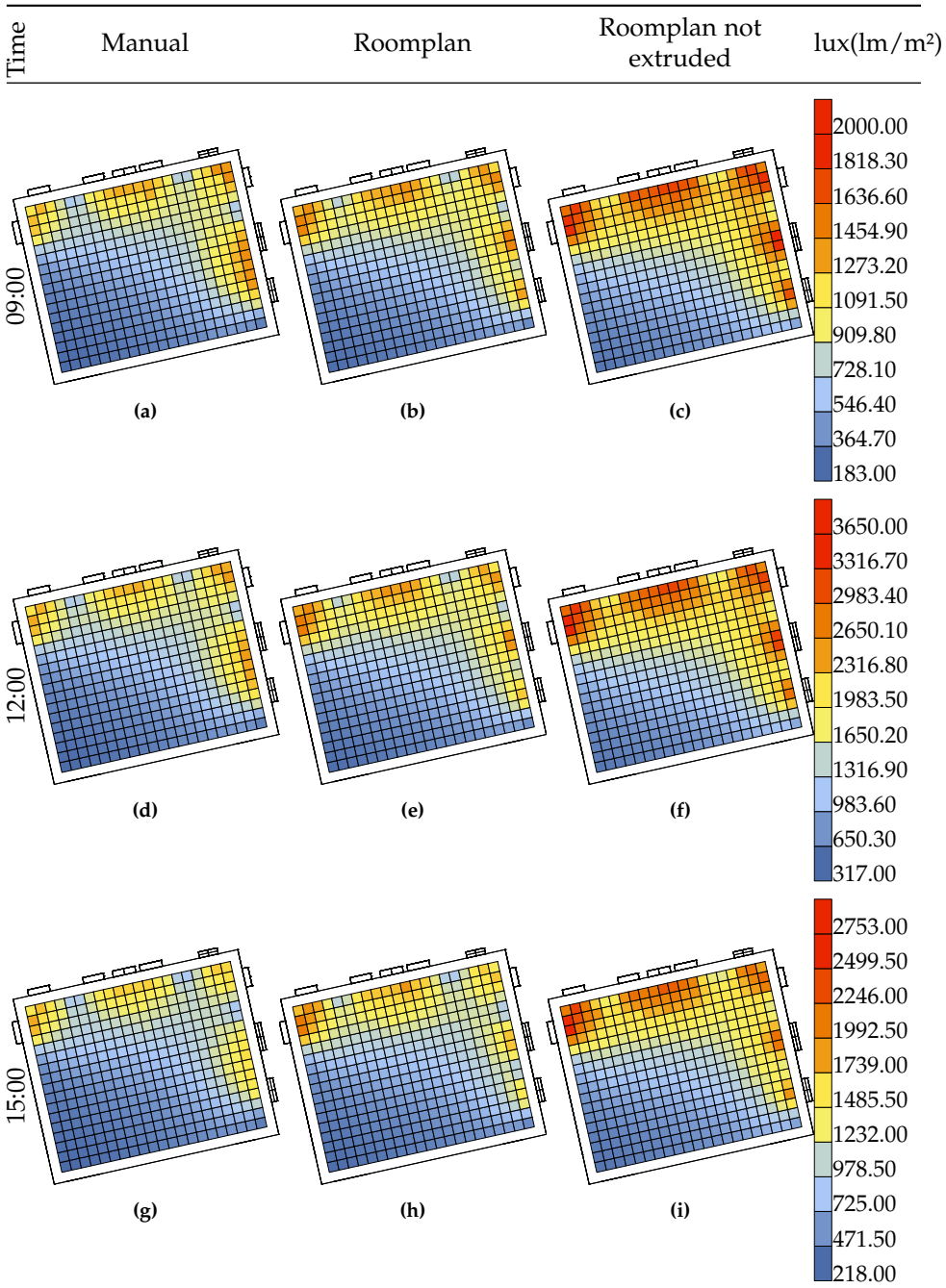

Figure E.9.: Heatmaps of illuminance for the 20th of March (Spring Equinox) for GeoinfoLab.

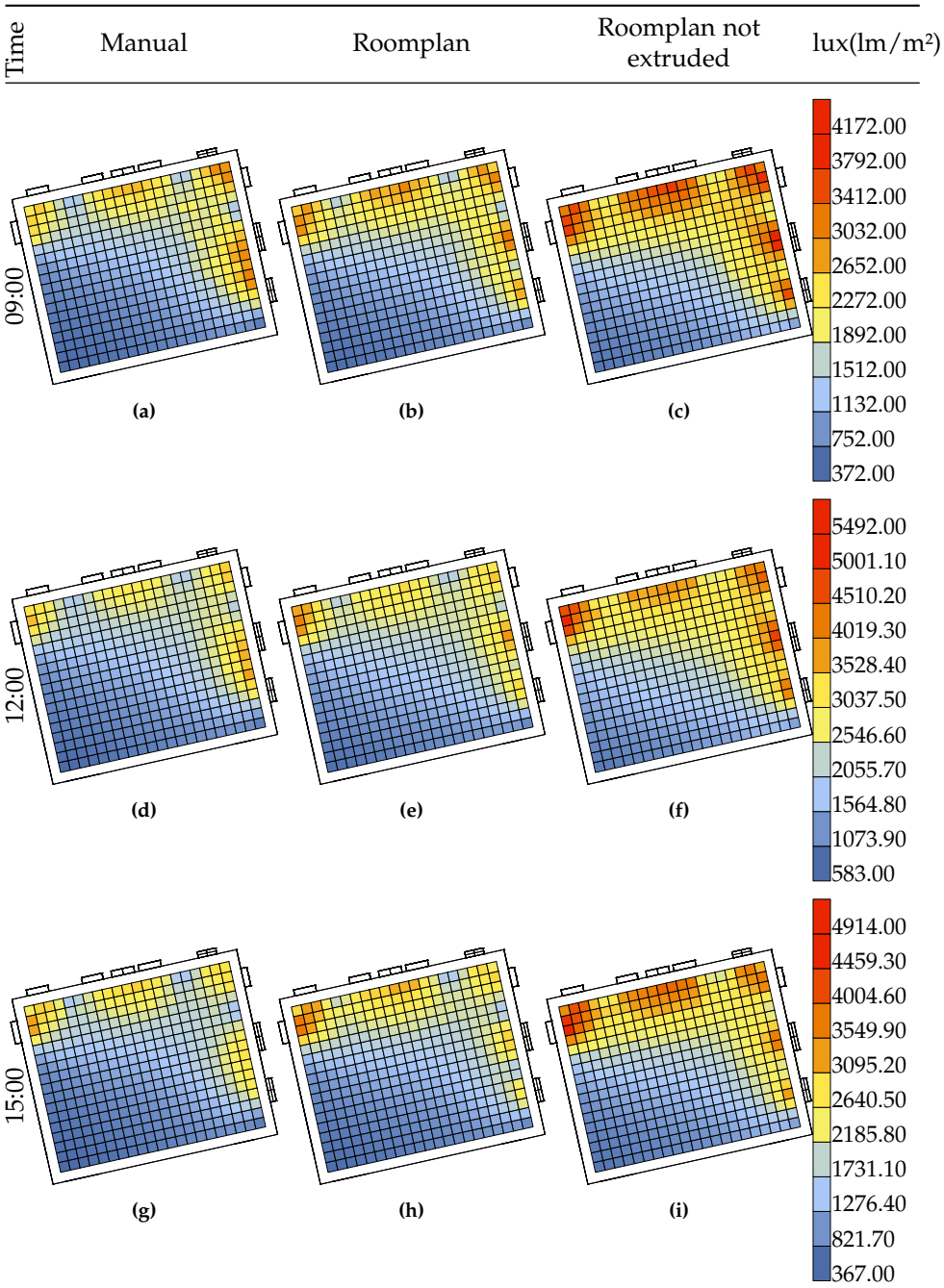

Figure E.10.: Heatmaps of illuminance for the 21th of June (Summer Solstice) for GeoinfoLab.

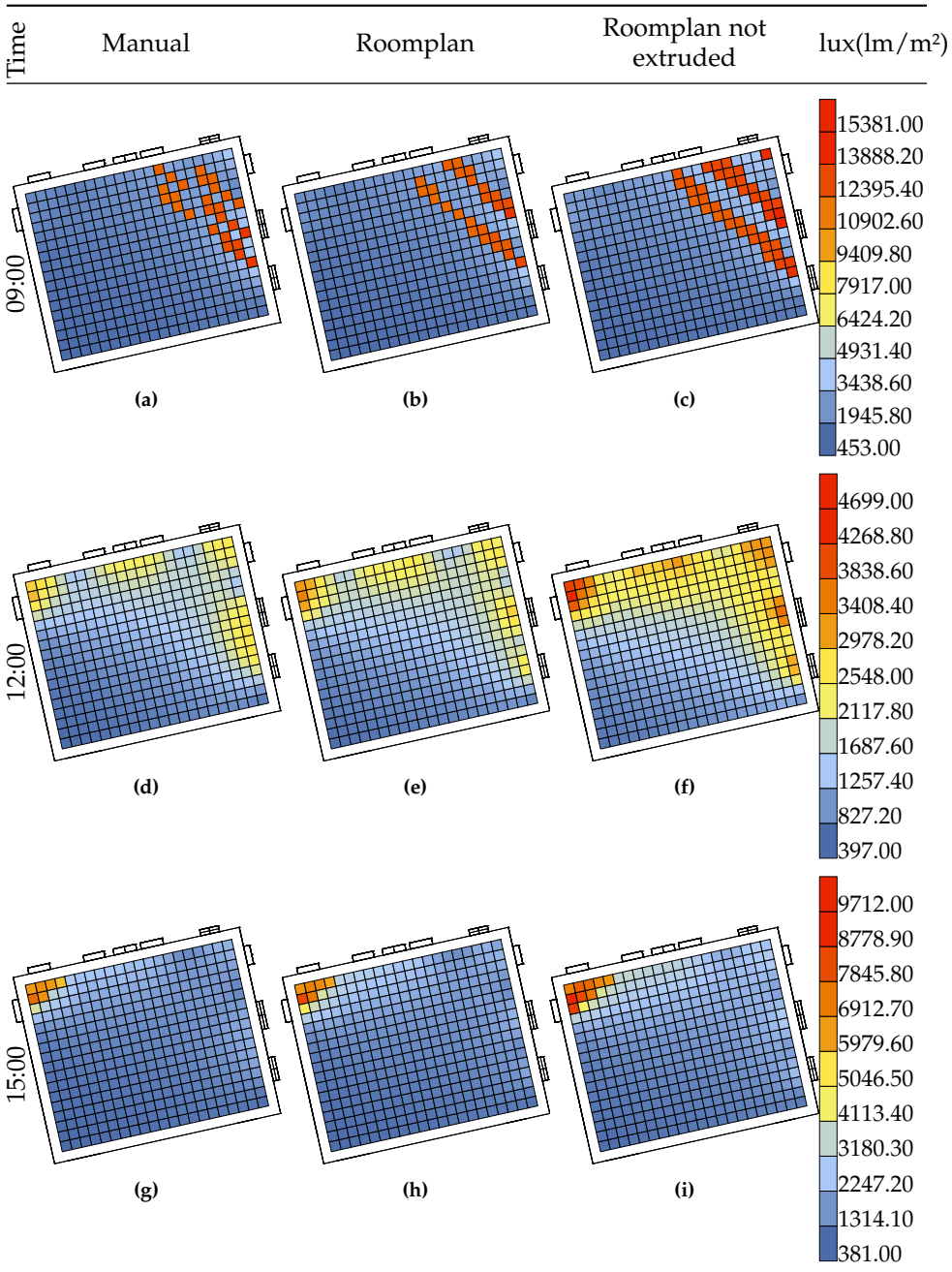

Figure E.11.: Heatmaps of illuminance for the 22nd of September (Autumn Equinox) for GeoinfoLab.

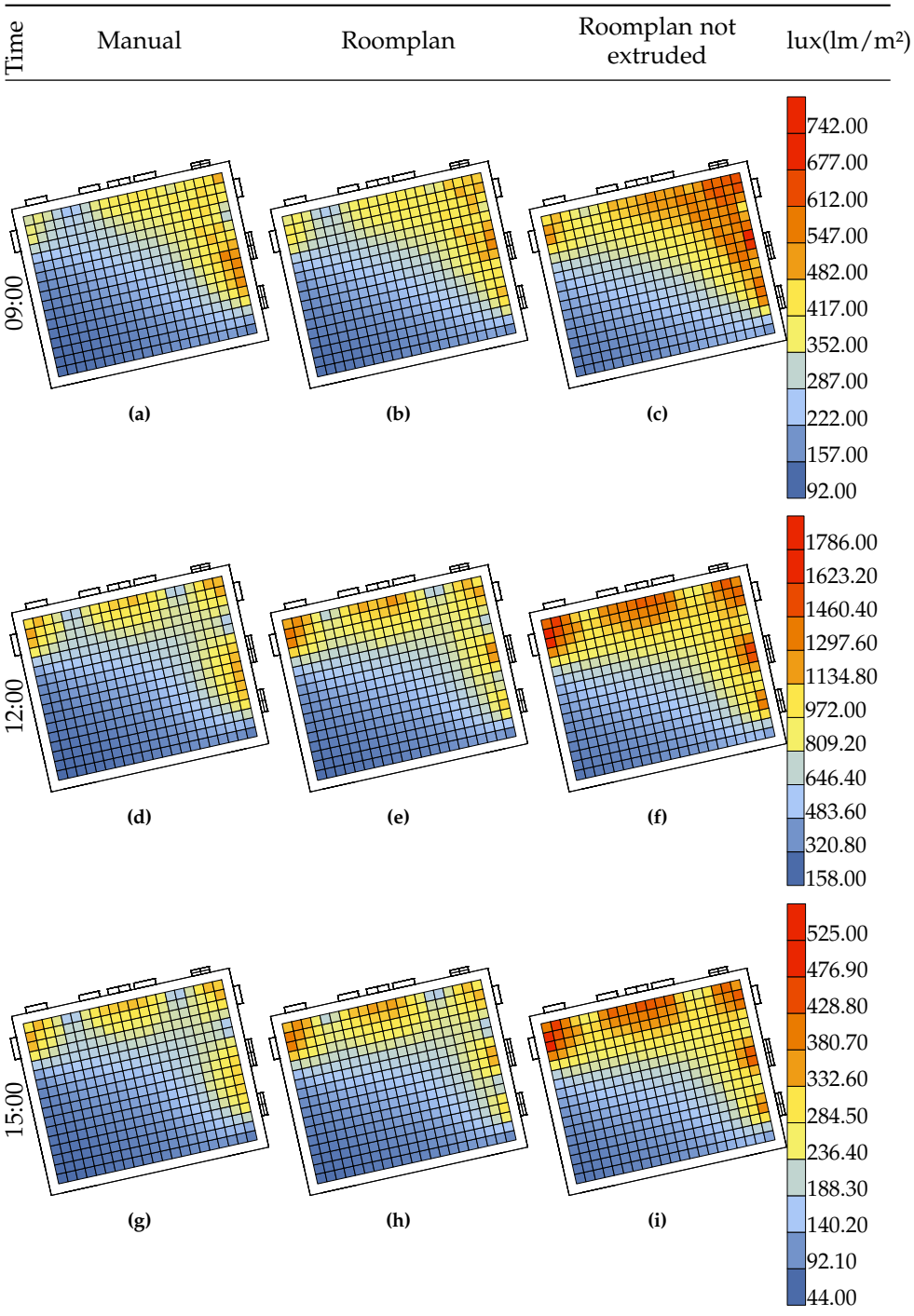

Figure E.12.: Heatmaps of illuminance for the 21st of December (Winter Solstice) for GeoinfoLab.

Bibliography

Directive (EU) 2024/1275 of the European Parliament and of the Council of 24 April 2024 on the energy performance of buildings (recast) (Text with EEA relevance). http://data.europa.eu/eli/dir/2024/1275/oj/eng, April 2024.

Nuno Abreu, Andry Pinto, Aníbal Matos, and Miguel Pires. Procedural Point Cloud Modelling in Scan-to-BIM and Scan-vs-BIM Applications: A Review. *ISPRS International Journal of Geo-Information*, 12(7):260, July 2023. ISSN 2220-9964. doi: 10.3390/ijgi12070260. https://www.mdpi.com/2220-9964/12/7/260.

Apple Inc. 3D Parametric Room Representation with RoomPlan. https://machinelearning.apple.com/research/roomplan, 2022a.

Apple Inc. CapturedRoom.USDExportOptions Documentation. https://developer.apple.com/documentation/roomplan/capturedroom/usdexportoptions, 2022b.

Apple Inc. RoomPlan Framework Documentation. https://developer.apple.com/documentation/RoomPlan, 2022c.

Apple Inc. Explore enhancements to RoomPlan - WWDC23 - Videos. https://developer.apple.com/videos/play/wwdc2023/10192/, 2023.

Apple Inc. Create a 3D model of an interior room by guiding the user through an AR experience. https://developer.apple.com/documentation/roomplan/create-a-3d-model-of-an-interior-room-by-guiding-the-user-through-an-ar-experience, 2025a.

Apple Inc. Providing custom models for captured rooms and structure exports. https://developer.apple.com/documentation/roomplan/providing-custom-models-for-captured-rooms-and-structure-exports, 2025b.

Cigdem Askar and Harald Sternberg. Use of Smartphone Lidar Technology for Low-Cost 3D Building Documentation with iPhone 13 Pro: A Comparative Analysis of Mobile Scanning Applications. *Geomatics*, 3(4):563–579, December 2023. ISSN 2673-7418. doi: 10.3390/geomatics3040030. https://www.mdpi.com/2673-7418/3/4/30.

Ramen Munir Baloch, Cara Nichole Maesano, Jens Christoffersen, Corinne Mandin, Eva Csobod, Eduardo de Oliveira Fernandes, Isabella Annesi-Maesano, and on behalf of the SINPHONIE Consortium. Daylight and School Performance in European Schoolchildren. *International Journal of Environmental Research and Public Health*, 18(1):258, January 2021. ISSN 1660-4601. doi: 10.3390/ijerph18010258. https://www.mdpi.com/1660-4601/18/1/258.

Mohamed Boubekri, Jaewook Lee, Piers MacNaughton, May Woo, Lauren Schuyler, Brandon Tinianov, and Usha Satish. The Impact of Optimized Daylight and Views on the Sleep Duration and Cognitive Performance of Office Workers. *International Journal of Environmental Research and Public Health*, 17(9):3219, January 2020. ISSN 1660-4601. doi: 10.3390/ijerph17093219. https://www.mdpi.com/1660-4601/17/9/3219.

Eleonora Brembilla, Shervin Azadi, and Pirouz Nourian. A Computational Approach for Checking Compliance with European View and Sunlight Exposure Criteria. http://arxiv.org/abs/2109.11037, September 2021.

Salvatore Carlucci, Francesco Causone, Francesco De Rosa, and Lorenzo Pagliano. A review of indices for assessing visual comfort with a view to their use in optimization processes to support building integrated design. *Renewable and Sustainable Energy Reviews*, 47:1016–1033, July 2015. ISSN 1364-0321. doi: 10.1016/j.rser.2015.03.062. https://www.sciencedirect.com/science/article/pii/S1364032115002154.

L. Díaz-Vilariño, S. Lagüela, J. Armesto, and P. Arias. Indoor daylight simulation performed on automatically generated as-built 3D models. *Energy and Buildings*, 68:54–62, January 2014. ISSN 0378-7788. doi: 10.1016/j.enbuild.2013.02.064. https://www.sciencedirect.com/science/article/pii/S0378778813006038.

Erika Dolníková. *Simulation Tools for Predicting Daylighting Conditions in Buildings*. Digital Innovations in Architecture, Engineering and Construction. Springer Nature Switzerland, Cham, 2025. ISBN 978-3-031-78329-6 978-3-031-78330-2. doi: 10.1007/978-3-031-78330-2. https://link.springer.com/10.1007/978-3-031-78330-2.

Lambros T. Doulos and Aris Tsangrassoulis. The Future of Interior Lighting Is Here. *Sustainability*, 14(12):7044, January 2022. ISSN 2071-1050. doi: 10.3390/su14127044. https://www.mdpi.com/2071-1050/14/12/7044.

Zahra Hamedani, Ebrahim Solgi, Trevor Hine, Henry Skates, Gillian Isoardi, and Ruwan Fernando. Lighting for work: A study of the relationships among discomfort glare, physiological responses and visual performance. *Building and Environment*, 167:106478, January 2020. ISSN 0360-1323. doi: 10.1016/j.buildenv.2019.106478. https://www.sciencedirect.com/science/article/pii/S0360132319306900.

Patrick Hübner, Martin Weinmann, Sven Wursthorn, and Stefan Hinz. Automatic voxel-based 3D indoor reconstruction and room partitioning from triangle meshes. *ISPRS Journal of Photogrammetry and Remote Sensing*, 181:254–278, November 2021. ISSN 0924-2716. doi: 10.1016/j.isprsjprs.2021.07.002. https://www.sciencedirect.com/science/article/pii/S0924271621001799.

International WELL Building Institute. Light. https://v2.wellcertified.com/en/wellv2/light, n.d.a.

International WELL Building Institute. WELL v2 Overview. https://v2.wellcertified.com/en/wellv2/overview, n.d.b.

Anne Iversen, Nicolas Roy, Mette Hvass, Michael Jørgensen, Jens Christoffersen, Werner Osterhaus, and Kjeld Johnsen. *Daylight Calculations in Practice: An Investigation of the Ability of Nine Daylight Simulation Programs to Calculate the Daylight Factor in Five Typical Rooms*. SBI. SBI forlag, København, 2013. ISBN 978-87-92739-49-0.

Roxana Jafarifiroozabadi, Anjali Joseph, William Bridges, and Andrea Franks. The impact of daylight and window views on length of stay among patients with heart disease: A retrospective study in a cardiac intensive care unit. *Journal of Intensive Medicine*, 03(02):155–164, April 2023. doi: 10.1016/j.jointm.2022.11.002. https://mednexus.org/doi/full/10.1016/j.jointm.2022.11.002.

Anja Jamrozik, Nicholas Clements, Syed Shabih Hasan, Jie Zhao, Rongpeng Zhang, Carolina Campanella, Vivian Loftness, Paige Porter, Shaun Ly, Selena Wang, and Brent Bauer. Access to daylight and view in an office improves cognitive performance and satisfaction and reduces eyestrain: A controlled crossover study. *Building and Environment*, 165: 106379, November 2019. ISSN 0360-1323. doi: 10.1016/j.buildenv.2019.106379. https://www.sciencedirect.com/science/article/pii/S036013231930589X.

Jan L.M. Hensen and Roberto Lamberts. *Building Performance Simulation for Design and Operation*, volume Second edition. Routledge, Abingdon, Oxon, 2019. ISBN 978-1-138-39219-9. https://search.ebscohost.com/login.aspx?direct=true&db=nlebk&AN=2138805&site=ehost-live&authtype=sso&custid=s1131660.

Zhizhong Kang, Juntao Yang, Zhou Yang, and Sai Cheng. A Review of Techniques for 3D Reconstruction of Indoor Environments. *ISPRS International Journal of Geo-Information*, 9(5):330, May 2020. ISSN 2220-9964. doi: 10.3390/ijgi9050330. https://www.mdpi.com/2220-9964/9/5/330.

Farzam Kharvari. An empirical validation of daylighting tools: Assessing radiance parameters and simulation settings in Ladybug and Honeybee against field measurements. *Solar Energy*, 207:1021–1036, September 2020. ISSN 0038-092X. doi: 10.1016/j.solener.2020.07.054. https://www.sciencedirect.com/science/article/pii/S0038092X20307866.

Ladybug Tools. Honeybee Schema. https://www.ladybug.tools/honeybee-schema/, 2024.

Ville V. Lehtola, Shayan Nikoohemat, and Andreas Nüchter. Indoor 3D: Overview on Scanning and Reconstruction Methods. In Martin Werner and Yao-Yi Chiang, editors, *Handbook of Big Geospatial Data*, pages 55–97. Springer International Publishing, Cham, 2021. ISBN 978-3-030-55462-0. doi: 10.1007/978-3-030-55462-0_3. https://doi.org/10.1007/978-3-030-55462-0_3.

Gahyeon Lim and Nakju Doh. Automatic Reconstruction of Multi-Level Indoor Spaces from Point Cloud and Trajectory. *Sensors*, 21(10):3493, January 2021. ISSN 1424-8220. doi: 10.3390/s21103493. https://www.mdpi.com/1424-8220/21/10/3493.

Zhaoji Lin, Yutao Huang, and Li Yao. Three-Dimensional Reconstruction of Indoor Scenes Based on Implicit Neural Representation. *Journal of Imaging*, 10(9):231, September 2024. ISSN 2313-433X. doi: 10.3390/jimaging10090231. https://www.mdpi.com/2313-433X/10/9/231.

Remedios M. López-Lovillo, Samuel Domínguez-Amarillo, Juan José Sendra, and Ignacio Acosta. How can a daylighting and user-oriented control system be configured? A state-of-the-art critical review. *Journal of Building Engineering*, 64:105704, April 2023. ISSN 2352-7102. doi: 10.1016/j.jobe.2022.105704. https://www.sciencedirect.com/science/article/pii/S2352710222017107.

Francisco Javier Montiel-Santiago, Manuel Jesús Hermoso-Orzáez, and Julio Terrados-Cepeda. Sustainability and Energy Efficiency: BIM 6D. Study of the BIM Methodology Applied to Hospital Buildings. Value of Interior Lighting and Daylight in Energy Simulation. *Sustainability*, 12(14):5731, January 2020. ISSN 2071-1050. doi: 10.3390/su12145731. https://www.mdpi.com/2071-1050/12/14/5731.

Pixar Animation Studios. USD Home — Universal Scene Description 25.05 documentation. https://openusd.org/release/index.html, 2021.

Radiance. SETTING RENDERING OPTIONS. https://radsite.lbl.gov/radiance/refer/Notes/rpict_options.htm

Royal Netherlands Standardization Institute (NEN). Daglicht in gebouwen Daylight in buildings. https://www.nen.nl.

Pingbo Tang, Daniel Huber, Burcu Akinci, Robert Lipman, and Alan Lytle. Automatic reconstruction of as-built building information models from laser-scanned point clouds: A review of related techniques. *Automation in Construction*, 19(7):829–843, November 2010. ISSN 0926-5805. doi: 10.1016/j.autcon.2010.06.007. https://www.sciencedirect.com/science/article/pii/S0926580510000907.

Christos Tzouvaras, Asimina Dimara, Alexios Papaioannou, Kanela Karatzia, Christos-Nikolaos Anagnostopoulos, Stelios Krinidis, Konstantinos I. Arvanitis, Dimosthenis Ioannidis, and Dimitrios Tzovaras. A Guide to Visual Comfort: An Overview of Indices and Its Applications. In *Artificial Intelligence Applications and Innovations. AIAI 2023 IFIP WG 12.5 International Workshops*, pages 183–194. Springer, Cham, 2023. ISBN 978-3-031-34171-7. doi: 10.1007/978-3-031-34171-7_14. https://link.springer.com/chapter/10.1007/978-3-031-34171-7_14.

Colophon

This document was typeset using LaTeX, using the KOMA-Script class `scrbook`. The main font is Palatino.